Spectrally and energy efficient ultra-wideband pulses based on spectrum shaping

Miloš, Ante

University of Zagreb
FACULTY OF ELECTRICAL ENGINEERING AND COMPUTING

Ante Miloš

SPECTRALLY AND ENERGY EFFICIENT ULTRA-WIDEBAND PULSES BASED ON SPECTRUM SHAPING

DOCTORAL THESIS

Zagreb, 2024

University of Zagreb
FACULTY OF ELECTRICAL ENGINEERING AND COMPUTING

Ante Miloš

SPECTRALLY AND ENERGY EFFICIENT ULTRA-WIDEBAND PULSES BASED ON SPECTRUM SHAPING

DOCTORAL THESIS

Supervisors:
Professor Mladen Vučić, Ph.D.
Adjunct Associate Professor Goran Molnar, Ph.D.

Zagreb, 2024

Sveučilište u Zagrebu
FAKULTET ELEKTROTEHNIKE I RAČUNARSTVA

Ante Miloš

SPEKTRALNO I ENERGETSKI UČINKOVITI ULTRA-ŠIROKOPOJASNI PULSOVI TEMELJENI NA OBLIKOVANJU SPEKTRA

DOKTORSKI RAD

Mentori:
Prof. dr. sc. Mladen Vučić
Nasl. izv. prof. dr. sc. Goran Molnar

Zagreb, 2024.

Doctoral thesis was written at the University of Zagreb Faculty of Electrical Engineering and Computing, Department of Electronic Systems and Information Processing.

The thesis was supported in part by Croatian Science Foundation under the Project IP-2019-04-4189 Efficient Signal Processing Systems for Software Defined Radio, and in part by Ericsson Nikola Tesla d.d. and University of Zagreb Faculty of Electrical Engineering and Computing under the project ILTERA.

Supervisors:
Professor Mladen Vučić, Ph.D.
Adjunct Associate Professor Goran Molnar, Ph.D.

PhD thesis contains 109 pages.
Thesis no: _____

About Supervisors

Mladen Vučić was born in Karlovac in 1965. He received B.Sc., M.Sc. and Ph.D. degrees in electrical engineering from the University of Zagreb, Faculty of Electrical Engineering and Computing (FER), Zagreb, Croatia, in 1989, 1993 and 1999, respectively.

Since March 1989 he has been working at the Department of Electronic Systems and Information processing at FER. In 2001 he was promoted to an Assistant Professor, in 2006 to an Associate Professor, in 2011 to a Professor and in 2016 to a Full Professor. He led three scientific and one research project, and participated in four other projects funded by the Ministry of Science and Technology of the Republic of Croatia. Furthermore, he participated in one EU FP7 project and one project funded by the European Regional Development Fund. Currently, he leads the project *Efficient signal processing systems for software defined radio*, which is funded by the Croatian Science Foundation. He is a member of the Centre of Research Excellence for Data Science and Cooperative Systems. He published more than 60 papers in journals and conference proceedings in the area of circuit theory, analog and digital signal processing, optimization theory and applications, digital system design, and embedded systems.

Prof. Vučić is a member of IEEE and KoREMA. From 2013 to 2016 he served as the chair of *IEEE Circuits and Systems Chapter Croatia*. From 2016 to 2018 he was Head of the Department of Electronic Systems and Information Processing at FER. In 1997, he was awarded from the Ministry of Defence and the Ministry of Science and Technology of the Republic of Croatia by the *Annual award for scientific contribution to the development and strengthening of the defence system of the Republic of Croatia*. In 2019, he received the *Fran Bošnjaković award* from the University of Zagreb.

Goran Molnar was born in Zagreb in 1978. He received the Diploma Engineer and Ph.D. degrees in electrical engineering from the University of Zagreb, Faculty of Electrical Engineering and Computing (FER), in 2001 and 2010. He received the *Silver medal Josip Lončar* from FER for outstanding Ph.D. thesis and *Award for Young Scientists Vera Johanides* from the Croatian Academy of Engineering for 2010th year, for the research in the field of synthesis and implementation of systems for analog and digital signal processing.

In 2001 he was employed as a Teaching and Research Assistant at the Department of Electronic Systems and Information Processing at FER. In 2010 he was employed as a Senior Teaching and Research Assistant at the same department. From 2001 to 2013 he participated in three scientific and one research project funded by the Ministry of Science and Technology of the Republic of Croatia. In 2013 he had the position of Experienced Researcher at *Centre of Research Excellence for Advanced Cooperative Systems* (*ACROSS*) funded by EU FP7 framework. In 2014 he was employed as a Senior FGPA Engineer and Project Leader at the electronic company Xylon. Since 2015 he works at the Research and Development Centre of Ericsson Nikola Tesla d.d., where he participates in two educational and research collaboration-projects between FER and Ericsson Nikola Tesla d.d. in the development of 4G/5G radio access networks, entitled *Improvements for LTE Radio Access Equipment* (*ILTERA*) and *Emerging Wireless and Information Technologies for 5G Radio Access Networks* (*EWITA*). Currently, he participates in the project *Efficient Signal Processing Systems for Software Defined Radio* funded by Croatian Science Foundation. In 2018 he was promoted to an Adjunct Assistant Professor at FER, and in 2022 to an Adjunct Associate Professor. In 2023 he was promoted to a Tenured Scientific Adviser in the area of technical sciences, scientific field of electrical engineering. He published 48 papers in journals and conference proceedings in the fields of filter theory and design, analog and digital signal processing, communication systems, optimization theory and applications, and digital system design.

Goran Molnar is a member of IEEE. From 2018 to 2021 he was serving as the chair of *IEEE Signal Processing Chapter Croatia*.

O mentorima

Mladen Vučić rođen je u Karlovcu 1965. godine. Diplomirao je, magistrirao i doktorirao u polju elektrotehnike na Sveučilištu u Zagrebu, Fakultetu elektrotehnike i računarstva (FER), 1989., 1993. odnosno 1999. godine.

Od ožujka 1989. godine radi na Zavodu za elektroničke sustave i obradbu informacija FER-a. Godine 2001. izabran je u znanstveno-nastavno zvanje docenta, 2006. u zvanje izvanrednog profesora, 2011. u zvanje redovitog profesora, a 2016. u zvanje redovitog profesora u trajnom izboru. Dosad je vodio tri znanstvenoistraživačka i jedan tehnologijski istraživačko razvojni projekt, te je sudjelovao na još četiri znanstvenoistraživačka projekta Ministarstva znanosti i tehnologije Republike Hrvatske. Također, bio je istraživač na jednom EU FP7 projektu te na jednom projektu financiranom iz Europskog fonda za regionalni razvoj. Trenutno vodi projekt *Učinkoviti sustavi za obradu signala namijenjeni programski definiranom radiju* koji je financiran od Hrvatske zaklade za znanost. Član je Znanstvenog centra izvrsnosti za znanost o podatcima i kooperativne sustave. Objavio je više od 60 radova u časopisima i zbornicima konferencija u području teorije električnih krugova, analogne i digitalne obrade signala, teorije i primjene optimizacijskih postupaka, dizajna digitalnih sustava te ugradbenih računalnih sustava.

Prof. Vučić član je udruga IEEE i KoREMA. Od 2013. do 2016. godine bio je predsjednik Odjela za električne krugove i sustave Hrvatske sekcije IEEE. Od 2016. do 2018. godine bio je predstojnik Zavoda za elektroničke sustave i obradbu informacija FER-a. 1997. godine dobio je *Godišnju nagradu za sveukupne znanstveno-istraživačke doprinose razvoju i jačanju sustava obrane Republike Hrvatske*, koju su zajednički dodijelili Ministarstvo obrane i Ministarstvo znanosti i tehnologije Republike Hrvatske. 2019. godine dobio je *Nagradu Fran Bošnjaković* koju je dodijelilo Sveučilište u Zagrebu.

Goran Molnar rođen je u Zagrebu 1978. godine. Diplomirao je i doktorirao u polju elektrotehnike na Sveučilištu u Zagrebu, Fakultetu elektrotehnike i računarstva (FER), 2001. i 2010. godine. Za istaknutu doktorsku disertaciju dobio je *Srebrnu plaketu Josip Lončar*. Za svoj znanstveno-istraživački rad u području sinteze i implementacije sustava za analognu i digitalnu obradu signala, uručena mu je *Nagrada mladom znanstveniku Vera Johanides* Akademije tehničkih znanosti Hrvatske za 2010. godinu.

Godine 2001. zapošljava se kao znanstveni novak na Zavodu za elektroničke sustave i obradbu informacija FER-a. Godine 2010. zapošljava se kao viši asistent na istom zavodu. Od 2001. do 2013. godine sudjeluje u radu na tri znanstveno-istraživačka i jednom tehnologijsko istraživačko razvojnom projektu Ministarstva znanosti i tehnologije Republike Hrvatske. Godine 2013. zapošljava se kao istraživač na infrastrukturnom europskom projektu *Centre of Research Excellence for Advanced Cooperative Systems* (*ACROSS*) financiranog iz EU FP7 okvirnog programa. Godine 2014. zapošljava se kao razvojni FPGA inženjer i voditelj industrijskih projekata u elektroničkoj tvrtki Xylon d.o.o. Od 2015. godine do danas, radi u Istraživačko-razvojnom centru kompanije Ericsson Nikola Tesla d.d. gdje sudjeluje u radu na dva projekta obrazovne i znanstveno-istraživačke suradnje između FER-a i Ericssona Nikole Tesle d.d. u području razvoja 4G/5G radijskih pristupnih mreža, pod nazivima *Poboljšanje karakteristika rada LTE radijskih pristupnih uređaja* (*ILTERA*) i *Nove bežične i informacijske tehnologije za 5G radijske pristupne mreže* (*EWITA*). Trenutno je istraživač na znanstveno istraživačkom projektu *Učinkoviti sustavi za obradu signala namijenjeni programski definiranom radiju* financiranom od Hrvatske zaklade za znanost. Godine 2018. izabran je u naslovno znanstveno-nastavno zvanje docenta na FERu, a 2022. u naslovnog izvanrednog profesora. Godine 2023. izabran je u znanstveno zvanje znanstveni savjetnik u trajnom zvanju u znanstvenom području tehničkih znanosti, polje elektrotehnika. Objavio je 48 radova u časopisima i zbornicima konferencija u području teorije i sinteze filtara, analogne i digitalne obrade signala, komunikacijskih sustava, teorije i primjene optimizacijskih postupaka te dizajna digitalnih sustava.

Goran Molnar član je udruge IEEE. Od 2018. do 2021. godine bio je predsjednik Odjela za obradu signala Hrvatske sekcije IEEE.

ABSTRACT

Ultra-wideband (UWB) impulse radio uses very short pulses to transmit data, resulting in high-rate transmission. These systems require pulses that efficiently fill desired spectral masks and exhibit high energy concentration. Since these requirements are in conflict, many methods for the design of UWB pulses make a trade-off between them. Common UWB pulses exploit Gaussian derivatives. These derivatives represent bandpass pulses well localized in time. However, they do not exploit UWB region efficiently. In this dissertation, two methods for the design of spectrally and energy efficient UWB pulses based on Gaussian derivatives as well as Gaussian pulses have been presented. First method considers the design of pulses based on sharpening technique. The sharpening was introduced in the design of FIR filters, where it was used to improve the filter's magnitude response. Here, it is used to develop a method for the design of UWB pulses which optimally fill a desired spectral mask. The method is based on the sharpening of the magnitude spectrum of an arbitrary Gaussian derivative by applying the Kaiser-Hamming polynomials. Such sharpening offers controllable flatness at the top of the magnitude spectrum as well as controllable steepness in spectrum's transition regions. Second method is inspired by Gaussian derivatives, in which the Gaussian is weighted by Hermite polynomials. Here, the polynomials are constructed by imposing maximum flatness at the peak of pulse’s amplitude spectrum. Furthermore, to obtain UWB pulses, frequency shift and bandwidth scaling are applied. In both methods, the pulse's magnitude spectrum is given in a closed form, thus ensuring fast and robust pulse design. Furthermore, compared to other Gaussian-based UWB waveforms, both methods bring the pulses which have significantly higher spectral efficiency and slightly lower energy concentration. In addition to these methods, the approximation of ideal UWB waveforms by using pulse shapers is also considered in the dissertation. In particular, the pulse shapers whose impulse responses approximate Gaussian derivatives, modified Hermite pulses, prolate spheroidal pulses, as well as the proposed sharpened Gaussian derivatives and flat-spectrum Gaussian pulses are presented. To obtain the optimum pulse shapers, least-squares error criterion is used. In their design, the transfer functions that exhibit spectral efficiency up to 78% are considered.

Keywords: Gaussian derivatives, impulse response approximation, maximally flat, optimum waveforms, polynomial sharpening, pulse shaping, time-domain synthesis, ultra-wideband (UWB) systems.

Spektralno i energetski učinkoviti ultra-širokopojasni pulsovi temeljeni na oblikovanju spektra

Ultra-širokopojasni (*ultra-wideband*, UWB) radio koristi pulsove kratkog trajanja za prijenos informacija. Ovi pulsovi moraju učinkovito popunjavati zadanu spektralnu masku te biti koncentrirani u vremenu. Često korišteni pulsovi temelje se na Gaussovim derivacijama. Ove derivacije su dobro vremenski koncentrirane, ali ne iskorištavaju učinkovito područje pod maskom. U disertaciji su predložene dvije metode za dizajn spektralno i energetski učinkovitih pulsova temeljenih na Gaussovom pulsu i njegovim derivacijama. Prva metoda se temelji na izoštravanju amplitudnih spektara Gaussovih derivacija Kaiser-Hammingovim polinomima. Takvo izoštravanje nudi kontroliranje glatkoće u maksimumu amplitudnog spektra kao i kontroliranje nagiba njegovog prijelaznog područja. Druga metoda inspirirana je Gaussovim derivacijama, u kojima je Gaussova funkcija otežana Hermitovim polinomima. U disertaciji je predložen optimalan težinski polinom koji osigurava maksimalnu glatkoću u vrhu amplitudnog spektra pulsa. Uspoređujući dobivene pulsove s drugim pulsovima temeljenim na Gaussovoj funkciji, obje metode nude značajno veće spektralne učinkovitosti s tek nešto slabijom energetskom koncentracijom. Konačno, razmatrana je aproksimacija idealnih pulsova pomoću impulsnih odziva vremenski kontinuiranih filtara. Dane su prijenosne funkcije ovih filtara pogodne za oblikovanje raznih konvencionalnih te predloženih UWB pulsova.

Disertacija je podijeljena u sedam poglavlja. U prvom, uvodnom, poglavlju provedeno istraživanje smješteno je u kontekst. Dana je definicija UWB radija i UWB signala. Nadalje, navedene su glavne značajke UWB prijenosnih sustava i područja njihove primjene te je opisana njihova interakcija s drugima kratkodometnim komunikacijskim sustavima. UWB prijenos reguliran je spektralnim maskama koje specificiraju razne regulatorne agencije. U ovoj disertaciji razmatrani su pulsovi koji zadovoljavaju maske za otvorene i zatvorene prostore koje propisuje Federalna komisija za komunikacije (*Federal Communications Commission,* FCC). Za obje maske izdvojeno je takozvano UWB područje koje obuhvaća frekvencije od 3.1 GHz do 10.6 GHz, a u kojem je, prema FCC specifikacijama, za prijenos pulsova dozvoljena maksimalna spektralna gustoća snage od −41.3 dBm/MHz. Pulsovi razmatrani u ovoj disertaciji dizajnirani su tako da učinkovito ispunjavaju spomenuto područje. Kao mjera kvalitete ispune,

uvedena je spektralna učinkovitost definirana kao omjer snage pulsa u UWB frekvencijskom području i ukupne snage koju u tom području dopušta spektralna maska. Nadalje, kao mjera kvalitete valnog oblika pulsa uvedena je energetska koncentracija definirana kao omjer energije korisnog dijela pulsa i njegove ukupne energije.

U drugom poglavlju opisana su dosadašnja postignuća u području dizajna UWB pulsova. Nadalje, razmotrene su prednosti i nedostatci postojećih pulsova te je dana njihova usporedba. Od konvencionalnih pulsova koji se koriste u UWB dizajnu razmatrane su Gaussove derivacije, modificirane Hermitove funkcije i izdužene sferoidne valne funkcije (*prolate spheroidal function*). UWB pulsovi temeljeni na Gaussovim derivacijama i izduženim sferoidnim valnim funkcijama imaju iznimno velike energetske koncentracije. Međutim, oni slabo ispunjavaju UWB područje spektralne maske. Hermitovi pulsovi također imaju veliku energetsku koncentraciju. Međutim, karakteristike njihovih spektralnih gustoća snaga imaju velike bočne latice što može uzrokovati jaku interferenciju s drugim komunikacijama. S druge strane, puls koji nudi vrlo veliku spektralnu učinkovitost je pojasno propusni sinc puls koji gotovo u potpunosti ispunjava UWB područje. Međutim, ovakav puls ima veliko i dugotrajno istitravanje, što uzrokuje slabu energetsku koncentraciju. Stoga se njegovo trajanje ograničava množenjem s odgovarajućim vremenskim otvorom. Dobar kompromis između spektralne učinkovitosti i energetske koncentracije nude linearne kombinacije konvencionalnih pulsova. U njima se često koriste frekvencijski transponirani Gaussovi i sinc pulsovi, te Gaussove derivacije.

S obzirom da se prva predložena metoda za dizajn pulsova temelji na Gaussovim derivacijama, u trećem poglavlju opisan je postupak dizajna UWB pulsova temeljen na njima. U ovakvom dizajnu potrebno je osigurati kompatibilnost Gaussovih derivacija s danom spektralnom maskom. Za to je potrebno odrediti faktore za skaliranje amplitude i frekvencijskog područja. U disertaciji je detaljno opisan postupak određivanja ovih faktora. Nadalje, dani su parametri pod kojima Gaussove derivacije optimalno popunjavaju vanjsku i unutarnju FCC spektralnu masku. Također, dan je programski kod u kojem je implementiran cjelovit dizajn pulsova temeljenih na Gaussovim derivacijama. Za dobivene pulsove izračunate se spektralne učinkovitosti i energetske koncentracije s obzirom na obje maske. Kod računanja energetske koncentracije, energija korisnog dijela pulsa određena je numerički, dok su za izračunavanje njegove ukupne energije izvedeni analitički izrazi.

Četvrto poglavlje opisuje prvu od predloženih metoda za dizajn pulsova. Ova metoda temelji se na izoštravanju amplitudnih spektara Gaussovih derivacija Kaiser-Hammingovim polinomima. Polinomno izoštravanje prvi je put primijenjeno za poboljšavanje amplitudnih

karakteristika filtara s konačnim impulsnim odzivom (*finite impulse response*, FIR). Međutim, iako je izoštravanje dobro poznato u dizajnu FIR filtara, do sada nije razmatrana njegova primjena u sintezi valnih oblika. Izoštravanje Kaiser-Hammingovim polinomima pogodno je za dizajn UWB pulsova jer omogućava kontrolu glatkoće u maksimumu amplitudnog spektra i kontrolu nagiba njegovog prijelaznog područja. Da bi ovo izoštravanje moglo biti primijenjeno na Gaussove derivacije, maksimumi njihovih amplitudnih spektara normirani su na jedinične vrijednosti. Na ovako dobivene spektre primijenjeni su polinomi za izoštravanje s raznim stupnjevima glatkoće. Nadalje, izvedeni su analitički izrazi za amplitudne spektre izoštrenih Gaussovih derivacija te za pripadajuće valne oblike. Uočeno je da valni oblici dobivenih pulsova predstavljaju linearne kombinacije Gaussovih derivacija i njihovih Hilbertovih transformacija. Stoga je izveden i analitički izraz za ove Hilbertove transformacije. U ovom poglavlju opisan je i dizajn ultra-širokopojasnih pulsova temeljenih na izoštrenim Gaussovim derivacijama. Kako bi bila osigurana kompatibilnost pulsova s danom spektralnom maskom, za pojedine redove Gaussovih derivacija potrebno je odrediti faktore za skaliranje frekvencijskog područja te redove glatkoća polinoma. U disertaciji je predložen postupak za određivanje ovih parametara. Također, dan je programski kod u kojem je implementiran cjelovit dizajn pulsova kompatibilnih s FCC maskama. Za dobivene pulsove izračunate su spektralne učinkovitosti i energetske koncentracije. Nadalje, dani su primjeri koji pokazuju superiornost spektralne učinkovitosti predloženih pulsova u odnosu na različite gaussovske i sinc pulsove. Također, dana je usporedba njihovih energetskih koncentracija.

Forsiranje glatkoće u vrhu amplitudnog spektra UWB pulsa značajno povećava spektralnu učinkovitost, a istovremeno zadržava dobru energetsku koncentraciju. Kod izoštrenih Gaussovih derivacija, glatkoća je nametnuta posredno, kao kompozicija maksimalno glatkih polinoma i Gaussovih derivacija. Kao posljedica ovakvog pristupa, prilagođavanje spektra pulsa na zadanu spektralnu masku bilo je potrebno provesti pomoću optimizacije. Osim toga, dio UWB područja i dalje je ostao neiskorišten. Peto poglavlje opisuje metodu koja bolje iskorištava UWB područje, a istovremeno omogućava analitičko oblikovanje pulsa. Ova metoda koristi Gaussovu funkciju otežanu polinomom dobivenim po maksimalno glatkom kriteriju. Ovakav model inspiriran je valnim oblicima Gaussovih derivacija, u kojima je Gaussova funkcija otežana Hermitovim polinomima. U predloženoj metodi, najprije je izveden analitički izraz za valni oblik i amplitudni spektar pulsova u kojem je Gaussova funkcija otežana proizvoljnim polinomom. Nadalje, optimalan težinski polinom je određen po maksimalno glatkom kriteriju. Ovaj kriterij je zadovoljen na frekvenciji koja osigurava optimalnu glatkoću amplitude. U ovom poglavlju, detaljno je opisano i prilagođavanje dobivenih pulsova

spektralnim maskama. Ako je dobiveni amplitudni spektar maksimalno gladak na nultoj frekvenciji, valni oblik UWB pulsa dobiva se frekvencijskom translacijom dvostranog spektra pulsa iz osnovnog frekvencijskog područja. S druge strane, ukoliko je amplitudni spektar maksimalno gladak na frekvenciji različitoj od nule, UWB puls dobiva se frekvencijskom translacijom jednostranog spektra pulsa iz osnovnog frekvencijskog područja. U oba slučaja, translacija se izvodi uz frekvenciju miješanja koja osigurava kompatibilnost pulsa sa spektralnom maskom na frekvencijama na kojima dozvoljena spektralna gustoća snage ima diskontinuitet. Na taj način osigurava se optimalno ispunjavanje UWB područja te time i visoka spektralna učinkovitost. Polinom dobiven po maksimalno glatkom kriteriju u frekvencijskoj domeni ujedno osigurava dobru energetsku koncentraciju pulsova. U disertacija je dan i programski kod u kojem je implementiran cjelovit dizajn pulsova kompatibilnih s FCC maskama. Kako bi se prikazale značajke predloženog pristupa, napravljena je usporedba dobivenih oblika i konvencionalnih UWB pulsova kao što su Gaussove derivacije te linearne kombinacije translatiranih sinc pulsova i translatiranih Gaussovih derivacija.

Šesto poglavlje opisuje metodu za dizajn vremenski kontinuiranih filtara čiji impulsni odzivi aproksimiraju kauzalne reprezentacije raznih idealnih pulsova. Kauzalnost pulsova je dobivena kašnjenjem koje je određeno tako da kauzalna reprezentacija sadrži najmanje 99.9 % energije originalnog pulsa. U disertaciji je detaljno opisana metoda kojom su pronađene optimalne prijenosne funkcije filtara po kriteriju najmanje kvadratne pogreške koja je definirana u vremenskoj domeni. Ta metoda koristi iterativan postupak u kojem se u svakom koraku rješava problem optimizacije linearne funkcije nad prostorom omeđenim stošcima drugog reda (*second order cone programming*). Metoda koristi model prijenosne funkcije filtara koji sadrži nultočke, polove i pojačanje (*zeros, poles and gain coeffcient*, ZPK) sustava. Ovakav model omogućava jednostavnu kontrolu stabilnosti sustava te osigurava malu osjetljivost postupka na numeričke pogreške. Da bi se aproksimirani pulsovi mogli lakše usporediti s originalnim pulsovima, izvedene su mjere spektralne učinkovitosti i energetske koncentracije impulsnih odziva filtara u analitičkom obliku. Ove mjere također koriste ZPK model sustava. U disertaciji je detaljno opisan postupak za sintezu optimalnih prijenosnih funkcija vremenski kontinuiranih filtara čiji impulsni odzivi aproksimiraju Gaussove derivacije, modificirane Hermitove funkcije i izdužene sferoidne valne funkcije, kao i predložene izoštrene Gaussove derivacije te Gaussove pulsove s maksimalno glatkim amplitudnim spektrom. Navedeni pulsovi namijenjeni su komunikacijama u kojima dano frekvencijsko područje koristi jedan korisnik. Osim njih, razmatrani su i impulsni odzivi koji aproksimiraju idealne pulsove temeljene na izduženim sferoidnim valnim funkcijama,

namijenjeni komunikacijama u kojima isto frekvencijsko područje koriste dva korisnika. Za ovakve pulsove izvedena je mjera njihove ortogonalnosti u analitičkom obliku. Konačno, za predložene aproksimacije pulsova izračunata je spektralna učinkovitost i energetska koncentracija.

U posljednjem, sedmom, poglavlju sažeta su svojstva predloženih metoda za dizajn idealnih UWB pulsova te svojstva njihovih kauzalnih aproksimacija. Metoda za dizajn UWB pulsova koja se temelji na izoštravanju, kao kriterij za dizajn koristi glatkoću spektra. Time osigurava veliku spektralnu učinkovitost i dobru energetsku koncentraciju. Jednostavna je za upotrebu, a njena primjena značajno poboljšava spektralna svojstva Gaussovih derivacija. Metoda podržava proizvoljnu spektralnu masku. Pulsovi oblikovani s obzirom na FCC maske pokazuju značajno veću spektralnu učinkovitost od ostalih gaussovskih pulsova, a istovremeno zadržavaju dobru energetsku koncentraciju. Polinomno otežavanje Gaussovog pulsa također koristi glatkoću spektra kao kriterij za dizajn. U ovom slučaju, oblikovanje je izvedeno pomoću translacije i skaliranja frekvencijskog područja. Taj pristup se pokazao kao vrlo učinkovit pri ispunjavanju UWB područja spektralne maske. Pulsovi oblikovani s obzirom na FCC maske pokazuju značajno veću spektralnu učinkovitost nego konvencionalni pulsovi, uz istovremeno dobru energetsku koncentraciju. Predložene aproksimacije idealnih pulsova jako dobro prate valne oblike idealnih pulsova, te stoga osiguravaju približno jednake spektralne učinkovitosti kao i njihovi idealni parnjaci.

Ključni pojmovi: ultra-širokopojasnost (*UWB*), Gaussov puls, maksimalno glatki kriterij, ravan amplitudni spektar, Gaussove derivacije, polinomijalno izoštravanje, optimalni valni oblici, oblikovanje pulsa, spektralna učinkovitost, energetska koncentracija, sinteza pulsa u vremenskoj domeni, kriterij najmanje kvadratne pogreške.

TABLE OF CONTENTS

1. INTRODUCTION 1

2. STATE-OF-THE-ART UWB PULSES 6

2.1 Gaussian derivatives 6
2.2 Modified Hermite pulses 8
2.3 Prolate spheroidal wave functions 12
2.4 Translated sinc pulse 14
2.5 Linear combination of translated sinc pulses 15
2.6 Linear combination of translated Gaussian pulses 16
2.7 Linear combination of Gaussian derivatives 17
2.8 Overview 18

3. DESIGN OF UWB PULSES BASED ON GAUSSIAN DERIVATIVES 20

3.1 Design method 20
3.2 FCC-compliant Gaussian derivatives 23
3.3 Spectral efficiency and energy concentration of Gaussian derivatives 27

4. SHARPENED GAUSSIAN DERIVATIVES 31

4.1 Preparation of Gaussian derivatives for sharpening 31
4.2 Polynomial sharpening 31
4.3 Waveforms of sharpened Gaussian derivatives 33
4.4 Design of UWB pulses 40
4.5 FCC-compliant sharpened Gaussian derivatives 44

5. FLAT-SPECTRUM GAUSSIAN PULSES 52

5.1 Polynomially weighted Gaussian pulse 52
5.2 Maximally flat criterion 54
5.3 Optimum polynomials 56
5.4 Pulse shaping 61
5.5 FCC-compliant flat-spectrum Gaussian pulses 65
5.6 Comparison with other FCC-compliant pulses 70

6. TRANSFER FUNCTIONS OF FCC-COMPLIANT PULSE SHAPERS 75

6.1 Time-domain synthesis based on least squares approximation 75

6.2 Zero-pole-gain model of pulse shaper 76
6.3 Spectral efficiency and energy concentration of impulse response 78
6.4 Optimum pulse shapers 79
6.4.1 Pulse shapers forming Gaussian derivatives 79
6.4.2 Pulse shapers forming modified Hermite pulses 84
6.4.3 Pulse shapers forming prolate spheroidal pulses 85
6.4.4 Pulse shapers forming sharpened Gaussian derivatives 90
6.4.5 Pulse shapers forming flat-spectrum Gaussian pulses 92
7. CONCLUSION 101
8. REFERENCES 102
Biography 107
Životopis 109

1. INTRODUCTION

Ultra-wideband (UWB) impulse radio is a short-range communication system providing simple design, low power consumption, multipath immunity, and high data rates [1]. UWB technology has been originally developed for military communications and radar applications. The definition of UWB signal is based on the fractional bandwidth being greater than 25 % of the signal bandwidth, where fractional bandwidth is measured within −3 dB points in the spectrum. The signal is also considered as UWB if its bandwidth is wider than 500 MHz [2].

UWB impulse radio offers rates up to several Gbps at distances of 1 to 10 meters [2], what makes it suitable for personal area network communications such as Bluetooth or Wi-Fi. Also, UWB finds its application in local area networks, indoor data streaming, tracking, wireless monitoring, sensor networks, etc. In recent years, it emerged as the most promising technology in positioning applications, where it offers localization accuracy in range of 0.1 to 0.5 meters. Such an application has been successfully tested with Communications-Based Train Control in New York subway trains in 2020 [3]. In addition, in 2021 Apple designed a chip that uses UWB technology for spatial awareness, allowing iPhone models to precisely locate other devices [4]. In the same year, UWB finds its application in the automotive industry as well, where it is employed to enable secure keyless entry in BMW iX [5].

In 2002 US Federal Communications Commission (FCC) regulated the usage of UWB radio for commercial purposes by providing indoor and outdoor power spectral masks as shown in Figure 1.1 [6]. For both masks, the FCC defines the UWB region from 3.1 GHz to 10.6 GHz, with the maximum power spectral density (PSD) value of −4l.3 dBm/MHz. Later, other regulatory organizations allocated particular bands in Europe [7] and Japan [8].

UWB impulse radio utilizes very short pulses to transfer data. It is well-known that continuous generation of train of short pulses leads to strong spectral lines at multiples of the pulse repetition frequency [2]. Therefore, in the UWB transmitter, randomizing the pulse repetition frequency needs to be performed. Two most prominent techniques are time hopping and direct sequencing. Time hopping is based on adding a delay in the UWB pulse dependent on a time hopping code, where the code repeats after a certain interval [2]. In the direct sequencing technique, a pseudo random code is used to spread each data bit into multiple waveforms [1]. In both techniques, pulse amplitude modulation, on-off keying, and pulse position modulation are commonly used as modulation schemes.

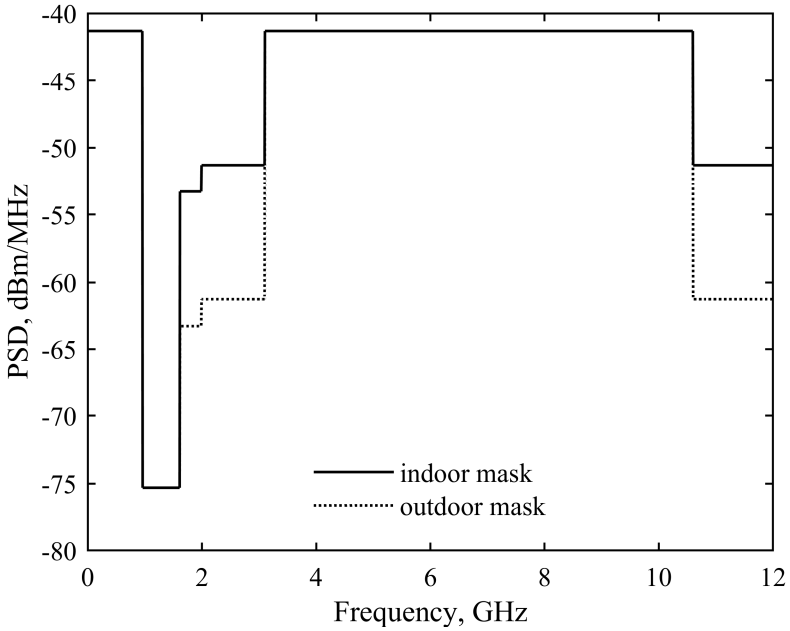

Figure 1.1 FCC spectral masks for indoor and outdoor UWB communications.

The spectrum of the transmitted UWB signal depends on the used pulse shaping method, randomizing technique, and modulation scheme [9]. Due to strict regulations, the key part of UWB transmitter is pulse shaping. Well-established pulse shaping techniques are lowpass filtering followed by up-conversion, bandpass pulse shaping filtering, and combined analog-digital waveform synthesis [10]. The first technique employs a lowpass filter to form a baseband pulse, which is then transposed to the UWB region. In the second technique, UWB pulse is obtained directly by using bandpass filter called pulse shaper whose impulse response approximates the desired waveform. The third technique employs discrete-time pulse synthesis followed by a simple bandpass filter. Despite the fact that lowpass filters are less complex than bandpass filters, using the lowpass filters in pulse shaping is paid by additional circuitry, which implements mixer and local oscillator. Therefore, UWB pulse transmission usually employs the pulse shaper approach. A block diagram of such transmission is shown in Figure 1.2. Several methods for the design of pulse shapers have been developed, considering Padé [11], elliptic [12], and least squares [13] approximation. In addition, the design of pulse shapers incorporating the frequency response of UWB antennas is considered in [14] and [15].

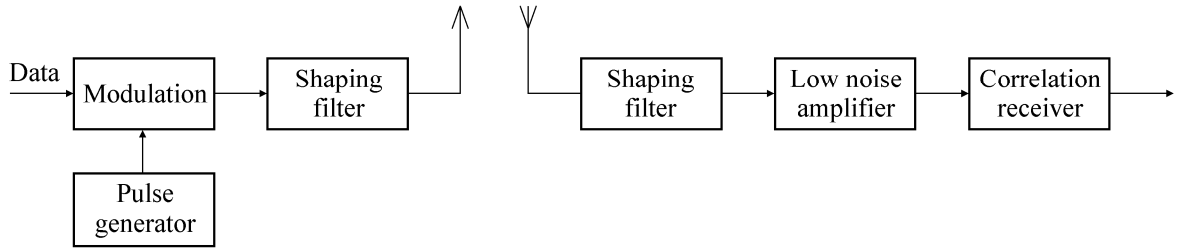

Figure 1.2 Block diagram of UWB pulse transmission [2].

In UWB pulse shaping, common figures of merit are spectral efficiency and energy concentration. The spectral efficiency is defined as the average power of pulse normalized to the total allowed power within the UWB region, that is,

$$\eta = \frac{\int_{f_L}^{f_U} |W(f)|^2 \, df}{\int_{f_L}^{f_U} M(f) \, df} \tag{1.1}$$

where $W(f)$ is Fourier transform of the UWB pulse, $M(f)$ is spectral mask, and f_L and f_U are lower and upper boundaries of the UWB region. The relative energy concentration of the UWB pulse is defined as

$$\lambda = \frac{\int_{-T/2}^{T/2} w^2(t) \, dt}{E_w} \tag{1.2}$$

where $w(t)$ is pulse waveform, E_w is the total energy of $w(t)$, and T is period within which the energy concentration is measured.

In the design of pulse shapers, conventional UWB waveforms are Gaussian derivatives [9], [16], modified Hermite polynomials [17], and prolate spheroidal wave functions [18], [19]. From the spectrum utilization point of view, these waveforms provide acceptable efficiency. High spectral efficiency is achieved by utilizing frequency translated sinc pulse [20]. However, it is paid by poor energy concentration. The spectral efficiency and energy concentration are both optimized in [21]. Furthermore, a good tradeoff between these parameters is offered by

doublet Hermite pulses [22], root-raised-cosine pulses [23], Gaussian windowed Gaussian derivatives [24], modified prolate-spheroidal wave functions [25], a family of functions obtained by solving the Sturm-Liouville differential equation in the frequency domain [26], modulated modified and normalized Hermite pulses [17], Hamming and Hann windowed pulses [27], sinusoidal-like [28], [29] and square-like [30] pulse, as well as the linear combinations of conventional pulses, such as spectrum-shifted Gaussian [31], [32], Gaussian derivatives of different orders [14], [33], [34], Hermite pulses [35], wavelets [36], [37], and sinc [31] pulses.

Besides analog pulses, high spectral efficiency can be reached by employing the finite-impulse-response (FIR) filters [38], [39]. However, generating UWB pulses by using FIR filters requires high-speed analog to digital converters. To eliminate the need for such converters, in [40] the authors presented an FIR-based architecture which implements UWB waveforms entirely in the continuous-time domain. In [41], the optimum design of FIR-based UWB waveforms for an arbitrary spectral mask has been considered.

In this dissertation, two methods for the design of spectrally and energy efficient UWB pulses based on Gaussian derivatives as well as Gaussian pulses have been presented. The former considers the design of pulses based on sharpening technique. The sharpening has been introduced in the design of FIR filters, where it has been used to improve the filter's magnitude response. Here, it is used to develop a method for the design of UWB pulses which optimally fill a desired spectral mask. The method is based on the sharpening of the magnitude spectrum of an arbitrary Gaussian derivative by applying the Kaiser-Hamming polynomials. Such sharpening offers controllable flatness at the top of the magnitude spectrum as well as controllable steepness in spectrum's transition regions. The latter method is inspired by Gaussian derivatives, in which the Gaussian is weighted by Hermite polynomials. Here, the polynomials are constructed by imposing maximum flatness at the peak of pulse’s amplitude spectrum. Furthermore, to obtain UWB pulses, frequency shift and bandwidth scaling are applied. It brings so-called flat-spectrum Gaussian pulses. In addition to these two methods, the approximation of ideal UWB pulses by using pulse shapers' transfer functions is also considered in the dissertation. In particular, the pulse shapers whose impulse responses approximate Gaussian derivatives, modified Hermite pulses, and prolate spheroidal pulses, as well as the sharpened Gaussian derivatives and flat-spectrum Gaussian pulses are presented. To obtain the optimum pulse shapers, least-squares error criterion is used.

The dissertation is organized as follows. The second chapter describes conventional and state-of-the-art UWB pulses. The third chapter describes the optimum design of UWB pulses

by using Gaussian derivatives. In the fourth chapter the sharpened Gaussian derivatives and their utilization in the design of optimum UWB pulses are presented. The fifth chapter presents flat-spectrum Gaussian pulses. Finally, the sixth chapter presents the time-domain synthesis of pulse shapers and provides various zero-pole-gain models of their transfer functions.

2. STATE-OF-THE-ART UWB PULSES

In this chapter, conventional and state-of-the-art UWB pulses obtained by analytical procedures are described in the time and frequency domain, and the examples of their waveforms and power spectral densities designed for FCC masks are provided. In particular, Gaussian derivatives, modified Hermite pulses, prolate spheroidal wave functions, and translated sinc pulse are considered as conventional pulses, whereas linear combinations of translated sinc and Gaussian pulses as well as linear combinations of Gaussian derivatives are considered as state-of-the-art pulses.

2.1 Gaussian derivatives

The most popular UWB pulses are the derivatives of Gaussian pulse. These pulses are characterized by very good time and frequency localization [9], [16].

An *n*th derivative of the Gaussian pulse

$$g_0(t) = \alpha e^{-(t/\tau)^2} \tag{2.1}$$

is given by [9]

$$g_n(t) = \frac{d^n g_0(t)}{dt^n} = (-1)^n \frac{1}{\tau^n} H_n\left(\frac{t}{\tau}\right) g_0(t) \tag{2.2}$$

where α and τ are amplitude and bandwidth scaling factors and $H_n(t)$ is the Hermite polynomial of order n. A closed-form expression for the nth order Hermite polynomial is given by [42]

$$H_n(t) = n! \sum_{m=0}^{\lfloor n/2 \rfloor} \frac{(-1)^m}{m!(n-2m)!} (2t)^{n-2m} \tag{2.3}$$

where $\lfloor u \rfloor$ denotes the greatest integer equal to or smaller than u.

The first six Gaussian derivatives obtained for $\alpha = 1$ and $\tau = 1$ s are shown in Figure 2.1. Clearly, even-order derivatives represent even functions, while odd-order derivatives are odd functions. In addition, according to (2.2), the Gaussian derivative can be considered as a

polynomially weighted Gaussian. Since the Gaussian suppresses the tail of a polynomial regardless of how high the polynomial order is, the Gaussian derivatives are well localized in time.

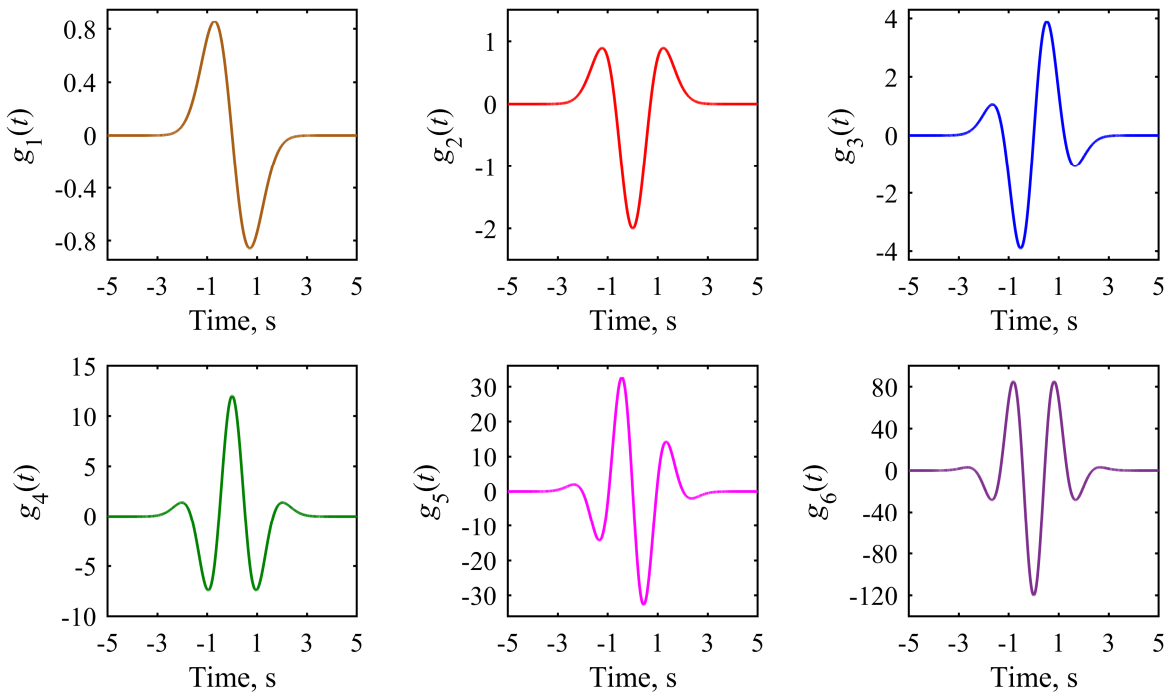

Figure 2.1 First six Gaussian derivatives obtained for $\alpha = 1$ and $\tau = 1$ s.

The spectrum of $g_n(t)$ is obtained as [43]

$$G_n(\omega) = j^n \omega^n G_0(\omega) \tag{2.4}$$

where $G_0(\omega)$ is the Fourier transform of Gaussian pulse given by [1]

$$G_0(\omega) = \alpha\tau\sqrt{\pi}e^{-(\omega\tau/2)^2} \tag{2.5}$$

The magnitude spectrum of $g_n(t)$ given by

$$|G_n(\omega)| = |\omega|^n G_0(\omega) \tag{2.6}$$

The peak of $|G_n(\omega)|$is placed at [44]

$$\omega_n = \frac{\sqrt{2n}}{\tau} \tag{2.7}$$

The shapes of $|G_n(\omega)|$ are illustrated in Figure 2.2 for the derivatives from Figure 2.1. For comparison, the magnitudes $|G_n(\omega)|$ are divided by $|G_n(\omega_n)|$ to ensure unity peaks. It is clear that $|G_n(\omega)|$ is a bandpass function whose lower transition band is steeper than the upper one.

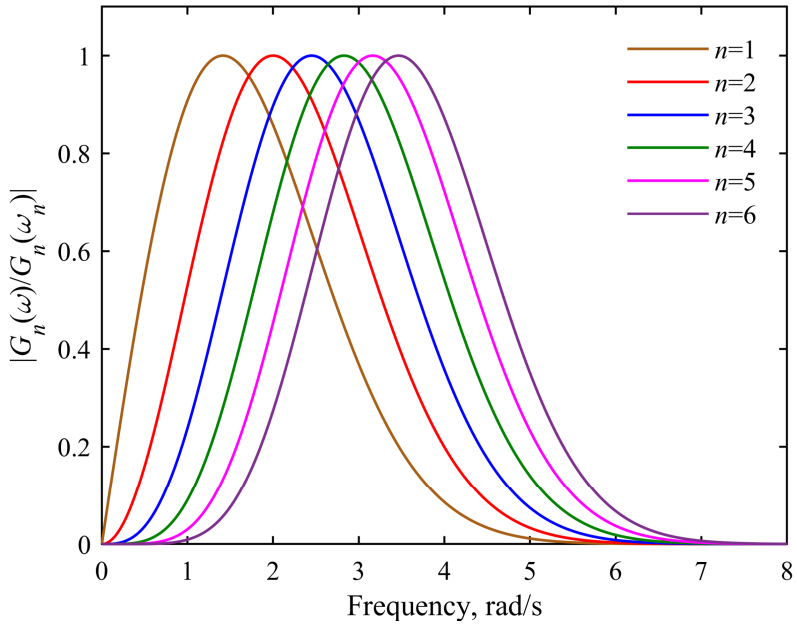

Figure 2.2 Magnitude spectra of first six Gaussian derivatives with peak magnitudes normalized to unity, obtained for $\tau = 1$ s.

The compliance of Gaussian derivatives to a given spectral mask is achieved by using the appropriate value of τ. A detailed description of the design of UWB-compliant Gaussian derivatives will be described in Chapter 3. Here, the PSDs of the fourth Gaussian derivative complaint with FCC indoor mask and the seventh Gaussian derivative compliant with FCC outdoor mask are illustrated in Figure 2.3. They are obtained for $\tau = 0.067$ ns and $\tau = 0.091$ ns, respectively [9].

2.2 Modified Hermite pulses

Authors in [17] proposed utilization of modified Hermite pulses in UWB impulse radio applications. They used a Hermite polynomial as the pulse basis and modified it to impose mutual orthogonality. In such manner pulses can utilize the same frequency region without interfering. Consequently, by utilizing multiple pulses in the same region, spectral efficiency is enhanced. In such a scenario, each pulse can be assigned to different user to form multiaccess communication system.

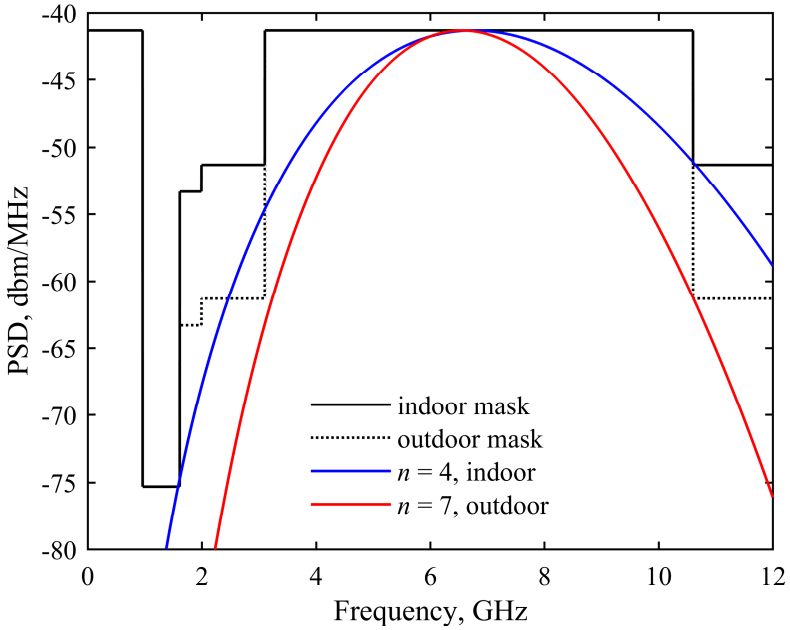

Figure 2.3 Power spectral densities of FCC-compliant Gaussian derivatives, obtained for $n = 4$ and $n = 7$.

An nth order modified Hermite pulse is given by [17]

$$m_n(t) = e^{\left(t/\sqrt{2}\tau\right)^2} g_n(t) \tag{2.8}$$

where weighting function $e^{\left(t/\sqrt{2}\tau\right)^2}$ is introduced to provide orthogonality [19]. The modified Hermite pulses for $\tau = 1$ s are shown in Figure 2.4. Clearly, the pulses' durations are similar for all n. Consequently, their bandwidths have also similar values.

The modified Hermite pulses satisfy the following differential equation [19]

$$m_{n+1}(t) = \frac{d^n}{dt^n}\left(m_n(t)\right) - \frac{t}{\tau^2} m_n(t) \tag{2.9}$$

By using time and frequency derivative property of the Fourier transform, spectra of modified Hermite pulses can be obtained from expression in (2.9) as [17]

$$M_{n+1}(\omega) = j\omega M_n(\omega) - j\frac{1}{\tau^2}\frac{d}{d\omega} M_n(\omega) \tag{2.10}$$

For illustration, the first three $M_n(\omega)$ take the form

$$
\begin{aligned}
M_0(\omega) &= \tau\sqrt{2\pi e}\,e^{-\left(\omega\tau/\sqrt{2}\right)^2} \\
M_1(\omega) &= j2\omega\tau\sqrt{2\pi e}\,e^{-\left(\omega\tau/\sqrt{2}\right)^2} \\
M_2(\omega) &= \frac{1}{\tau}\left(2-4\omega^2\tau^2\right)\sqrt{2\pi e}\,e^{-\left(\omega\tau/\sqrt{2}\right)^2} \\
M_3(\omega) &= j\frac{1}{\tau}4\omega\left(3-2\omega^2\tau^2\right)\sqrt{2\pi e}\,e^{-\left(\omega\tau/\sqrt{2}\right)^2}
\end{aligned}
\tag{2.11}
$$

The first three magnitude spectra of modified Hermite pulses with peak magnitudes normalized to unity are illustrated in Figure 2.5.

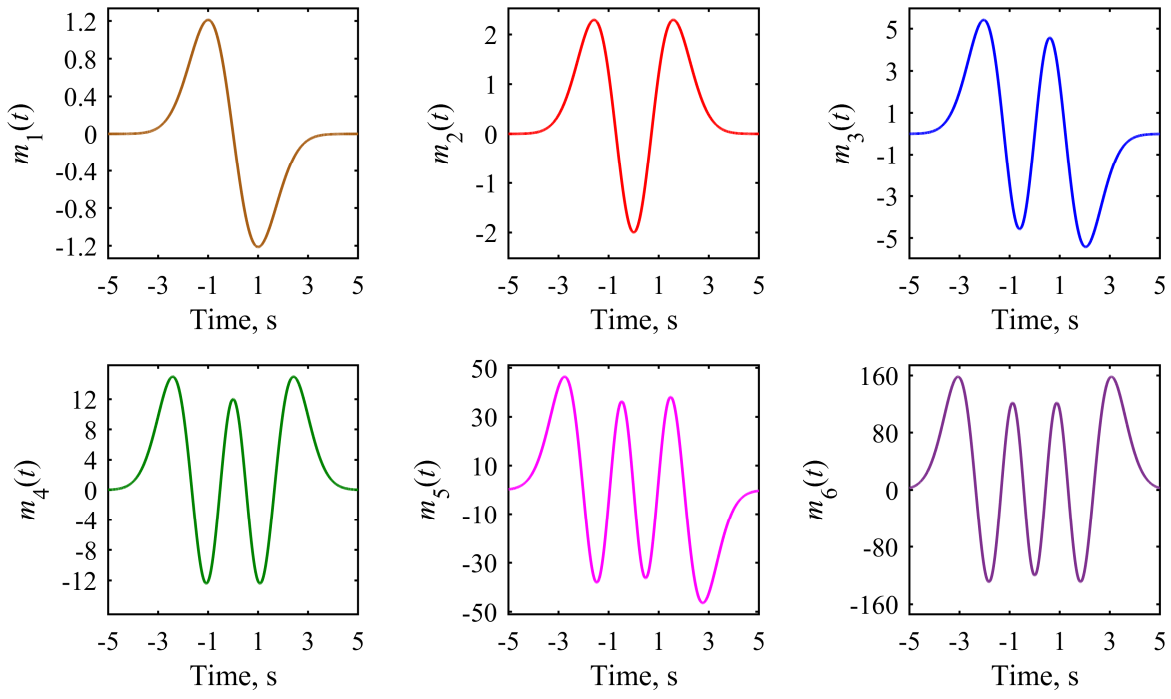

Figure 2.4 First six modified Hermite pulses obtained for $\tau = 1$ s.

Clearly, the pulse's peak frequency increases with an increase in n. In addition, the peak frequency and the bandwidth increase with a decrease in the value of τ. The compliance of modified Hermite pulses with a given spectral mask is satisfied by finding the optimum values of τ, similar as for Gaussian derivatives. The PSDs of the first three modified Hermite pulses which are compliant with FCC indoor mask are shown in Figure 2.6. It is clear that modified Hermite pulses of order $n > 1$ contain large sidelobes. In addition, even-order pulses have DC components, whereas odd-order pulses do not have DC components but contain significant

components at low frequencies [17]. Therefore, to meet the requirements of a spectral mask, additional bandpass filtering is required. Nulls in the pulse spectrum can be utilized to mitigate interferences from known signal sources which appear in the UWB region, such as Wi-Fi signals.

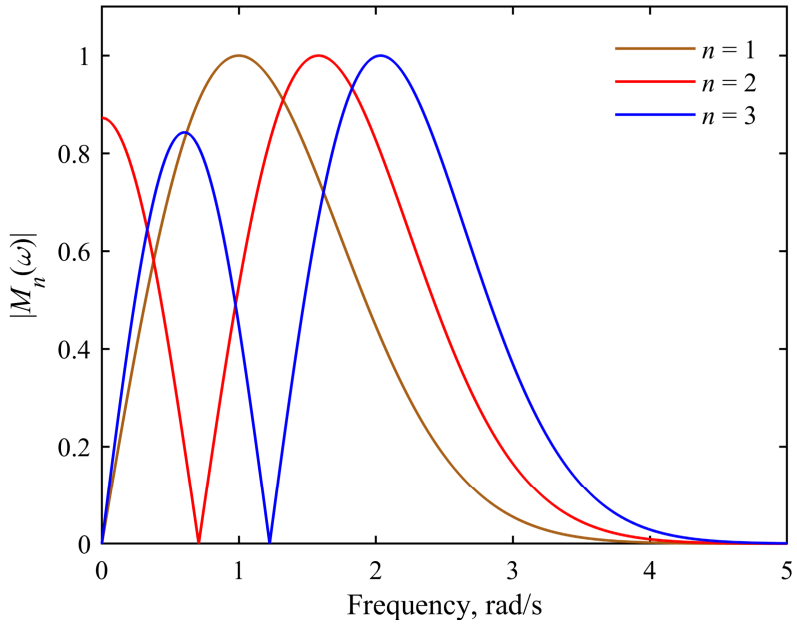

Figure 2.5 Magnitude spectra of first three modified Hermite pulses with peak magnitudes normalized to unity.

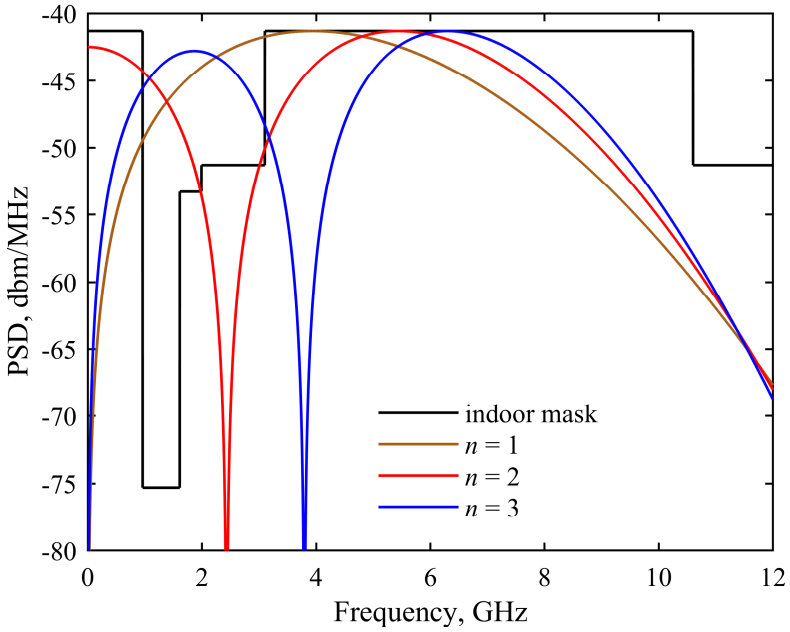

Figure 2.6 Power spectral densities of modified Hermite pulses for $n \leq 3$, for values of τ fitting UWB region of FCC indoor mask.

2.3 Prolate spheroidal wave functions

The most popular algorithm for the design of orthogonal pulses is based on prolate spheroidal wave functions. This algorithm has been proposed in [18]. In the algorithm, $\psi(t)$ denotes a pulse that fits the FCC mask and is time-limited with $-T_P/2 \le t \le T_P/2$. This pulse satisfies the following equation [18]

$$\lambda\psi(t) = \psi(t) * h(t) = \int_{-T_P/2}^{T_P/2} \psi(\tau) h(t-\tau)\,\mathrm{d}\tau \tag{2.12}$$

where T_P is pulse's duration, and λ and $h(t)$ are the gain constant and impulse response of an ideal bandpass filter. The solutions of the equation in (2.12) are known as prolate spheroidal wave functions [45]. For the FCC masks, $h(t)$ is given by

$$h(t) = 2f_U \operatorname{sinc}(2f_U t) - 2f_L \operatorname{sinc}(2f_L t) \tag{2.13}$$

where

$$\operatorname{sinc}(u) = \begin{cases} \dfrac{\sin(\pi u)}{\pi u} & \text{for } u \neq 0 \\ 1 & \text{for } u = 0 \end{cases} \tag{2.14}$$

and f_U = 10.6 GHz and f_L = 3.1 GHz are upper and lower band-edge frequency of the UWB region. To solve the equation in (2.12), a finite number of samples, Q+1, within $-T_P/2 \le t \le T_P/2$ is used. For an even Q, equation (2.12) can be written in the form

$$\lambda \begin{bmatrix} \psi(t_{-Q/2}) \\ \vdots \\ \psi(t_0) \\ \vdots \\ \psi(t_{Q/2}) \end{bmatrix} = \begin{bmatrix} h(t_0) & \cdots & h(t_{-Q}) \\ \vdots & \vdots & \vdots \\ h(t_{Q/2}) & \cdots & h(t_{-Q/2}) \\ \vdots & \vdots & \vdots \\ h(t_Q) & \cdots & h(t_0) \end{bmatrix} \times \begin{bmatrix} \psi(t_{-Q/2}) \\ \vdots \\ \psi(t_0) \\ \vdots \\ \psi(t_{Q/2}) \end{bmatrix} \tag{2.15}$$

or shortly

$$\lambda \boldsymbol{\psi} = \mathbf{H}\boldsymbol{\psi} \tag{2.16}$$

It is clear that **H** is a symmetric Toeplitz matrix. Furthermore, the solutions for $\boldsymbol{\psi}$ are eigenvectors of **H**. As shown in [45], when $T_P \rightarrow \infty$, the solutions and the corresponding pulses $\psi_n(t)$, $n = 1, 2, ..., Q+1$, are orthonormal. Therefore, the following equation holds [45]

$$\int_{-\infty}^{\infty} \psi_n(t)\psi_m(t)dt = \begin{cases} 0 & \text{for} \quad n \neq m \\ 1 & \text{for} \quad n = m \end{cases} \quad n, m = 1, 2, 3 \ \ldots \tag{2.17}$$

Even-order pulses are odd functions, whereas odd-order pulses are even functions.

For a finite value of T, it has been shown in [45] that

$$\int_{-T/2}^{T/2} \psi_n(t)\psi_m(t)dt = \begin{cases} 0 & \text{for} \quad n \neq m \\ \lambda_n & \text{for} \quad n = m \end{cases} \quad n, m = 1, 2, 3 \ \ldots \tag{2.18}$$

From expressions (2.17) and (2.18), it is recognized that λ_n, $n = 1, 2, ..., Q+1$, represent the energy concentration of pulses $\psi_n(t)$ within the interval $-T/2 \leq t \leq T/2$.

Considering maximum power of pulses, the eigenvectors corresponding to the largest two eigenvalues are chosen for UWB pulses. These pulses are called prolate spheroidal pulses. They are denoted here as ψ_1 and ψ_2. Waveforms and PSDs of ψ_1 and ψ_2 compliant with the FCC indoor and outdoor mask are shown in Figure 2.7. Both pulses are well localized in time.

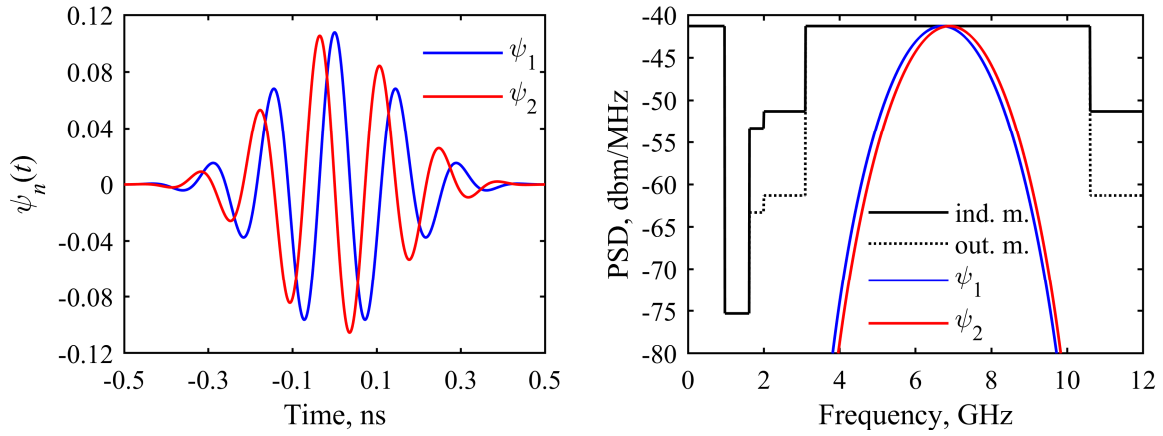

Figure 2.7 Waveforms (left) and power spectral densities (right) of prolate spheroidal FCC-compliant pulses ψ_1 and ψ_2.

2.4 Translated sinc pulse

The UWB region of the FCC spectral masks has a constant PSD. Consequently, a frequency translated sinc pulse is the best candidate for filling this region [20]. However, the translated sinc pulse suffers from high ringing. In [20], this ringing is limited by pulse truncation.

The spectrum of sinc pulse translated to the UWB band $f_L < f < f_U$ is given by [20]

$$P(f) = \begin{cases} C & \text{for} \quad f_L < f < f_U \\ 0 & \text{for} \quad \text{otherwise} \end{cases} \tag{2.19}$$

where C is a magnitude limit in the UWB region. The waveform of the translated sinc pulse is given by [20]

$$p(t) = 8C f_W \operatorname{sinc}(2 f_W t) \cos(2\pi f_c t) \tag{2.20}$$

where f_W is the cut-off frequency of the original sinc pulse and f_c is the center frequency of the UWB region. In [20], the authors used a rectangular window with the duration of 16 ns to truncate the pulse in (2.20). The waveform and PSD of the obtained pulse meeting the FCC masks are shown in Figure 2.8. As a consequence of the truncation, the PSD contains overshoots and sidelobes which can violate spectral mask. However, their influence can be controlled by changing the width of the truncation window.

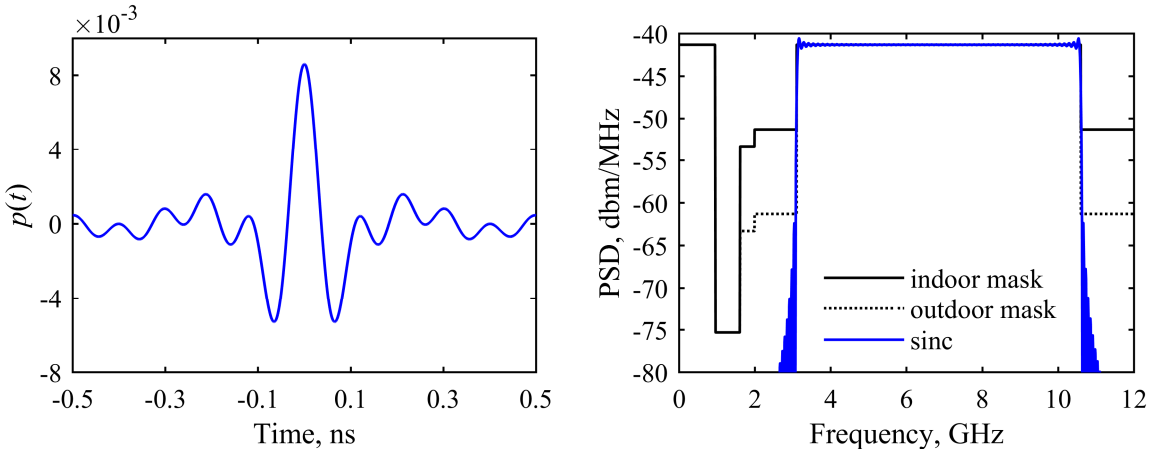

Figure 2.8 Waveform (left) and power spectral density (right) of translated sinc pulse truncated to 16 ns, which is compliant with FCC masks.

2.5 Linear combination of translated sinc pulses

In terms of spectral properties, frequency translated sinc pulse fits a rectangular mask the best. However, it suffers from large ringing. To solve this problem, a linear combination of sinc pulses has been utilized in [31] yielding a good time localization while still maintaining high spectral efficiency.

A linear combination of two translated sinc pulses is given by [31]

$$c_{1,2}(t) = a_1 p(t) + a_2 p(t-\delta) \tag{2.21}$$

where $p(t)$ is given in (2.20), a_1 and a_2 are weighting factors, and δ is a delay [31]. The spectrum of the pulse in (2.21) is given by [31]

$$C_{1,2}(f) = a_1 P(f) + a_2 P(f) e^{-2\pi f \delta j} \tag{2.22}$$

A linear combination of three translated sinc pulses takes the form [31]

$$c_{1,2,3}(t) = a_1 p_1(t) + a_2 p_2(t-\delta_1) + a_3 p_3(t-\delta_2) \tag{2.23}$$

where a_1, a_2 and a_3 are weighting factors, and δ_1 and δ_2 are delays. Note that unlike the pulse in (2.21), the linear combination in (2.23) employs different sinc pulses, $p_1(t)$, $p_2(t)$, $p_3(t)$. They are obtained by using the cut-off frequencies f_{W1}, f_{W2}, f_{W3}, and translation frequencies f_{c1}, f_{c2}, f_{c3}. The amplitude spectrum of the pulse in (2.23) is given by [31]

$$C_{1,2,3}(t) = a_1 P_1(f) + a_2 P_2(f) e^{-2\pi f \delta_1 j} + a_3 P_3(f) e^{-2\pi f \delta_2 j} \tag{2.24}$$

where $P_1(f)$, $P_2(f)$ and $P_3(f)$ are the spectra of $p_1(t)$, $p_2(t)$ and $p_3(t)$.

To ensure that $c_{1,2}(t)$ and $c_{1,2,3}(t)$ fit the UWB spectral mask, appropriate values of pulses' cut-off frequencies and the translation frequencies, as well as the weighting coefficients and delays should be found. In [31], the authors provided pulses which satisfy the criterion for maximum efficiency in fitting several UWB spectral masks. The pulses are found by an interior point optimization algorithm. As an example, the optimum linear combination of three translated sinc pulses which meets the FCC indoor mask is obtained for C = 8.61e–3, $a_1 = -1$, f_{W1} = 3.245 GHz, f_{c1} = 6.47 GHz, $a_2 = 3$, f_{W2} = 3.325 GHz, f_{c2} = 7.19 GHz, δ_1 = 0.017 ns, a_3 = 4.35, f_{W3} = 3.705 GHz, f_{c3} = 6.73 GHz, and δ_2 = 0.04 ns. The corresponding waveform and the PSD are shown in Figure 2.9.

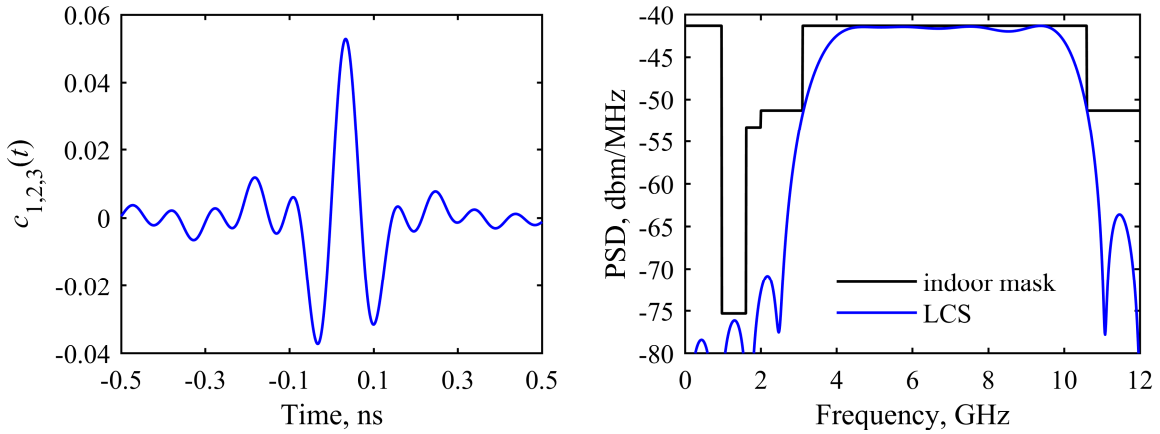

Figure 2.9 Waveform (left) and power spectral density (right) of linear combination of three translated sinc pulses meeting FCC indoor mask.

2.6 Linear combination of translated Gaussian pulses

Unlike sinc pulses, Gaussian pulses have low spectral efficiency but rather high energy concentration. These properties are preserved in their frequency translations as well. Therefore, by combining translated Gaussian pulses, an increase in spectral efficiency is expected together with high energy concentration.

A general expression for the linear combination of K Gaussian pulses is given by

$$g_c(t) = \sum_{k=0}^{K} a_k g_0(t) \cos(2\pi f_k t) \tag{2.25}$$

where a_k and f_k, $k = 0, 1, ..., K$, are the weighting factors and central frequencies of translated Gaussian pulses. The corresponding amplitude spectrum is obtained as

$$G_c(f) = \sum_{k=0}^{K} a_k G_0(f - f_k) \tag{2.26}$$

where $G_0(f)$ is given by (2.5) and $f = \omega/2\pi$.

The linear combinations of two and three translated Gaussian pulses fitted to arbitrary spectral masks have been proposed in [31]. In [32], this technique has been utilized for the FCC indoor mask. In the paper referred to, the linear combination of eight Gaussian pulses which meets this mask up to 12 GHz is presented. The mask is first divided into five regions, with the widest being the UWB region. Then, the weighting factors and translation frequencies are

optimized to ensure maximum flatness of the spectrum in the UWB region. The weighting factors are found by an iterative trial and error procedure for each of the five bands. The translation frequencies are found by fitting the bandwidths of the Gaussian pulses. After combining the bands, some modification is needed to ensure that the combination fits the mask at the UWB edges. The pulse is obtained in a form [32]

$$g_c(t) = Ce^{-\frac{t^2}{4\beta}}\left[a_1\cos(2\pi f_1 t) + a_2\cos(2\pi f_2 t) + a_3\sum_{k=3}^{7}\cos(2\pi f_k t) + a_4\cos(2\pi f_8 t)\right] \quad (2.27)$$

where $C = 8.61\text{e}{-3}$, $\beta = 0.0317$, $a_1 = 0.0823$, $f_1 = 0.48$ GHz, $a_2 = 1.9790$, $f_2 = 3.85$ GHz, $a_3 = 1.9822$, $f_3 = 4.85$ GHz, $f_4 = 5.85$ GHz, $f_5 = 6.85$ GHz, $f_6 = 7.85$ GHz, $f_7 = 8.85$ GHz, $a_4 = 1.9790$, and $f_8 = 9.85$ GHz. The waveform and PSD of the pulse in (2.27) are shown in Figure 2.10.

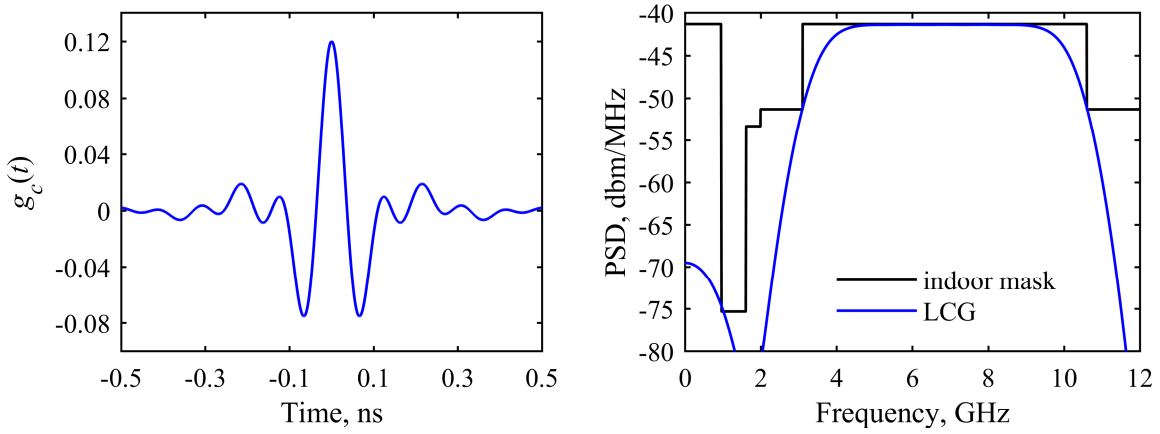

Figure 2.10 Waveform (left) and power spectral density (right) of linear combination of eight translated Gaussian pulses, which is compliant with FCC indoor mask.

2.7 Linear combination of Gaussian derivatives

Linear combinations of sinc and linear combinations of Gaussian pulses require frequency translations to fill the spectral masks. However, Gaussian derivatives are bandpass pulses. Therefore, the design of UWB pulses based on linear combinations of Gaussian derivatives contains smaller number of variables then do the design based on linear combination of sinc or Gaussian pulses. Consequently, the overall design is simpler. The number of waveforms used in the combination is preferably small to keep the pulse generating system

simple [34]. In [33], a linear combination of two second-order Gaussian derivatives has been proposed.

Linear combination of Gaussian derivatives of different orders has been considered in [34]. In the paper referred to, the authors proposed a combination of one sixth- and two seventh-order Gaussian derivatives. It is given by [34]

$$g_{6,7,7}(t) = a_1 g_6(t,\tau_1) + a_2 g_7(t,\tau_2) + a_3 g_7(t,\tau_3) \tag{2.28}$$

where $a_1 = 0.4368$, $a_2 = -0.6775$, $a_3 = 0.3498$, $\tau_1 = 0.1069$ ns, $\tau_2 = 0.1069$ ns, and $\tau_3 = 0.0537$ ns. The corresponding amplitude spectrum is given by

$$G_{6,7,7}(\omega) = a_1 G_6(\omega,\tau_1) + a_2 G_7(\omega,\tau_2) + a_3 G_7(\omega,\tau_3) \tag{2.29}$$

where $G_6(\omega, \tau_1)$, $G_7(\omega, \tau_2)$ and $G_7(\omega, \tau_3)$ are obtained by using (2.4) and (2.5). The waveform and PSD of the triplet in (2.28) that meets the FCC indoor mask are shown in Figure 2.11.

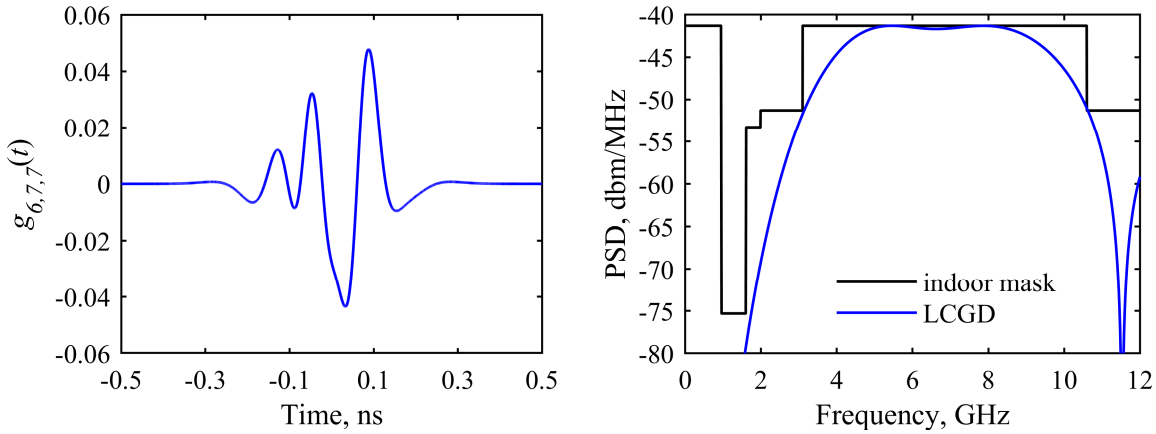

Figure 2.11 Waveform (left) and power spectral density (right) of linear combination of one sixth- and two seventh-order Gaussian derivatives, which is compliant with FCC indoor mask.

2.8 Overview

The Gaussian derivatives, modified Hermite pulses, and prolate spheroidal wave functions represent bandpass pulses well localized in time. However, they do not exploit the UWB region efficiently. On the other hand, the truncated and translated sinc pulse offers very high spectral efficiency which is paid by poor time localization A good trade-off between

spectral efficiency and energy concentration is achieved by linear combinations of translated Gaussian pulses, different Gaussian derivatives, and translated sinc pulses. Using (1.1) and (1.2), the spectral efficiency for $f_L = 3.1$ GHz and $f_U = 10.6$ GHz as well as the energy concentration for $T = 0.5$ ns are calculated and listed in Table 2.1 for the aforementioned FCC-compliant indoor pulses.

Table 2.1 Spectral efficiency and energy concentration of various FCC-compliant indoor pulses.

	Pulse	η, %	λ, %
Conventional	Fourth Gaussian derivative [9]	54.3	>99.99
	Modified Hermite pulse [17]	55.5	>99.99
	Prolate spheroidal pulse [18]	25.5	>99.99
Sinc	Translated and truncated sinc pulse [20]	98.9	95.82
	Linear combination of three translated sinc pulses [31]	82.6	98.53
Gaussian	Linear combination of Gaussian derivatives [34]	72.0	99.97
	Linear combination of three translated Gaussians [31]	77.5	99.78
	Linear combination of eight translated Gaussians [32]	82.8	99.56

3. DESIGN OF UWB PULSES BASED ON GAUSSIAN DERIVATIVES

In this chapter, the design of UWB pulses whose waveforms correspond to Gaussian derivatives is described in detail. In the design, the Gaussian derivatives that fit a given spectral mask are considered. As an example, the optimum FCC-compliant Gaussian derivatives are provided.

3.1 Design method

For an *n*th-order Gaussian derivative containing bandwidth scaling factor τ, the objective is to find the value of τ which optimally fill a desired spectral mask. The filling is formulated as the minimization of the distance between the spectral mask and the magnitude spectrum of the Gaussian derivative calculated at the edge frequencies of the UWB region. That distance is defined as

$$\varepsilon(\tau) = A_L - \left|G_n(f_L)\right| + A_U - \left|G_n(f_U)\right| \tag{3.1}$$

where f_L and f_U are the lower and the upper band-edge frequency whereas A_L and A_U are magnitude limits at f_L and f_U. For a given mask, the optimum value of τ is obtained by solving the problem

$$\begin{aligned} &\underset{\tau}{\text{minimize}} && \varepsilon(\tau) \\ &\text{subject to} && \left|G_n(f)\right|^2 \le M(f) \end{aligned} \tag{3.2}$$

where $M(f)$ denotes the PSD mask. To ensure the maximum PSD value of Gaussian derivative corresponds to maximum PSD value of the spectral mask, the magnitude spectrum $|G_n(f)|$ is normalized to unity magnitude at its peak, and $M(f)$ is normalized to unity density in the UWB region. Using (2.5), (2.6), and (2.7), the amplitude scaling factor of Gaussian derivative which ensures unity peak magnitude is obtained as

$$\alpha = \frac{\tau^{n-1}}{\sqrt{\pi}}\left(\frac{e}{2n}\right)^{\frac{n}{2}} \tag{3.3}$$

Since $|G_n(f)|$ has a bell shape, the problem in (3.2) is simplified as

$$\begin{aligned} \underset{\tau}{\text{maximize}} \quad & \left|G_n(f_L)\right| + \left|G_n(f_U)\right| \\ \text{subject to} \quad & \left|G_n(f_L)\right| \le A_L \\ & \left|G_n(f_U)\right| \le A_U \\ & \left|G_n(f_k)\right| \le A_k \ , k = 1,2,...,K \end{aligned} \tag{3.4}$$

where f_k are frequencies outside the UWB region at which the mask changes, $A_L = \sqrt{M(f_L)}$, $A_U = \sqrt{M(f_U)}$, and $A_k = \sqrt{M(f_k)}$. A typical relation between magnitude limits corresponding to discontinuities in normalized FCC indoor mask and the magnitude spectrum of a Gaussian derivative is illustrated in Figure 3.1.

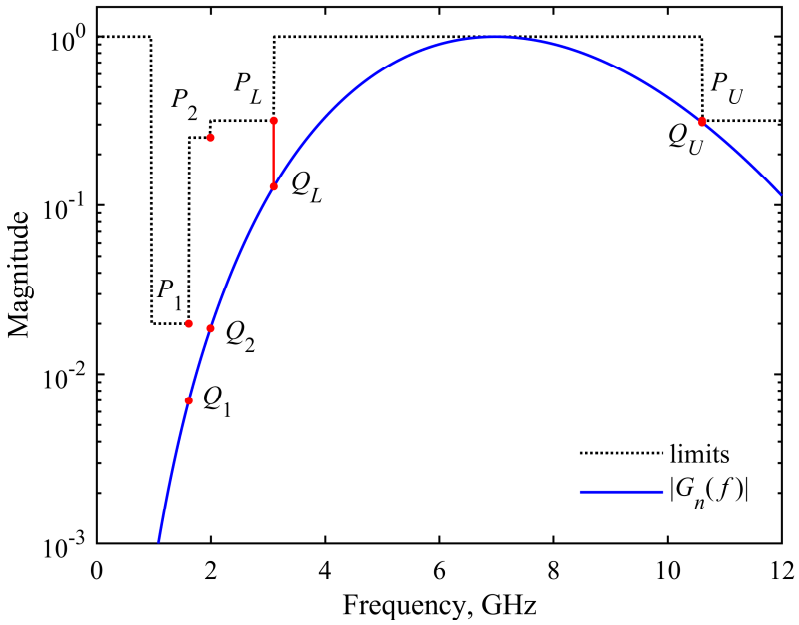

Figure 3.1 Magnitude limits corresponding to normalized FCC indoor mask and magnitude spectrum of Gaussian derivative. Red dots show used magnitude limits, $P_1 = (f_1, A_1)$, $P_2 = (f_2, A_2)$, $P_L = (f_L, A_L)$, $P_U = (f_U, A_U)$, and corresponding magnitudes, $Q_1 = (f_1, |G_n(f_1)|)$, $Q_2 = (f_2, |G_n(f_2)|)$, $Q_L = (f_L, |G_n(f_L)|)$, and $Q_U = (f_U, |G_n(f_U)|)$.

In the design process it is expected that the peak frequency of Gaussian derivative, f_n, is placed within the band $f_L < f_n < f_U$. According to (2.7), for a given f_n, the corresponding τ equals

$$\tau = \frac{\sqrt{2n}}{2\pi f_n} \tag{3.5}$$

From (3.5) it follows that the design deals with τ which is limited to the interval

$$\sqrt{\frac{n}{2}}\frac{1}{\pi f_U} < \tau < \sqrt{\frac{n}{2}}\frac{1}{\pi f_L} \tag{3.6}$$

Since τ is bounded by a finite interval, the optimum value of τ can be easily found by using the direct search. In this search, the objective function $\varepsilon(\tau)$ is evaluated on the uniformly spaced grid of τ with steps of $\Delta\tau$ defined within the interval in (3.6).

Assuming that the spectral mask $M(f)$ limits the magnitude spectrum $|G_n(f)|$ to the value of C in the UWB region, the Gaussian derivative is given by

$$w_n(t) = Cg_n(t) \tag{3.7}$$

By substituting (3.3) into (2.2), and (2.2) into (3.7), $w_n(t)$ takes the form

$$w_n(t) = C\frac{(-1)^n}{\tau\sqrt{\pi}}\left(\frac{e}{2n}\right)^{n/2} H_n\left(\frac{t}{\tau}\right)e^{-(t/\tau)^2} \tag{3.8}$$

The amplitude spectrum of $w_n(t)$ is given by

$$W_n(\omega) = \begin{cases} C(-1)^{n/2}\left|G_n(\omega)\right| & \text{for even } n \\ C(-1)^{(n-1)/2}\,\mathrm{sgn}(\omega)\left|G_n(\omega)\right| & \text{for odd } n \end{cases} \tag{3.9}$$

The waveforms $w_n(t)$ exhibit even symmetry for even n and odd symmetry for odd n, as it is illustrated in Figure 2.1. In addition, in both cases their polarity alternates with n. Therefore, the amplitude spectrum of $w_n(t)$ satisfies $W_n(\omega_n) = \beta C$, where $\beta = (-1)^{n/2}$ for an even n, and $\beta = (-1)^{(n-1)/2}$ for an odd n.

An example of MATLAB [47] code implementing the entire design is given by Algorithm 3.1 for convenience. The function is called *uwbdesign_gaussder*. Its input parameters are the order of Gaussian derivative, *n*, vector of mask frequencies expressed in GHz, *F*, vector of mask PSDs having the same size as *F* expressed in dBm/MHz, *M*, PSD in

the UWB region, M_0, and indices of the elements in F corresponding to the lower and upper UWB-edge frequencies, L and U. The function *uwbdesign_gaussder* calls the function *gaussdermag* which calculates $|G_n(\omega)|$. In the code, $\Delta\tau$ = 1e–4 ns is used.

Algorithm 3.1 Design of UWB Gaussian derivative of order n.

```
function tau=uwbdesign_gaussder(n,F,M,M0,L,U)

dtau=1e-4; % the step of tau in ns

k=sqrt(n/2)/pi; tauL=k/F(U); tauU=k/F(L);
A=10.^((M-M0)/20); w=2*pi*F; K=length(F);

% search for optimum tau
yold=0; tau=[];
for taui=(ceil(tauL/dtau):ceil(tauU/dtau))*dtau
 Gn=gaussdermag(n,taui,w);
 if sum(Gn<=A)==K % satisfies mask
  ynew=Gn(L)+Gn(U);
  if ynew > yold
   yold=ynew; tau=taui;
end, end, end

function Gn=gaussdermag(n,tau,w)

alpha=tau^(n-1)/sqrt(pi)*(exp(1)/2/n)^(n/2);
G0=alpha*tau*sqrt(pi)*exp(-(w*tau/2).^2);
Gn=abs(w).^n.*G0;
```

3.2 FCC-compliant Gaussian derivatives

To illustrate the design procedure, several Gaussian derivatives that fill the FCC indoor and outdoor mask are designed. In both masks, the UWB region is placed between f_L = 3.1 GHz and f_U = 10.6 GHz. This region is bounded by the points that are 10 dB and 20 dB below the highest PSD. It brings $A_L = A_U = 0.316$ for the indoor and $A_L = A_U = 0.1$ for the outdoor mask. Outside the UWB region, the frequencies f_1 = 1.61 GHz and f_2 = 1.99 GHz are taken into account. It brings $A_1 = 0.020$ for both masks, and $A_2 = 0.251$ and $A_2 = 0.079$ for the indoor and the outdoor mask, respectively. For both masks C = 8.61e–3 is used.

The Gaussian derivatives which optimally fill the FCC indoor and outdoor mask are obtained for $n \geq 5$ and $n \geq 7$, respectively. However, the fourth Gaussian derivative slightly crosses the indoor mask in the GPS band. Since it is considered acceptable in practice [9], this derivative is taken into account by adjusting the GPS magnitude limit to $A_1 = 0.022$. For both FCC masks, the optimum values of τ and the corresponding peak frequencies f_n are given in

Table 3.1. Similar values of τ are obtained in [16], where the 3dB-bandwidths of Gaussian derivatives are maximized under the FCC constraints.

The power spectral densities of FCC-compliant Gaussian derivatives are shown in Figures 3.2 and 3.3, separately for the indoor and the outdoor mask. Clearly, the indoor Gaussian derivative with $n = 4$ and the outdoor Gaussian derivative with $n = 7$ fill the UWB region the best. Figure 3.4 shows their waveforms. Clearly, both pulses are well localized in time.

Table 3.1 Optimum peak frequencies and bandwidth scaling factors of FCC-compliant Gaussian derivatives.

	indoor mask		outdoor mask	
n	f_n, GHz	τ, ns	f_n, GHz	τ, ns
4	6.719	0.0670	-	-
5	7.010	0.0718	-	-
6	7.235	0.0762	-	-
7	7.416	0.0803	6.544	0.0910
8	7.570	0.0841	6.723	0.0947
9	7.699	0.0877	6.876	0.0982
10	7.813	0.0911	7.006	0.1016

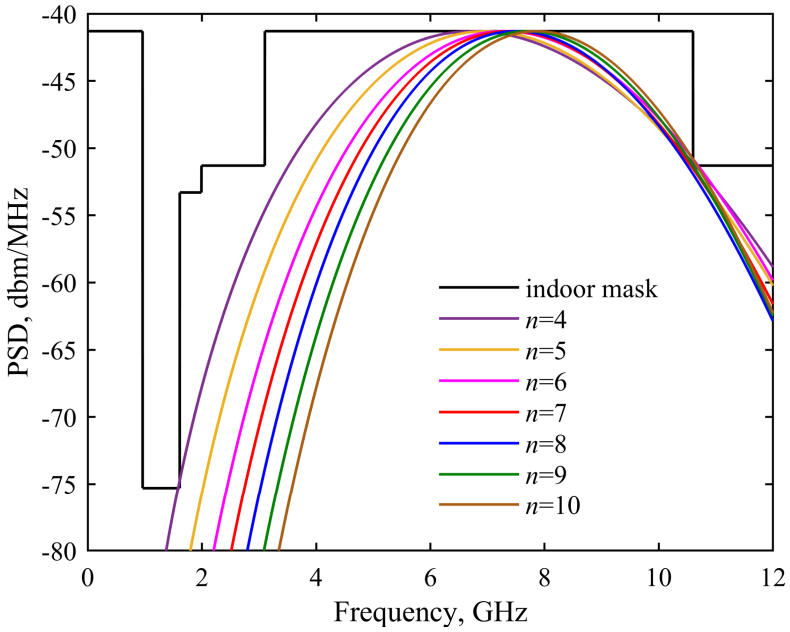

Figure 3.2 Power spectral densities of optimum nth-order Gaussian derivatives obtained for FCC indoor mask.

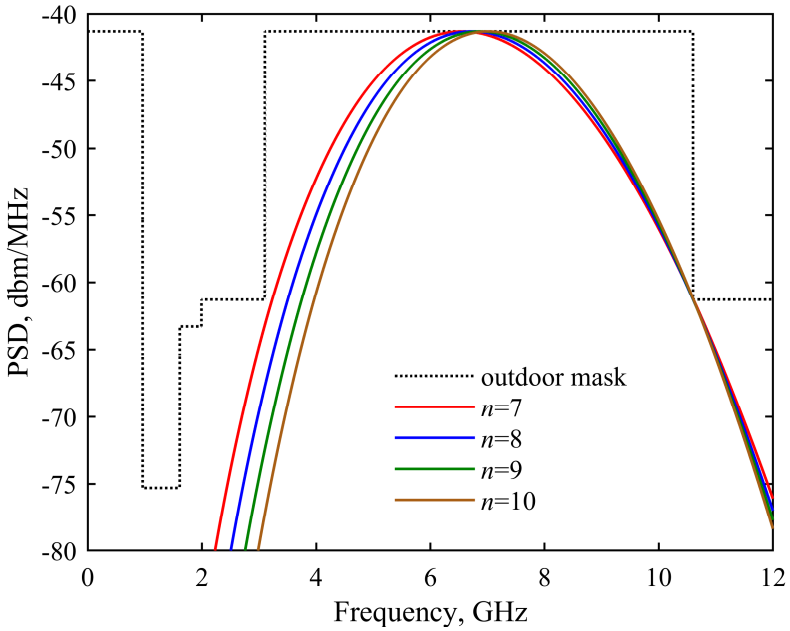

Figure 3.3 Power spectral densities of optimum *n*th-order Gaussian derivatives obtained for FCC outdoor mask.

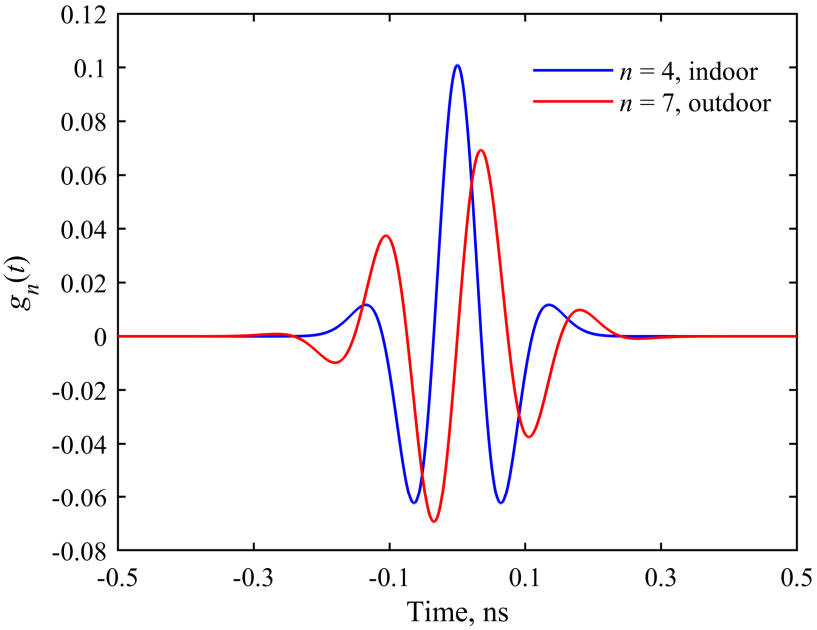

Figure 3.4 Waveforms of optimum FCC-compliant Gaussian derivatives with $n = 4$ and $n = 7$.

An example of MATLAB code for calculating the values of waveform $w_n(t)$ and of its amplitude spectrum $W_n(\omega)$ is given by Algorithm 3.2. The function is called *uwbgaussder*. Its input parameters are the order of Gaussian derivative, n, amplitude and bandwidth scaling factors, C and τ, the vector of time points in s, t, and the vector of frequency points in rad/s, w. The function *uwbgaussder* calls the function *gaussder* which calculates $g_n(t)$, the function *hermitepoly* which calculates the values of nth-order Hermite polynomial H_n, and the function *gaussdermag* which is given by Algorithm 3.1.

Algorithm 3.2 Calculating values of waveform and amplitude spectrum of UWB Gaussian derivative of order n.

```
function [wn,Wn]=uwbgaussder(n,C,tau,t,w)

% waveform gn(t)
alpha=tau^(n-1)/sqrt(pi)*(exp(1)/2/n)^(n/2);
gn=gaussder(n,alpha,tau,t);

% magnitude spectrum |Gn(w)|
Gn=gaussdermag(n,tau,w);

% waveform wn(t)
wn=C*gn;

% amplitude spectrum Wn(w)
if mod(n,2)==0, Wn=C*(-1)^(n/2)*Gn;
else Wn=C*(-1)^((n-1)/2)*sign(w).*Gn;
end

function gn=gaussder(n,alpha,tau,t)

g0=alpha*exp(-(t/tau).^2);
if n==0, gn=g0;
else gn=(-1)^n/tau^n*hermitepoly(n,t/tau).*g0;
end

function Hn=hermitepoly(n,x)

Hn=zeros(size(x));
for m=0:floor(n/2)
 Hn=Hn+(-1)^m/prod(1:m)/prod(1:n-2*m)*(2*x).^(n-2*m);
end
Hn=prod(1:n)*Hn;
```

An example of MATLAB code implementing the FCC mask $M(f)$ is given by Algorithm 3.3. The function is called *fccmask*. Its input parameters are the vector of frequency points in GHz, f, and a string containing the mask type, *mask*, which can be set to *'indoor'* or *'outdoor'*.

Algorithm 3.3 Implementation of FCC mask.

```
function M=fccmask(f,mask)

F=abs(f); M=ones(size(f));
if strcmp(mask,'indoor')
 M=-51.3*M; M(F>=1.61 & F<1.99)=-53.3;
elseif strcmp(mask,'outdoor')
 M=-61.3*M; M(F>=1.61 & F<1.99)=-63.3;
end
M(F>=0 & F<0.96 | F>=3.1 & F<=10.6)=-41.3;
M(F>=0.96 & F<1.61)=-75.3;
```

For example, the design of the FCC-compliant indoor pulse with $n = 4$ is given by the following call

```
n=4; F=[1.61, 1.99, 3.1, 10.6]; M=[-74.5, -53.3, -51.3, -51.3];
M0=-41.3; L=3; U=4;
tau=uwbdesign_gaussder(n,F,M,M0,L,U);
C=10^(M0/20);
t=linspace(-0.5,0.5,1001); f=linspace(0,12,1001); w=2*pi*f;
[wn,Wn]=uwbgaussder(n,C,tau,t,w);
figure, plot(t,wn/C);
figure, plot(f,20*log10(abs(Wn)),'g',f,fccmask(f,'indoor'),'r');
axis([f(1) f(end) -80 -40]);
```

The design of the FCC-compliant outdoor pulse with $n = 7$ is given by the call

```
n=7; F=[1.61, 1.99, 3.1, 10.6]; M=[-75.3, -63.3, -61.3, -61.3];
M0=-41.3; L=3; U=4;
tau=uwbdesign_gaussder(n,F,M,M0,L,U);
C=10^(M0/20);
t=linspace(-0.5,0.5,1001); f=linspace(0,12,1001); w=2*pi*f;
[wn,Wn]=uwbgaussder(n,C,tau,t,w);
figure, plot(t,wn/C);
figure, plot(f,20*log10(abs(Wn)),'g',f,fccmask(f,'outdoor'),'r');
axis([f(1) f(end) -80 -40]);
```

3.3 Spectral efficiency and energy concentration of Gaussian derivatives

According to (1.1), the spectral efficiency of Gaussian derivative $w_n(t)$ in the UWB region is given by

$$\eta = \frac{\int_{f_L}^{f_U} |W_n(f)|^2 \, df}{\int_{f_L}^{f_U} M(f) \, df} \tag{3.10}$$

Since $M(f) = C^2$ for $f_L < f < f_U$, the denominator in (3.10) equals $C^2(f_U - f_L)$. The value of the integral in the numerator can be easily found by applying numerical integration.

The spectral efficiencies of the optimum FCC-compliant Gaussian derivatives from Table 3.1 are given in Table 3.2. As expected, the maximum spectral efficiency for the indoor and outdoor mask is achieved for $n = 4$ and $n = 7$, respectively. For other Gaussian derivatives, the spectral efficiency decreases by an increase in n.

According to (1.2), the relative energy concentration of $w_n(t)$ is given by

$$\lambda = \frac{\int_{-\infty}^{-T/2} w_n^2(t) \, dt}{\int_{-\infty}^{\infty} w_n^2(t) \, dt} \tag{3.11}$$

Since $w_n(t)=Cg_n(t)$, the energy concentration is reduced to

$$\lambda = \frac{1}{E_n} \int_{-T/2}^{T/2} g_n^2(t) \, dt \tag{3.12}$$

where E_n is the total energy of $g_n(t)$.

To compute the energy concentration, the total energy of nth Gaussian derivative should be determined. Here, it is derived in an analytic form. On the other hand, the value of the integral in the numerator should be calculated by applying numerical integration.

The total energy of the Gaussian derivative is given by

$$\begin{aligned} E_n &= \int_{-\infty}^{+\infty} g_n^2(t) \, dt \\ &= \frac{2\alpha^2}{\tau^{2n}} \int_0^{+\infty} H_n^2\left(\frac{t}{\tau}\right) e^{-2(t/\tau)^2} \, dt \end{aligned} \tag{3.13}$$

To solve the integral in (3.13), Hermite polynomials $H_n(t)$ are written in a power-series form as

$$H_n(t)=\begin{cases}\sum_{r=0}^{n/2} b_r t^{2r} & \text{for even } n\\ \sum_{r=0}^{(n-1)/2} b_r t^{2r+1} & \text{for odd } n\end{cases} \tag{3.14}$$

where

$$b_r=\begin{cases} n!\dfrac{(-1)^{\frac{n}{2}-r}\,2^{2r}}{(2r)!\left(\frac{n}{2}-r\right)!} & \text{for even } n\\ n!\dfrac{(-1)^{\frac{n-1}{2}-r}\,2^{(2r+1)}}{(2r+1)!\left(\frac{n-1}{2}-r\right)!} & \text{for odd } n\end{cases} \tag{3.15}$$

By substituting (3.14) and (3.15) into (3.13), the total energy of $g_n(t)$ for even n takes the form

$$E_n=\frac{2\alpha^2}{\tau^{2n}}\sum_{r=0}^{n/2}\sum_{k=0}^{n/2} b_r b_k \int_0^{+\infty}\left(\frac{t}{\tau}\right)^{2(r+k)} e^{-2(t/\tau)^2}\,dt \tag{3.16}$$

By simplifying the integral in (3.16), E_n is reduced to

$$E_n=\frac{2\alpha^2}{\sqrt{2}\tau^{2n-1}}\sum_{r=0}^{n/2}\sum_{k=0}^{n/2}\frac{b_r b_k}{2^{r+k}}\int_0^{+\infty} x^{2(r+k)}e^{-x^2}\,dx \tag{3.17}$$

For solving the integral in (3.17), the following equality is used [42]

$$\int_0^{+\infty} x^m e^{-\beta x^l}\,dx=\frac{\Gamma(\gamma)}{l\beta^{\gamma}} \quad \text{for} \quad \gamma=\frac{m+1}{l},\quad \beta>0,\quad l>0,\quad m\ge 0 \tag{3.18}$$

where Γ is the gamma function. By setting $\beta = 1$ and $l = 2$ in (3.18), the total energy of $g_n(t)$ for even n is given by

$$E_n=\frac{\sqrt{2}\alpha^2}{2\tau^{2n-1}}\sum_{r=0}^{n/2}\sum_{k=0}^{n/2}\frac{b_r b_k}{2^{r+k}}\Gamma\left[\frac{2(r+k)+1}{2}\right] \tag{3.19}$$

A similar procedure is used to obtain the total energy of $g_n(t)$ for odd n. In this case, it is given by

$$E_n = \frac{2\alpha^2}{\sqrt{2}\tau^{2n}} \sum_{r=0}^{(n-1)/2} \sum_{k=0}^{(n-1)/2} b_r b_k \int_0^{+\infty} \left(\frac{t}{\tau}\right)^{2(r+k+1)} e^{-2(t/\tau)^2} dt \tag{3.20}$$

By solving the integral in (3.20), E_n takes the form

$$E_n = \frac{\sqrt{2}\alpha^2}{2\tau^{2n-1}} \sum_{r=0}^{(n-1)/2} \sum_{k=0}^{(n-1)/2} \frac{b_r b_k}{2^{r+k+1}} \Gamma\left(\frac{2(r+k+1)+1}{2}\right) \tag{3.21}$$

The energy concentrations of the optimum Gaussian derivatives from Table 3.1 calculated for $T = 0.5$ ns are given in Table 3.2. Since Gaussian derivatives have exponentially decaying tails, high energy concentrations are obtained.

Table 3.2 Spectral efficiency and energy concentration of FCC-compliant Gaussian derivatives from Table 3.1. Their highest values are highlighted in bold.

	indoor mask		outdoor mask	
n	η, %	λ, %	η, %	λ, %
4	**54.3**	**99.9999**	-	-
5	50.9	99.9999	-	-
6	48.1	99.9992	-	-
7	45.7	99.9966	**41.0**	**99.9877**
8	43.7	99.9976	39.4	99.9855
9	41.9	99.9940	38.1	99.9355
10	40.4	99.9801	36.8	99.9710

4. SHARPENED GAUSSIAN DERIVATIVES

Gaussian derivatives are bandpass waveforms well localized in time. However, their efficiency in filling the UWB spectral mask is low. To increase the efficiency, their modification is proposed. It is based on a well-known technique called polynomial sharpening. To obtain high spectral efficiency, the magnitude spectrum of a Gaussian derivative is sharpened with the Kaiser-Hamming polynomials [48]. These polynomials impose flatness at spectrum's peak, while maintaining good time localization.

4.1 Preparation of Gaussian derivatives for sharpening

The Fourier transform of nth Gaussian derivative can be written as

$$\begin{aligned} G_n(\omega) &= j^n \omega^n G_0(\omega) \\ &= \begin{cases} (-1)^{n/2} \left| G_n(\omega) \right| & \text{for even } n \\ j(-1)^{(n-1)/2} \operatorname{sgn}(\omega) \left| G_n(\omega) \right| & \text{for odd } n \end{cases} \end{aligned} \tag{4.1}$$

where $|G_n(\omega)|$ is the magnitude spectrum of the Gaussian derivative, given by

$$\left| G_n(\omega) \right| = \begin{cases} \omega^n G_0(\omega) & \text{for even } n \\ \operatorname{sgn}(\omega) \omega^n G_0(\omega) & \text{for odd } n \end{cases} \tag{4.2}$$

To perform sharpening, the magnitude spectra of Gaussian derivatives are normalized to ensure unity magnitude at their peaks. This is obtained by applying the amplitude scaling factor given in (3.3).

4.2 Polynomial sharpening

Kaiser and Hamming proposed the polynomial $f_{p,q}(x)$ which has a pth order of flatness at $x = 1$, qth order of flatness at $x = 0$, and passes through the points (1,1) and (0,0). This polynomial is given by [49]

$$f_{p,q}(x) = x^{q+1} \sum_{r=0}^{p} \frac{(q+r)!}{q!r!} (1-x)^r \tag{4.3}$$

where p and q are non-negative integers. The graphs of $f_{p,q}(x)$ are illustrated in Figure 4.1 for $p = 0$, 1, 2, 4, and 8, assuming $q = p$.

By applying α given in (3.3), the magnitude spectrum in (4.2) satisfies $0 \le |G_n(\omega)| \le 1$. Therefore, the sharpened magnitude spectra are obtained as

$$|S_n(\omega)| = f_{p,q}\left(|G_n(\omega)|\right) \tag{4.4}$$

They are illustrated in Figure 4.2 for $n = 2$, $\tau = 1$ s, and the polynomials from Figure 4.1. Note that this sharpening preserves requirement for zero DC [26]. The case $p = q = 0$ corresponds to the original Gaussian derivative. Clearly, an increase in p brings flatter top and sharper transition regions and, consequently, a larger bandwidth. In addition, the peaks of $|S_n(\omega)|$ and $|G_n(\omega)|$ are placed at the same point.

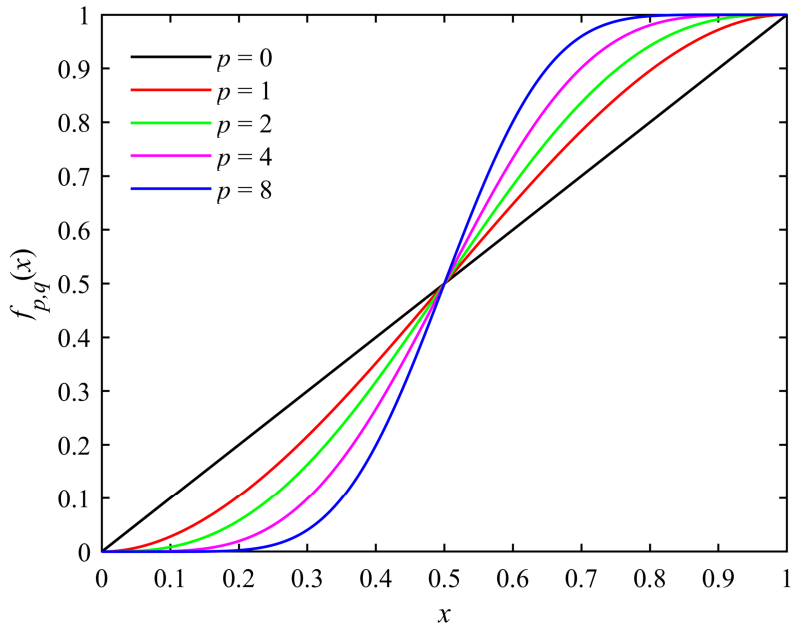

Figure 4.1 Kaiser-Hamming polynomials of various orders of flatness p, obtained for $q = p$.

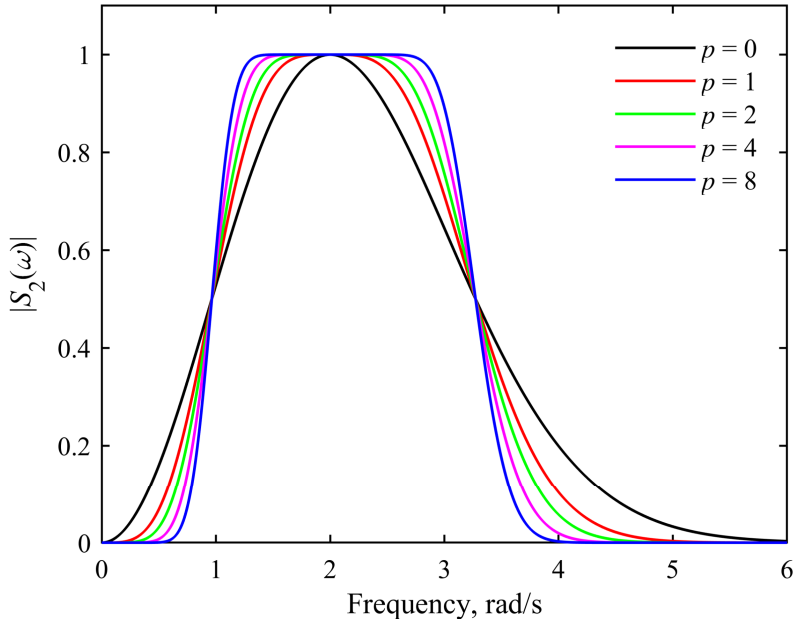

Figure 4.2 Magnitude spectra of second Gaussian derivative with $\tau = 1$ s sharpened with Kaiser-Hamming polynomials having $p = 0, 1, 2, 4,$ and 8 and $q = p$. Case $p = q = 0$ denotes original derivative [48].

4.3 Waveforms of sharpened Gaussian derivatives

To obtain the waveforms of sharpened Gaussian derivatives, polynomial $f_{p,q}(x)$ is first expressed in a power-series form. To obtain this form, $f_{p,q}(x)$ is expanded as

$$\begin{aligned} f_{p,q}(x) &= x^{q+1}\sum_{r=0}^{p}\frac{(q+r)!}{q!r!}(1-x)^r \\ &= x^{q+1}\sum_{r=0}^{p}\frac{(q+r)!}{q!r!}\sum_{k=0}^{r}\binom{r}{k}1^{r-k}(-x)^k \\ &= \sum_{r=0}^{p}\frac{(q+r)!}{q!}\sum_{k=0}^{r}\frac{(-1)^k}{k!(r-k)!}x^{k+q+1} \end{aligned} \tag{4.5}$$

Clearly, $f_{p,q}(x)$ contains the powers running from x^{q+1} to x^{p+q+1}. Therefore, its power-series form is given by

$$f_{p,q}(x) = \sum_{m=q+1}^{M} a_m x^m \tag{4.6}$$

where $M = p + q + 1$ is polynomial order and a_m are polynomial coefficients. By substituting $k = m - q - 1$ into (4.5), the coefficients a_m are obtained as

$$a_m = \frac{(-1)^{m-q-1}}{(m-q-1)!} \sum_{r=m-q-1}^{p} \frac{(q+r)!}{q!(r+q+1-m)!} \quad \text{for } m = q+1, q+2, \ldots, M \tag{4.7}$$

After substituting $x = |G_n(\omega)|$ into (4.6), the sharpened magnitude spectrum takes the form

$$\left|S_n(\omega)\right| = \sum_{m=q+1}^{M} a_m \left|G_n(\omega)\right|^m \tag{4.8}$$

By applying (4.2), the term $|G_n(\omega)|^m$ is given by

$$\left|G_n(\omega)\right|^m = \begin{cases} \omega^{mn} G_0^m(\omega) & \text{for even } n \\ \operatorname{sgn}^m(\omega)\, \omega^{mn} G_0^m(\omega) & \text{for odd } n \end{cases} \tag{4.9}$$

By using (2.5), $G_0^m(\omega)$ can be written as

$$G_0^m(\omega) = \left(\alpha\tau\sqrt{\pi}\right)^{m-1} G_0\left(\sqrt{m}\omega\right) \tag{4.10}$$

By substituting (4.10) into (4.9), applying the identity

$$\omega^{mn} \operatorname{sgn}^m(\omega) = \begin{cases} \omega^{mn} & \text{for even } m \\ \omega^{mn} \operatorname{sgn}(\omega) & \text{for odd } m \end{cases} \tag{4.11}$$

and taking into account that mn is even if m or n is even, it follows

$$\left|G_n(\omega)\right|^m = \begin{cases} \left(\alpha\tau\sqrt{\pi}\right)^{m-1} \omega^{mn} G_0\left(\sqrt{m}\omega\right) & \text{for even } mn \\ \left(\alpha\tau\sqrt{\pi}\right)^{m-1} \operatorname{sgn}(\omega)\, \omega^{mn} G_0\left(\sqrt{m}\omega\right) & \text{for odd } mn \end{cases} \tag{4.12}$$

The expression in (4.12) is recognized in a compact form as

$$\left|G_n(\omega)\right|^m = \frac{\left(\alpha\tau\sqrt{\pi}\right)^{m-1}}{\left(\sqrt{m}\right)^{mn}} \left|G_{mn}\left(\sqrt{m}\omega\right)\right| \tag{4.13}$$

where $|G_{mn}(\omega)|$ is the magnitude spectrum of mnth Gaussian derivative. Finally, by substituting (4.13) into (4.8), the sharpened magnitude spectrum is obtained as

$$\left|S_n(\omega)\right| = \sum_{m=q+1}^{M} a_m \frac{\left(\alpha\tau\sqrt{\pi}\right)^{m-1}}{\left(\sqrt{m}\right)^{mn}} \left|G_{mn}\left(\sqrt{m}\omega\right)\right| \tag{4.14}$$

Note that $|S_n(\omega)|$ is a linear combination of the magnitude spectra of Gaussian derivatives of orders mn.

In the sharpening process, the phase spectrum of the original derivative in (4.1) is retained. Therefore, the Fourier transform of the sharpened derivative is given by

$$S_n(\omega) = \begin{cases} (-1)^{n/2} \left|S_n(\omega)\right| & \text{for even } n \\ j(-1)^{(n-1)/2} \operatorname{sgn}(\omega) \left|S_n(\omega)\right| & \text{for odd } n \end{cases} \tag{4.15}$$

By substituting (4.14) into (4.15) and by using (4.2) to express $\left|G_{mn}(\sqrt{m}\omega)\right|$, the spectrum $S_n(\omega)$ is obtained as

$$S_n(\omega) = (-1)^{n/2} \sum_{m=q+1}^{M} a_m \frac{\left(\alpha\tau\sqrt{\pi}\right)^{m-1}}{\left(\sqrt{m}\right)^{mn}} (-1)^{mn/2} G_{mn}\left(\sqrt{m}\omega\right) \tag{4.16}$$

for an even n and as

$$S_n(\omega) = (-1)^{(n-1)/2} \sum_{m=q+1}^{M} a_m \frac{\left(\alpha\tau\sqrt{\pi}\right)^{m-1}}{\left(\sqrt{m}\right)^{mn}} \tilde{G}_{mn}\left(\sqrt{m}\omega\right) \tag{4.17}$$

for an odd n, where

$$\tilde{G}_{mn}\left(\sqrt{m}\omega\right) = \begin{cases} j(-1)^{mn/2} \operatorname{sgn}(\omega) G_{mn}\left(\sqrt{m}\omega\right) & \text{for even } mn \\ (-1)^{(mn-1)/2} G_{mn}\left(\sqrt{m}\omega\right) & \text{for odd } mn \end{cases} \tag{4.18}$$

The waveforms of sharpened Gaussian derivatives are obtained by applying the inverse Fourier transform to $S_n(\omega)$. Using (4.16) and (4.17) it results in

$$s_n(t)=\begin{cases}(-1)^{n/2}\displaystyle\sum_{m=q+1}^{M}a_m\frac{\left(\alpha\tau\sqrt{\pi}\right)^{m-1}}{\left(\sqrt{m}\right)^{mn}}\mathcal{F}^{-1}\left\{G_{mn}\left(\sqrt{m}\omega\right)\right\} & \text{for even } n\\ (-1)^{(n-1)/2}\displaystyle\sum_{m=q+1}^{M}a_m\frac{\left(\alpha\tau\sqrt{\pi}\right)^{m-1}}{\left(\sqrt{m}\right)^{mn}}\mathcal{F}^{-1}\left\{\tilde{G}_{mn}\left(\sqrt{m}\omega\right)\right\} & \text{for odd } n\end{cases} \tag{4.19}$$

For an even n, mn is also even. Therefore, the inverse Fourier transform of $G_{mn}(\sqrt{m}\omega)$ is given by

$$\mathcal{F}^{-1}\left\{G_{mn}\left(\sqrt{m}\omega\right)\right\}=(-1)^{mn/2}\frac{1}{\sqrt{m}}g_{mn}\left(\frac{t}{\sqrt{m}}\right) \tag{4.20}$$

By substituting (4.20) into (4.19), $s_n(t)$ for an even n is given by

$$s_n(t)=(-1)^{n/2}\sum_{m=q+1}^{M}(-1)^{mn/2}a_m\frac{(\alpha\tau\sqrt{\pi})^{m-1}}{(\sqrt{m})^{mn+1}}g_{mn}\left(\frac{t}{\sqrt{m}}\right) \tag{4.21}$$

For an odd n, the inverse Fourier transform of $\widetilde{G}_{mn}(\sqrt{m}\omega)$ is given by

$$\mathcal{F}^{-1}\left\{\tilde{G}_{mn}\left(\sqrt{m}\omega\right)\right\}=\frac{1}{\sqrt{m}}\begin{cases}(-1)^{mn/2-1}\,\hat{g}_{mn}\left(\dfrac{t}{\sqrt{m}}\right) & \text{for even } mn\\ (-1)^{(mn-1)/2}\,g_{mn}\left(\dfrac{t}{\sqrt{m}}\right) & \text{for odd } mn\end{cases} \tag{4.22}$$

where $\hat{g}_{mn}(t)$ is the Hilbert transform of $g_{mn}(t)$. By substituting (4.22) into (4.19), $s_n(t)$ for an odd n is given by

$$s_n(t)=(-1)^{(n-1)/2}\sum_{m=q+1}^{M}a_m\frac{\left(\alpha\tau\sqrt{\pi}\right)^{m-1}}{\left(\sqrt{m}\right)^{mn+1}}\begin{cases}(-1)^{mn/2-1}\,\hat{g}_{mn}\left(\dfrac{t}{\sqrt{m}}\right) & \text{for even } mn\\ (-1)^{(mn-1)/2}\,g_{mn}\left(\dfrac{t}{\sqrt{m}}\right) & \text{for odd } mn\end{cases} \tag{4.23}$$

In (4.22) and (4.23), the Hilbert transforms of even-order Gaussian derivatives $\hat{g}_{mn}(t)$ are required. The Hilbert transforms of Gaussian derivatives are given by the integral [50]

$$\hat{g}_{mn}(t) = \frac{1}{\sqrt{\pi}} \int_0^{\infty} x^n e^{-x^2/4} \sin\left(x t + \frac{n\pi}{2} \right) \mathrm{d}x \tag{4.24}$$

This integral can be solved numerically. However, the Hilbert transforms of Gaussian derivatives can also be obtained by using analytical approximations. One such approximation is proposed in [51]. Finally, the Hilbert transforms of Gaussian derivatives can be expressed in a closed form via the imaginary error function erfi. The latter approach is presented in the following text.

For simplicity, an *mn*th Gaussian derivative with $\alpha = 1$ and $\tau = 1$ s is considered. It is given by

$$g_{mn}(t) = (-1)^{mn} H_{mn}(t) e^{-t^2} \tag{4.25}$$

By using (3.14) and (3.15), and assuming *mn* is even, the Hilbert transform of $g_{mn}(t)$ takes the form

$$\begin{aligned} \hat{g}_{mn}(t) &= \mathcal{H}\left\{ \sum_{r=0}^{mn/2} b_r t^{2r} e^{-t^2} \right\} \\ &= \begin{cases} \mathcal{H}\left\{ e^{-t^2} \right\} & \text{for } r = 0 \\ \sum_{r=1}^{mn/2} b_r \mathcal{H}\left\{ t^{2r} e^{-t^2} \right\} & \text{for } r > 0 \end{cases} \end{aligned} \tag{4.26}$$

where

$$\begin{aligned} \mathcal{H}\left\{ e^{-t^2} \right\} &= \frac{1}{\pi} (v.p.) \int_{-\infty}^{\infty} \frac{e^{-u^2}}{t-u} du \\ &= e^{-t^2} \operatorname{erfi}(t) \end{aligned} \tag{4.27}$$

where erfi is the imaginary error function. This function is defined as [52]

$$\operatorname{erfi}(jt) = j \operatorname{erf}(t) \tag{4.28}$$

where

$$\operatorname{erf}(t) = \frac{2}{\sqrt{\pi}} \int_0^t e^{u^2}\, du \tag{4.29}$$

For $r > 0$, the Hilbert transform of $t^{2r} e^{-t^2}$ is calculated by using the recurrence expression

$$\mathcal{H}\left\{t^{2r} e^{-t^2}\right\} = t^2 \mathcal{H}\left\{t^{2(r-1)} e^{-t^2}\right\} - \frac{\left(2(r-1)-1\right)!!}{\sqrt{\pi}\, 2^{r-1}} t \tag{4.30}$$

By using (4.27) and (4.30), the Hilbert transform of $t^{2r} e^{-t^2}$ for $r \geq 0$ is obtained as

$$\mathcal{H}\left\{t^{2r} e^{-t^2}\right\} = t^{2r} e^{-t^2} \operatorname{erfi}(t) - \frac{2}{\sqrt{\pi}} t^{2r+1} \left(1 - \sum_{k=0}^{r} \frac{\prod_{i=0}^{k} (2i-1)}{2^k t^{2k} (2k-1)} \right) \quad \text{for } t \neq 0 \tag{4.31}$$

By substituting (4.31) into (4.26), it follows

$$\hat{g}_{mn}(t) = H_{mn}(t) e^{-t^2} \operatorname{erfi}(t) - \frac{2}{\sqrt{\pi}} \sum_{r=0}^{mn/2} b_r t^{2r+1} \left(1 - \sum_{k=0}^{r} \frac{\prod_{i=0}^{k} (2i-1)}{2^k t^{2k} (2k-1)} \right) \quad \text{for } t \neq 0 \tag{4.32}$$

By using (4.25), the Hilbert transforms of Gaussian derivatives are obtained as

$$\hat{g}_{mn}(t) = g_{mn}(t) \operatorname{erfi}(t) - \frac{2}{\sqrt{\pi}} \sum_{r=0}^{mn/2} b_r t^{2r+1} \left(1 - \sum_{k=0}^{r} \frac{\prod_{i=0}^{k} (2i-1)}{2^k t^{2k} (2k-1)} \right) \text{for } t \neq 0 \tag{4.33}$$

It is known that the Hilbert transform of an even function is an odd function. Consequently, $\hat{g}_{mn}(t) = 0$ for $t = 0$. Finally, for even-order Gaussian derivatives with arbitrary values α and τ, their Hilbert transforms take the form

$$\hat{g}_{mn}(t)=\begin{cases} g_{mn}(t)\,\mathrm{erfi}\left(\dfrac{t}{\tau}\right)-\dfrac{2\alpha}{\sqrt{\pi}\tau^{mn}}\displaystyle\sum_{r=0}^{mn/2} b_r\left(\dfrac{t}{\tau}\right)^{2r+1}\left(1-\sum_{q=0}^{r}\dfrac{\displaystyle\prod_{i=0}^{q}(2i-1)}{2^q\left(\dfrac{t}{\tau}\right)^{2q}(2q-1)}\right) & \text{for } t\neq 0 \\ 0 & \text{for } t=0 \end{cases} \tag{4.34}$$

Since the sharpened Gaussian derivatives have the same phase spectra as the original derivatives, the waveforms $s_n(t)$ exhibit even symmetry for an even n and odd symmetry for an odd n. In addition, in both cases their polarity alternates with n. The pulses $s_n(t)$ are illustrated in Figure 4.3 for $n = 2$ and the polynomials from Figure 4.1.

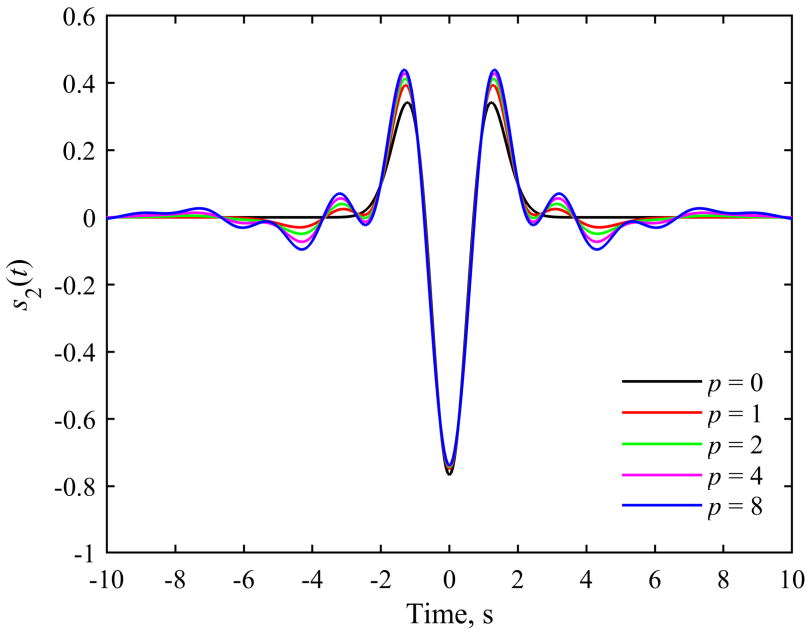

Figure 4.3 Waveforms of second Gaussian derivative with $\tau = 1$ s sharpened with Kaiser-Hamming polynomial having $p = 0$, 1, 2, 4, and 8 and $q = p$. Case $p = q = 0$ denotes waveform of original derivative [48].

4.4 Design of UWB pulses

In this section, the sharpened Gaussian derivatives are applied in the design of UWB pulses which optimally fill a desired spectral mask. For given n and p, our objective is to find the values of q and τ that ensure optimum filling of a given UWB region. The design utilizes the method shown in Section 3.1, which is here tailored for sharpened Gaussian derivatives. The filling is formulated via the minimization of distance between the spectral mask and the sharpened magnitude spectrum calculated at the edge frequencies of the UWB region. This distance is defined as

$$\varepsilon(q,\tau) = A_L - \left|S_n(f_L)\right| + A_U - \left|S_n(f_U)\right| \tag{4.35}$$

where f_L and f_U are the lower and the upper band-edge frequency, whereas A_L and A_U are magnitude limits at f_L and f_U. For a given mask, the optimum values of q and τ are obtained by solving the problem

$$\begin{aligned} &\underset{q,\tau}{\text{minimize}} && \varepsilon(q,\tau) \\ &\text{subject to} && \left|S_n(f)\right|^2 \le M(f) \end{aligned} \tag{4.36}$$

where $M(f)$ denotes the PSD mask normalized to unity density in the UWB region.

Since $|S_n(f)|$ has a bell shape, the problem in (4.36) is simplified as [48]

$$\begin{aligned} &\underset{q,\tau}{\text{maximize}} && \left|S_n(f_L)\right| + \left|S_n(f_U)\right| \\ &\text{subject to} && \left|S_n(f_L)\right| \le A_L \\ &&& \left|S_n(f_U)\right| \le A_U \\ &&& \left|S_n(f_k)\right| \le A_k \ , k = 1,2,...,K \end{aligned} \tag{4.37}$$

where f_k are frequencies outside the UWB region at which the mask changes, $A_L = \sqrt{M(f_L)}$, $A_U = \sqrt{M(f_U)}$, and $A_k = \sqrt{M(f_k)}$. The magnitude limits corresponding to normalized FCC indoor mask and the magnitude spectrum of a sharpened Gaussian derivative are illustrated in Figure 4.4, for convenience.

In the design process the peak of $|S_n(f)|$ should be placed within the band $f_L < f < f_U$. As shown in Section 3.1, τ is limited to the interval given in (3.6). Since τ is bounded by a finite

interval and q is a non-negative integer, the problem in (4.37) can be easily solved by using the direct search. In this search, the objective function is evaluated on the uniformly spaced grid of τ with steps of $\Delta\tau$ defined within the interval in (3.6). This evaluation is repeated for each q running from 0 to some limit q_{max}. Using the value of τ corresponding to the midpoint of the interval in (3.6), q_{max} can be estimated as the lowest value of q for which the constraints in (4.37) are met.

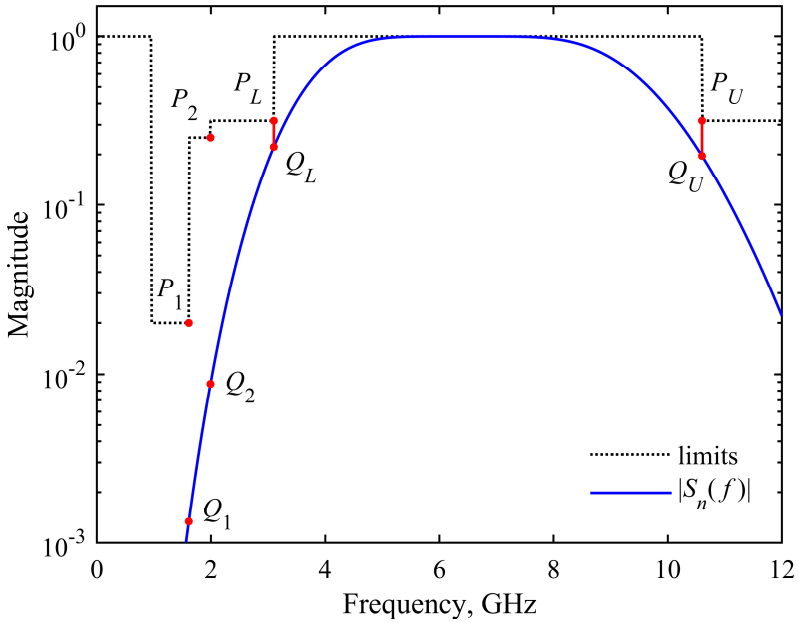

Figure 4.4 Magnitude limits corresponding to normalized FCC indoor mask and magnitude spectrum of sharpened Gaussian derivative. Red dots show used magnitude limits, $P_1 = (f_1, A_1)$, $P_2 = (f_2, A_2)$, $P_L = (f_L, A_L)$, $P_U = (f_U, A_U)$, and corresponding magnitudes, $Q_1 = (f_1, |S_n(f_1)|)$, $Q_2 = (f_2, |S_n(f_2)|)$, $Q_L = (f_L, |S_n(f_L)|)$, and $Q_U = (f_U, |S_n(f_U)|)$ [48].

To preserve the same polarity of all UWB pulses and enable the change of peak values of their magnitude spectra, the waveforms are scaled as in

$$w_n(t) = \beta C s_n(t) \tag{4.38}$$

where C is the magnitude limit in the UWB region, $\beta = (-1)^{n/2}$ for an even n, and $\beta = (-1)^{(n-1)/2}$ for an odd n. Using (4.15), the amplitude spectrum of the pulse in (4.38) is given by

$$W_n(\omega) = \begin{cases} C\left|S_n(\omega)\right| & \text{for even } n \\ C\,\mathrm{sgn}(\omega)\left|S_n(\omega)\right| & \text{for odd } n \end{cases} \tag{4.39}$$

Clearly, it satisfies $W_n(\omega_n) = C$.

An example of MATLAB code implementing the entire design is given by Algorithm 4.1, for convenience. The function is called *uwbdesign_sharpgaussder* [48]. Its input parameters are the order of Gaussian derivative, n, order of flatness, p, vector of mask frequencies expressed in GHz, F, vector of mask PSDs having the same size as F expressed in dBm/MHz, M, PSD in UWB region, M_0, and indices of the elements in F corresponding to the lower and upper UWB-edge frequencies, L and U. The function *uwbdesign_sharpgaussder* calls the function *sharpmag* which calculates $|S_n(\omega)|$. In the code, $\Delta\tau$ = 1e–4 ns is used.

Algorithm 4.1 Design of UWB sharpened Gaussian derivative of order n.

```
function [q,tau]=uwbdesign_sharpgaussder(n,p,F,M,M0,L,U)

dtau=1e-4; % the step of tau in ns

k=sqrt(n/2)/pi; tauL=k/F(U); tauU=k/F(L);
taum=(tauL+tauU)/2;
A=10.^((M-M0)/20); w=2*pi*F; K=length(F);

% search for qmax
qi=0; taum=ceil(taum/dtau)*dtau;
while 1
 qi=qi+1; Sn=sharpmag(n,taum,p,qi,w);
 if sum(Sn<=A)==K % satisfies mask
  qmax=qi; break
end, end

% search for optimum q and tau
yold=0; q=[]; tau=[];
for qi=0:qmax
 for taui=(ceil(tauL/dtau):ceil(tauU/dtau))*dtau
  Sn=sharpmag(n,taui,p,qi,w);
  if sum(Sn<=A)==K % satisfies mask
   ynew=Sn(L)+Sn(U);
   if ynew > yold
    yold=ynew; q=qi; tau=taui;
end, end, end, end

function Sn=sharpmag(n,tau,p,q,w)

alpha=tau^(n-1)/sqrt(pi)*(exp(1)/2/n)^(n/2);
G0=alpha*tau*sqrt(pi)*exp(-(w*tau/2).^2);
Gn=abs(w).^n.*G0;
S=ones(size(w));
for r=1:p
 S=S+prod(q+1:q+r)/prod(1:r)*(1-Gn).^r;
end
Sn=Gn.^(q+1).*S;
```

An example of MATLAB code for calculating the values of the waveform $w_n(t)$ and its amplitude spectrum $W_n(\omega)$ is given by Algorithm 4.2 . The function is called *sharpgaussder*. Its input parameters are the order of Gaussian derivative, n, orders of flatness, p and q, amplitude and bandwidth scaling factors, C and τ, vector of time points in s, t, and vector of frequency points in rad/s, w. The function *sharpgaussder* calls the function *ht_gaussder* which calculates $\hat{g}_m(t)$, the function *gaussder* which is given by Algorithm 3.2, and the function *sharpmag* which is given by Algorithm 4.1.

Algorithm 4.2 Calculating values of waveform and amplitude spectrum of sharpened Gaussian derivative of order n.

```
function [wn,Wn]=sharpgaussder(n,p,q,C,tau,t,w)

% amplitude scaling factor of original Gaussian derivative
alpha=tau^(n-1)/sqrt(pi)*(exp(1)/2/n)^(n/2);

% polynomial coefficients am
M=p+q+1; a=zeros(M,1);
for m=(q+1):M
 S=0;
 for r=(m-q-1):p, S=S+prod(q+1:q+r)/prod(1:r-(m-q-1)); end
 a(m)=(-1)^(m-q-1)/prod(1:(m-q-1))*S;
end

% waveform sn(t)
s=zeros(size(t));
if mod(n,2)==0 % even n
 beta=(-1)^(n/2);
 for m=(q+1):M
  gmn=gaussder(m*n,alpha,tau,t/sqrt(m)); % gmn(t/sqrt(m))
  s=s+(-1)^(m*n/2)*a(m)*(alpha*tau*sqrt(pi))^(m-1)/sqrt(m)^(m*n+1)*gmn;
 end
 sn=beta*s;
else % odd n
 beta=(-1)^((n-1)/2);
 for m=(q+1):M
  gmn=gaussder(m*n,alpha,tau,t/sqrt(m)); % gmn(t/sqrt(m))
  if mod(m*n,2)==0 % even mn
   % Hilbert transform of gmn(t/sqrt(m))
   gmn_ht=ht_gaussder(m*n,alpha,tau,gmn,t/sqrt(m));
   g=(-1)^(m*n/2-1)*gmn_ht;
  else % odd mn
   g=(-1)^((m*n-1)/2)*gmn;
  end
  s=s+a(m)*(alpha*tau*sqrt(pi))^(m-1)/sqrt(m)^(m*n+1)*g;
 end
 sn=beta*s;
end

% magnitude spectrum |Sn(w)|
Sn=sharpmag(n,tau,p,q,w);
```

```
% waveform wn(t)
wn=beta*C*sn;

% amplitude spectrum Wn(w)
if mod(n,2)==0, Wn=C*Sn;
else Wn=C*sign(w).*Sn;
end

function gnht=ht_gaussder(n,alpha,tau,gn,t)
% Hilbert transform of gn(t~=0)
gnht=zeros((size(t)));
for r=0:floor(n/2)
 br=factorial(n)*(-1)^(n/2-r)*2^(2*r)/factorial(2*r)/factorial(n/2-r);
 sum=0;
 for k=0:1:r
  I=zeros(1,k);
  for i=0:1:k
   I(1,i+1)=(2*i-1);
  end
  sum=sum+prod(I)/2^k./(t/tau).^(2*k)/(2*k-1);
 end
 gnht=gnht+br.*(t/tau).^(2*r+1).*(1-sum);
end
gnht=gn.*erfi(t/tau)-2*alpha/sqrt(pi)/tau^(n).*gnht;
% Hilbert transform of gn(t==0)
gnht(t==0)=0;
```

4.5 FCC-compliant sharpened Gaussian derivatives

To illustrate features of the proposed method, several pulses that fill the FCC indoor and outdoor mask are designed. The sharpened first and second Gaussian derivatives that fill the UWB region between $f_L = 3.1$ GHz and $f_U = 10.6$ GHz are considered. UWB region is bounded by the points that are 10 dB and 20 dB below the highest PSD. It brings $A_L = A_U = 0.316$ for the indoor and $A_L = A_U = 0.1$ for the outdoor mask. Outside the UWB region, the frequencies $f_1 = 1.61$ GHz and $f_2 = 1.99$ GHz are taken into account. It brings $A_1 = 0.020$ for both masks, and $A_2 = 0.251$ and $A_2 = 0.079$ for the indoor and the outdoor mask, respectively. For both masks $C = 8.61\text{e}{-3}$ is used.

Table 4.1 provides numerical values of the obtained q and τ for various p. In addition, pulse's spectral efficiency and energy concentration are calculated by expressions (1.1) and (1.2) for $T = 0.5$ ns. Clearly, both derivatives exhibit similar spectral efficiency and energy concentration. Furthermore, an increase in p results in the increase of spectral efficiency. A significant increase is achieved already for $p = 1$. In addition, since the indoor mask is less restrictive than the outdoor, the FCC-compliant indoor pulses exhibit higher efficiency. High energy concentration is obtained in all cases. The efficiency greater than 80 % is achieved for

the indoor mask and $p \geq 6$. The obtained PSDs and waveforms for both masks are illustrated in Figure 4.5 for $n = 2$ and $p = 8$.

Using Algorithm 4.1 and 4.2, the design of the FCC-compliant indoor pulse with $n = 2$ and $p = 8$ is given by the following call

```
n=2; p=8; F=[1.61, 1.99, 3.1, 10.6]; M=[-75.3, -53.3, -51.3, -51.3];
M0=-41.3; L=3; U=4;
[q,tau]=uwbdesign_sharpgaussder(n,p,F,M,M0,L,U);
C=10^(M0/20);
t=linspace(-0.5,0.5,1001); f=linspace(0,12,1001); w=2*pi*f;
[wn,Wn]=sharpgaussder(n,p,q,C,tau,t,w);
figure, plot(t,wn/C);
figure, plot(f,20*log10(abs(Wn)),'g',f,fccmask(f,'indoor'),'r');
axis([f(1) f(end) -80 -40]);
```

The design of the FCC-compliant outdoor pulse with same n and p is given by the call

```
n=2; p=8; F=[1.61, 1.99, 3.1, 10.6]; M=[-75.3, -63.3, -61.3, -61.3];
M0=-41.3; L=3; U=4;
[q,tau]=uwbdesign_sharpgaussder(n,p,F,M,M0,L,U);
C=10^(M0/20);
t=linspace(-0.5,0.5,1001); f=linspace(0,12,1001); w=2*pi*f;
[wn,Wn]=sharpgaussder(n,p,q,C,tau,t,w);
figure, plot(t,wn/C);
figure, plot(f,20*log10(abs(Wn)),'g',f,fccmask(f,'outdoor'),'r');
axis([f(1) f(end) -80 -40]);
```

As elaborated in Chapter 3, the original Gaussian derivatives which fill the FCC indoor and outdoor mask with maximum efficiency are obtained for $n = 4$ and $\tau = 0.0670$ ns, as well as for $n = 7$ and $\tau = 0.0910$ ns. These derivatives are here compared with the optimum pulses which correspond to the sharpened Gaussian derivatives obtained for $n = 1$ and $n = 2$, with $p = 1$. Figure 4.6 shows their PSDs and waveforms. Clearly, the pulses obtained from sharpened Gaussian derivatives fill the UWB region more tightly than do the pulses obtained by original derivatives.

Table 4.1 Parameters and properties of FCC-compliant sharpened Gaussian derivatives. Properties are highlighted in bold [48].

	indoor mask				outdoor mask			
p	q	τ, ns	η, %	λ, %	q	τ, ns	η, %	λ, %
$n = 1$								
0	4	0.0322	**50.8**	**> 99.99**	6	0.0344	**41.0**	**99.99**
1	6	0.0342	**66.2**	**99.84**	10	0.0346	**53.7**	**99.62**
2	9	0.0343	**71.7**	**99.68**	14	0.0345	**59.8**	**99.21**
3	11	0.0348	**76.3**	**99.60**	17	0.0347	**64.5**	**98.94**
4	14	0.0347	**78.3**	**99.48**	21	0.0345	**67.0**	**98.74**
5	17	0.0346	**79.8**	**99.38**	24	0.0346	**69.5**	**98.60**
6	20	0.0346	**80.8**	**99.26**	27	0.0347	**71.4**	**98.48**
7	22	0.0348	**82.5**	**99.21**	30	0.0347	**73.1**	**98.40**
8	25	0.0347	**83.2**	**99.11**	33	0.0347	**74.4**	**98.33**
$n = 2$								
0	2	0.0441	**48.0**	**> 99.99**	3	0.0474	**39.4**	**99.99**
1	2	0.0491	**67.6**	**99.96**	5	0.0478	**51.8**	**99.63**
2	4	0.0478	**70.1**	**99.85**	6	0.0489	**59.9**	**99.46**
3	5	0.0483	**74.5**	**99.84**	8	0.0485	**63.2**	**99.23**
4	6	0.0487	**77.4**	**99.80**	9	0.0490	**67.0**	**99.25**
5	7	0.0489	**79.6**	**99.75**	11	0.0486	**68.5**	**99.07**
6	8	0.0491	**81.1**	**99.68**	12	0.0489	**70.9**	**99.10**
7	9	0.0492	**82.5**	**99.62**	13	0.0491	**72.9**	**99.11**
8	11	0.0486	**82.1**	**99.51**	15	0.0487	**73.5**	**98.96**

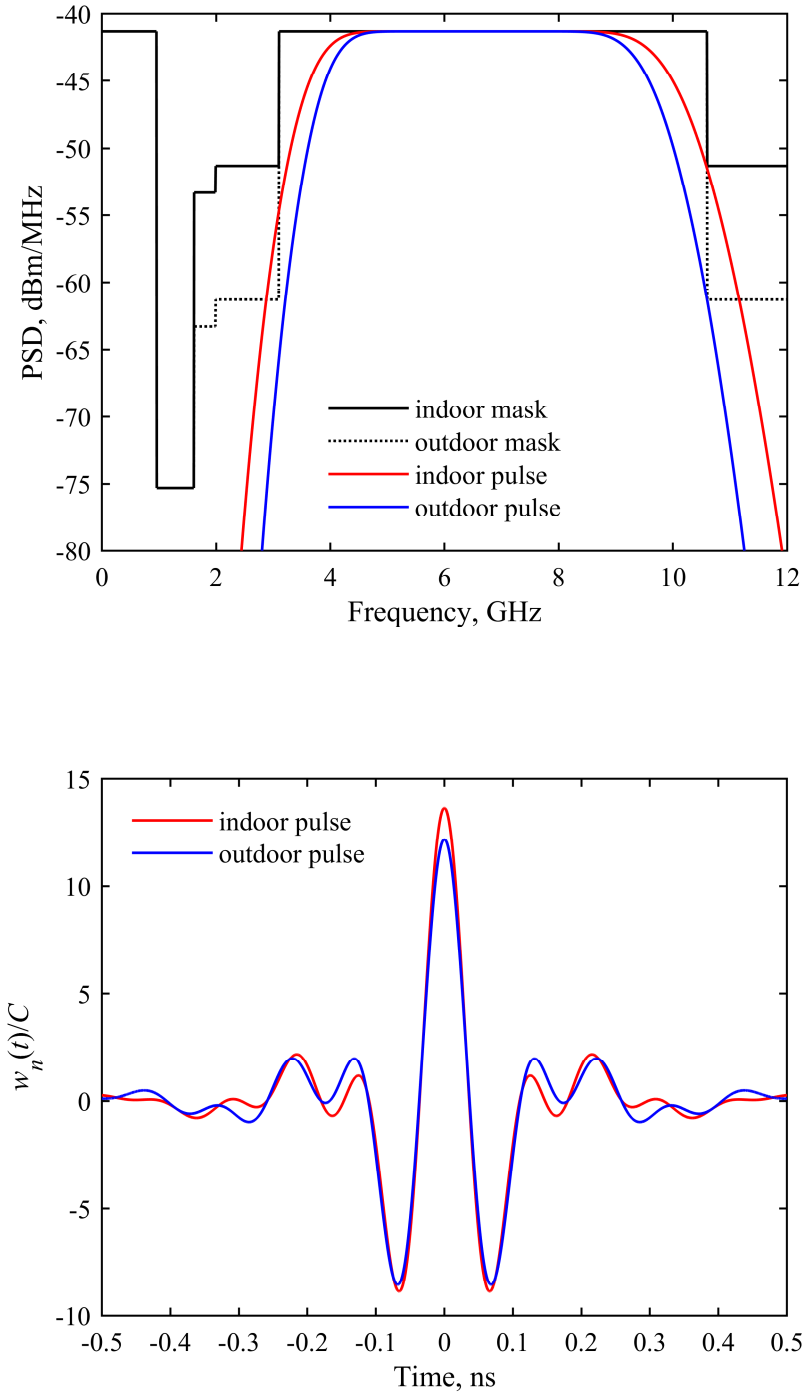

Figure 4.5 Power spectral densities (up) and waveforms (down) of FCC-compliant sharpened Gaussian derivatives obtained for $n = 2$ and $p = 8$ [48].

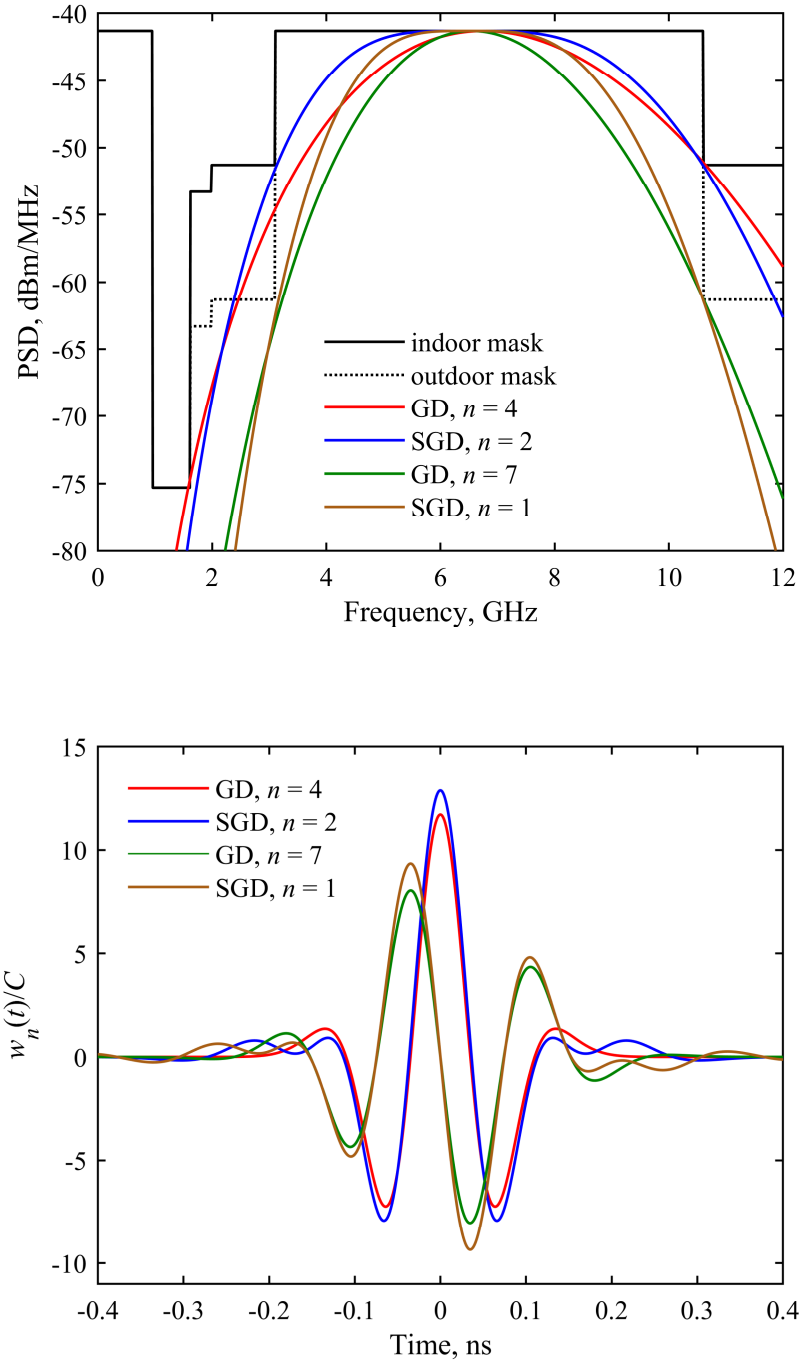

Figure 4.6 Power spectral densities (up) and waveforms (down) of nth Gaussian derivatives (GD) [9] and sharpened nth Gaussian derivatives (SGD) obtained for $p = 1$ [48].

Recently, a linear combination of three translated Gaussian pulses that fill the FCC indoor mask with maximum spectral efficiency has been proposed [31]. This pulse is compared with the optimally sharpened Gaussian derivative having $n = 2$ and $p = 4$. The PSDs and

waveforms of both pulses are shown in Figure 4.7. It is clear from the figure that somewhat better filling of the UWB region is encountered in the case of sharpening.

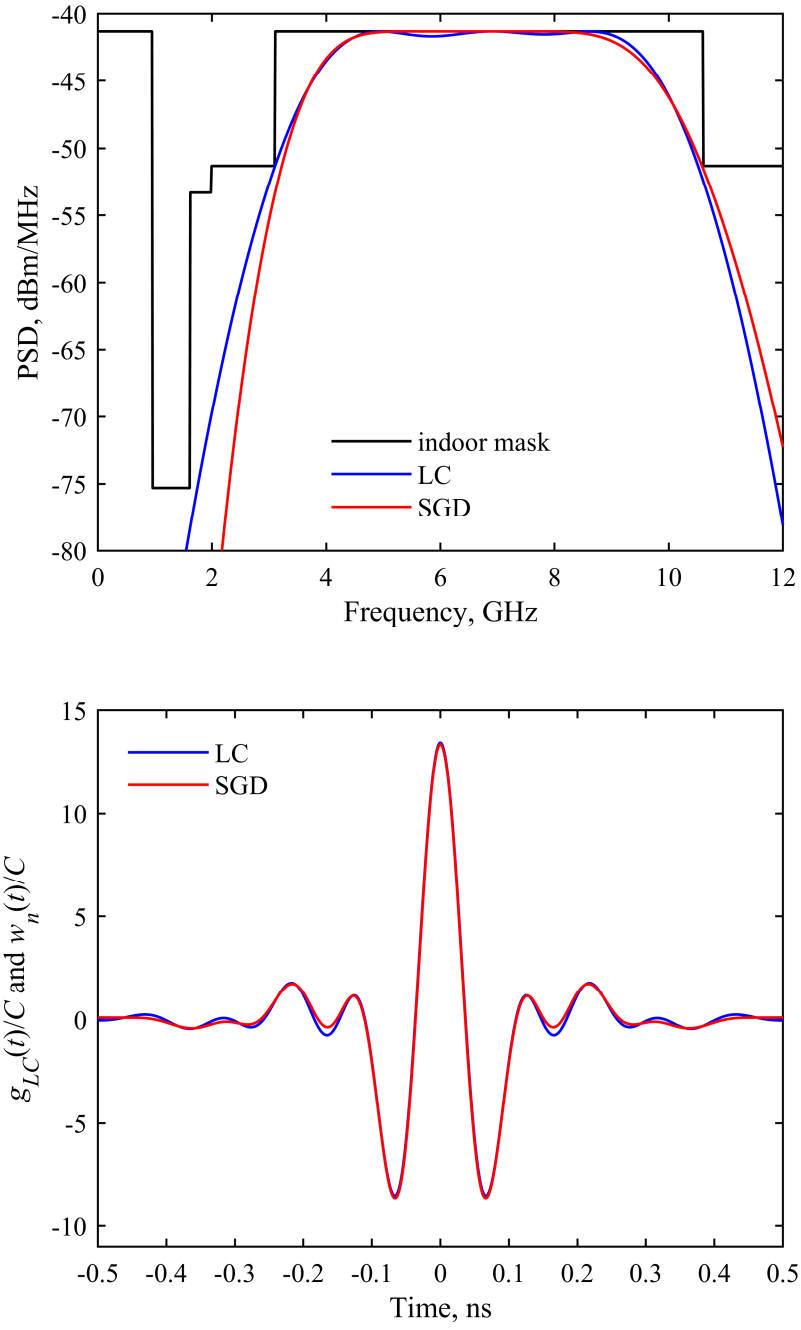

Figure 4.7 Power spectral densities (up) and waveforms (down) of linear combination of three translated Gaussian pulses (LC) [31] and sharpened Gaussian derivative (SGD) obtained for $n = 2$ and $p = 4$ [48].

A linear combination of eight translated Gaussian pulses that efficiently fill the FCC indoor mask has been proposed in [32]. This pulse is compared with the optimally sharpened Gaussian derivative obtained for $n = 1$ and $p = 8$. Their PSDs and waveforms are shown in Figure 4.8. It is clear that the sharpened derivative exhibits somewhat lower spectral efficiency, but higher energy concentration.

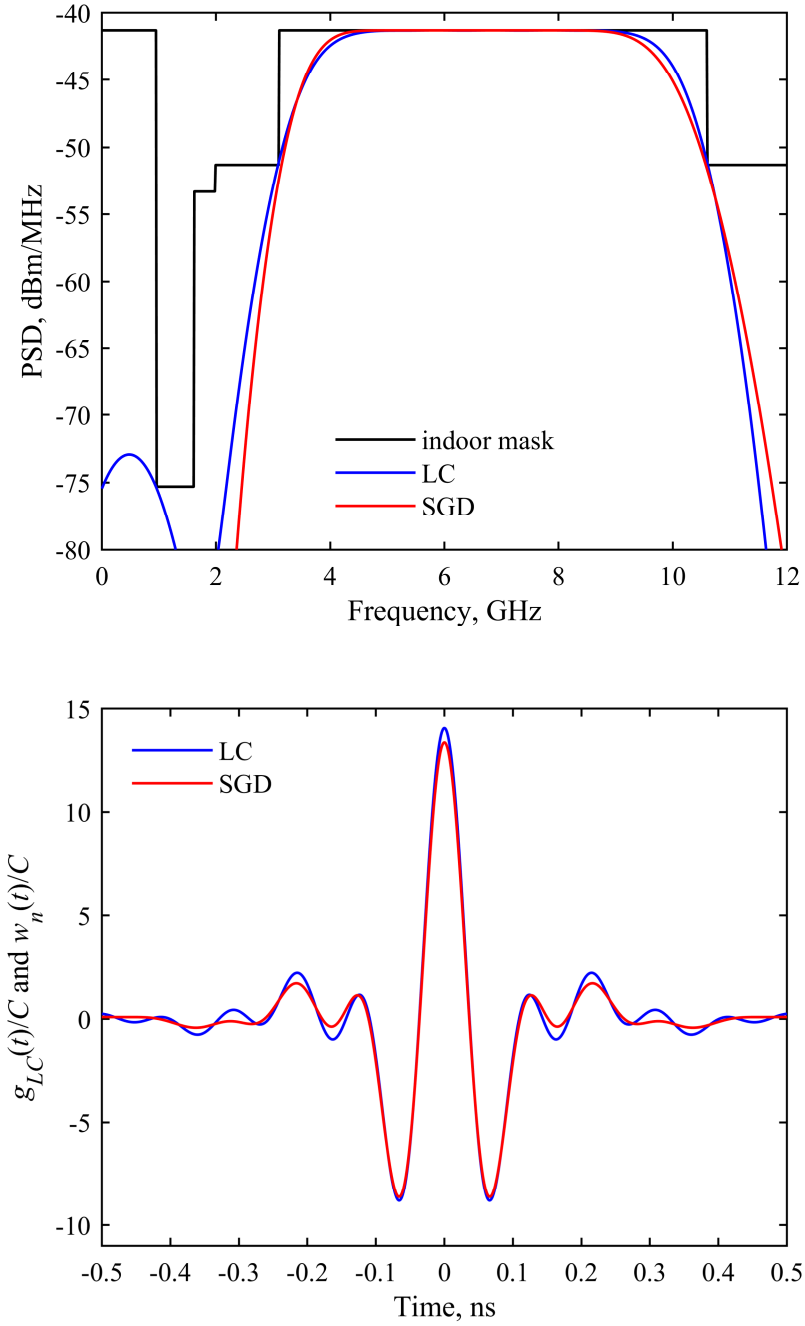

Figure 4.8 Power spectral densities (up) and waveforms (down) of linear combination of eight translated Gaussian pulses (LC) [32] and sharpened Gaussian derivative (SGD) obtained for $n = 1$ and $p = 8$ [48].

Considering FCC indoor mask, Table 4.2 shows the spectral efficiency and energy concentration of the pulses from [9], [31] and [32], which are shown in Figures 4.6, 4.7 and 4.8, the pulses presented in [20], [31], and [34] as well as of the optimally sharpened Gaussian derivative with $n = 1$ and $p = 8$. As expected, the sinc-based pulses have high spectral efficiency but relatively low energy concentration. Different behavior is encountered with Gaussian-based pulses. However, the sharpened Gaussian derivative exhibits the efficiency greater than 83 % and the concentration greater than 99 %.

Table 4.2 Comparisons of various FCC-compliant indoor pulses with sharpened Gaussian derivative.

	Pulse	η, %	λ, %
Sinc	Translated and truncated sinc pulse [20]	98.9	95.82
	Linear combination of three translated sinc pulses [31]	82.6	98.53
Gaussian	Fourth Gaussian derivative [9]	54.3	> 99.99
	Linear combination of Gaussian derivatives [34]	72.0	99.97
	Linear combination of three translated Gaussians [31]	77.5	99.78
	Linear combination of eight translated Gaussians [32]	82.8	99.56
	Sharpened Gaussian derivative with $n = 1$ and $p = 8$	83.2	99.11

5. FLAT-SPECTRUM GAUSSIAN PULSES

As elaborated in the previous chapter, imposing flatness in the peak of the magnitude spectrum of the UWB pulse significantly increases the spectral efficiency while maintaining good energy concentration. In the case of sharpened Gaussian derivatives, the flatness is imposed indirectly by using a composition of maximally flat polynomials and arbitrary Gaussian derivative. The consequence of such an approach is that pulse fitting in the UWB mask should be performed by an optimization procedure. In addition, a part of the UWB region still remains unfilled, as illustrated in Figure 4.7. In this chapter it will be shown that these drawbacks can be overcome by using a direct approach in flattening the magnitude spectrum. For this purpose, UWB pulse shaping based on polynomially weighted Gaussian pulses with maximally flat amplitude spectra is developed [53].

5.1 Polynomially weighted Gaussian pulse

Polynomially weighted Gaussian pulse is given by

$$f_n(t) = p_n(t)e^{-t^2} \tag{5.1}$$

where $p_n(t)$ is nth order polynomial. Note that in the above model the Gaussian pulse (2.1) with amplitude and bandwidth scaling factors set as $\alpha = 1$ and $\tau = 1$ s is used. Since symmetric pulses are considered, $p_n(t)$ contains only even or only odd powers. Therefore, the polynomials take the form

$$p_n(t) = \sum_{m=0}^{n/2} a_m t^{2m} \tag{5.2}$$

for an even n, and

$$p_n(t) = \sum_{m=0}^{(n-1)/2} a_m t^{2m+1} = t\sum_{m=0}^{(n-1)/2} a_m t^{2m} \tag{5.3}$$

for an odd n, where a_m are polynomial coefficients.

The Fourier transform of the pulse $f_n(t)$ for even n is given by

$$F_n(\omega) = \mathcal{F}\left\{ \sum_{m=0}^{n/2} a_m t^{2m} e^{-t^2} \right\} \tag{5.4}$$

Since the Fourier transform is linear operator, $F_n(\omega)$ becomes

$$F_n(\omega) = \sum_{m=0}^{n/2} a_m \mathcal{F}\left\{ t^{2m} e^{-t^2} \right\} \tag{5.5}$$

By applying the time derivative property of the Fourier transform, the expression in (5.5) is written as

$$F_n(\omega) = \sum_{m=0}^{n/2} a_m j^{2m} \frac{d^{2m}}{d\omega^{2m}} G_0(\omega) \tag{5.6}$$

where $G_0(\omega)$ is the Fourier transform of the Gaussian pulse given in (2.5). By substituting (2.5) into (5.6), the transform takes the form

$$F_n(\omega) = \sqrt{\pi} \sum_{m=0}^{n/2} (-1)^m a_m \frac{d^{2m}}{d\omega^{2m}} e^{-(\omega/2)^2} \tag{5.7}$$

Note that the derivative in (5.7) can be viewed as an even order derivative of the Gaussian function in the frequency domain. Therefore, it can be expressed similarly as in (2.2) by

$$\frac{d^{2m}}{d\omega^{2m}} e^{-(\omega/\beta)^2} = (-1)^{2m} \frac{1}{\beta^{2m}} H_{2m}\left(\frac{\omega}{\beta}\right) e^{-(\omega/\beta)^2} \tag{5.8}$$

Finally, by substituting $\beta = 2$ into (5.8), and (5.8) into (5.7), the Fourier transform of $f_n(t)$ for even n is given by

$$F_n(\omega) = \sqrt{\pi} \left[\sum_{m=0}^{n/2} (-1)^m 2^{-2m} a_m H_{2m}\left(\frac{\omega}{2}\right) \right] e^{-(\omega/2)^2} \tag{5.9}$$

For even n, the Fourier transform in (5.9) is real valued and therefore represents the amplitude spectrum of $f_n(t)$.

For odd n, the Fourier transform of $f_n(t)$ is obtained as

$$\begin{aligned}\mathcal{F}\{f_n(t)\} &= \sqrt{\pi}\left[\sum_{m=0}^{(n-1)/2} j^{2m+1}(-1)^{2m+1}2^{-(2m+1)}a_m H_{2m+1}\left(\frac{\omega}{2}\right)\right]e^{-(\omega/2)^2} \\ &= -j\frac{\sqrt{\pi}}{2}\left[\sum_{m=0}^{(n-1)/2}(-1)^m 2^{-2m}a_m H_{2m+1}\left(\frac{\omega}{2}\right)\right]e^{-(\omega/2)^2}\end{aligned} \tag{5.10}$$

In this case, the amplitude spectrum of $f_n(t)$ is given by

$$F_n(\omega) = -\frac{\sqrt{\pi}}{2}\left[\sum_{m=0}^{(n-1)/2}(-1)^m 2^{-2m}a_m H_{2m+1}\left(\frac{\omega}{2}\right)\right]e^{-(\omega/2)^2} \tag{5.11}$$

5.2 Maximally flat criterion

The design objective is to find polynomial coefficients a_m which ensure maximally flat-spectrum $F_n(\omega)$ at a given point $\omega = \omega_p$. In addition, the coefficients should provide unity magnitude at this point.

For even n, $F_n(\omega)$ is even function of ω. Therefore, we impose flatness at $\omega_p = 0$. The maximally flat criterion at this point is satisfied by setting the first $n + 1$ derivatives of $F_n(\omega)$ in (5.9) to 0. Since odd-order derivatives of an even function vanish at the origin, the flatness is imposed by setting

$$\begin{aligned}&F_n(0) = 1 \\ &\left.\frac{d^r F_n(\omega)}{d^r \omega}\right|_{\omega=0} = 0 \quad \text{for } r = 2, 4, \ldots, n\end{aligned} \tag{5.12}$$

For odd n, $F_n(\omega)$ is odd function of ω, Therefore, it satisfies $F_n(0) = 0$. Consequently, the flatness should be imposed at two frequencies $-\omega_p$ and ω_p. The maximally flat criterion at $\omega = \omega_p$ is satisfied by setting first $(n - 1)/2 + 1$ derivatives at $F_n(\omega)$ in (5.11) to 0 as in

$$\begin{aligned}&F_n(\omega_p) = 1 \\ &\left.\frac{d^r F_n(\omega)}{d^r \omega}(\omega)\right|_{\omega=\omega_p} = 0 \quad \text{for } r = 1, 2, \ldots, \frac{n-1}{2} + 1\end{aligned} \tag{5.13}$$

The derivatives in (5.12) and (5.13) are obtained by deriving $F_n(\omega)$ in (5.9) and (5.11). However, from (5.1), (5.2) and (5.3), it is clear that $f_n(t) = tf_{n-1}(t)$ for odd n. Consequently, $F_n(\omega)$ in (5.11) can be expressed as $F_n(\omega) = dF_{n-1}(\omega)/d\omega$. Since $n - 1$ is even, the derivatives in (5.13) can also be obtained by deriving $F_n(\omega)$ in (5.9). It follows

$$\begin{aligned}\frac{d^r F_n(\omega)}{d^r \omega} &= \frac{d^r}{d^r \omega}\left(\sqrt{\pi}\left[\sum_{m=0}^{L/2}(-1)^m 2^{-2m} a_m H_{2m}\left(\frac{\omega}{2}\right)\right]e^{-(\omega/2)^2}\right) \\ &= \sqrt{\pi}\sum_{m=0}^{L/2}(-1)^m 2^{-2m} a_m \frac{d^r}{d^r \omega}\left(H_{2m}\left(\frac{\omega}{2}\right)e^{-(\omega/2)^2}\right)\end{aligned} \tag{5.14}$$

assuming $L = n$ for an even n, and $L = n - 1$ for an odd n. By applying general Leibniz rule for rth derivative of a product [42], it follows

$$\frac{d^r}{d^r \omega}\left(H_{2m}\left(\frac{\omega}{2}\right)e^{-(\omega/2)^2}\right) = \sum_{q=0}^{r}\binom{r}{q}\frac{d^{r-q}}{d^{r-q}\omega}\left(e^{-(\omega/2)^2}\right)\frac{d^q}{d^q \omega}H_{2m}\left(\frac{\omega}{2}\right) \tag{5.15}$$

Furthermore, using (2.2) the first term in the sum in (5.15) can be written as

$$\frac{d^{r-q}}{d^{r-q}\omega}e^{-(\omega/2)^2} = (-1)^{(r-q)}\left(\frac{1}{2}\right)^{(r-q)} H_{r-q}\left(\frac{\omega}{2}\right)e^{-(\omega/2)^2} \tag{5.16}$$

By using (2.3) the second term in the sum takes the form

$$\frac{d^q}{d^q \omega}H_{2m}\left(\frac{\omega}{2}\right) = \frac{(2m)!}{(2m-q)!}H_{2m-q}\left(\frac{\omega}{2}\right) \tag{5.17}$$

By substituting (5.16) and (5.17) and (5.17) into (5.15), and (5.15) into (5.14), the derivatives of $F_n(\omega)$ in (5.9) are obtained as

$$\begin{aligned}&\frac{d^r F_n(\omega)}{d^r \omega} = \\ &\sqrt{\pi}\left[\sum_{m=0}^{L/2}(-1)^m 2^{-2m} a_m \sum_{q=0,q\le 2m}^{k}\binom{k}{q}\left(-\frac{1}{2}\right)^{k-q}\frac{(2m)!}{(2m-q)!}H_{2m-q}\left(\frac{\omega}{2}\right)H_{k-q}\left(\frac{\omega}{2}\right)\right]e^{-(\omega/2)^2}\end{aligned} \tag{5.18}$$

where $k = r$ for an even n, and $k = r + 1$ for an odd n.

5.3 Optimum polynomials

It is known that $a_0 = 1/\sqrt{\pi}$ for $n = 0$ and $a_0 = -\sqrt{2e/\pi}$ for $n = 1$. Note that for $n = 1$ ω_p is derived from setting $F_1^{(1)}(\omega_p) = 0$ in (5.18) as $\omega_p = \sqrt{2}$. For $n > 1$, the optimum coefficients are found by using the following procedure. By substituting (5.18) into (5.12) or (5.13), a system of equations can be formed. By using $\mathbf{a} = [a_0, a_1, ..., a_{L/2}]^T$ as the vector of coefficients, the system can be written in a matrix form as

$$\mathbf{Aa} = \mathbf{b} \tag{5.19}$$

where $\mathbf{A} \in \Re^{M\times(L/2+1)}$, $\mathbf{b} \in \Re^{M}$, $M = L/2 + 1$ for an even n, and $M = L/2 + 2$ for an odd n. The elements of matrix $\mathbf{A} = [A_{u,v}]$ are given by

$$A_{u,v} = \begin{cases} (-1)^{v-1} 2^{-2(v-1)} \sum\limits_{\substack{q=0,\\ q\le v-1}}^{u-1} \binom{2u-2}{2q} 2^{-2(u-q-1)} \dfrac{(2v-2)!}{(2v-2q-2)!} H_{2v-2q-2}(0) H_{2u-2q-2}(0) & \text{for even } n \\ (-1)^{v-1} 2^{-2(v-1)} \sum\limits_{\substack{q=0,\\ q\le 2(v-1)}}^{u} \binom{u}{q} 2^{-(u-q)} \dfrac{(2v-2)!}{(2v-q-2)!} H_{2v-q-2}\left(\dfrac{\omega_p}{2}\right) H_{u-q}\left(\dfrac{\omega_p}{2}\right) & \text{for odd } n \end{cases} \tag{5.20}$$

and vector $\mathbf{b}$ is obtained as

$$\mathbf{b} = \begin{cases} \left[\dfrac{1}{\sqrt{\pi}} \quad 0, \quad \ldots, \quad 0\right]^T & \text{for even } n \\ \left[-\dfrac{2e^{\omega_p^2/4}}{\sqrt{\pi}} \quad 0, \quad \ldots, \quad 0\right]^T & \text{for odd } n \end{cases} \tag{5.21}$$

For even n, the system in (5.19) is formed assuming $\omega_p = 0$. Earlier, the coefficient a_0 is derived for $n = 0$. Now, by using (5.19), (5.20) and (5.21) and assuming $\omega_p = 0$, coefficients for

$n = 2$ are calculated as $a_0 = 3/2\sqrt{\pi}$ and $a_1 = -1/\sqrt{\pi}$. Generally, the solution of the system in (5.19) for an arbitrary even n is obtained in a closed form as

$$a_m = \begin{cases} \dfrac{1}{\sqrt{\pi}} \dfrac{(-1)^m \prod_{i=m+1}^{n/2} (2i+1)}{2^{n/2-m}\,(n/2-m)!\,m!} & \text{for } m = 0, 1, ..., \dfrac{n}{2}-1 \\ \dfrac{1}{\sqrt{\pi}} \dfrac{(-1)^m}{m!} & \text{for } m = \dfrac{n}{2} \end{cases} \tag{5.22}$$

The optimum coefficients a_m for even order polynomials are given in Table 5.1.

Table 5.1 Coefficients of optimum weighting polynomials, a_m, for even n [53].

n	$\mathbf{a} = [a_0, a_1, ..., a_{n/2}]$, for even n
0	$\mathbf{a} = \dfrac{1}{\sqrt{\pi}}$
2	$\mathbf{a} = \dfrac{1}{\sqrt{\pi}}\left[\dfrac{3}{2}, -1\right]$
4	$\mathbf{a} = \dfrac{1}{\sqrt{\pi}}\left[\dfrac{15}{8}, -\dfrac{5}{2}, \dfrac{1}{2}\right]$
6	$\mathbf{a} = \dfrac{1}{\sqrt{\pi}}\left[\dfrac{35}{16}, -\dfrac{35}{8}, \dfrac{7}{4}, -\dfrac{1}{6}\right]$
8	$\mathbf{a} = \dfrac{1}{\sqrt{\pi}}\left[\dfrac{315}{128}, -\dfrac{105}{16}, \dfrac{63}{16}, -\dfrac{3}{4}, \dfrac{1}{24}\right]$
10	$\mathbf{a} = \dfrac{1}{\sqrt{\pi}}\left[\dfrac{693}{256}, -\dfrac{1155}{128}, \dfrac{231}{32}, -\dfrac{33}{16}, \dfrac{11}{48}, -\dfrac{1}{120}\right]$

For odd n, ω_p is not known in advance. Therefore, it is considered as a design variable. Fortunately, its value can be found by using the direct search. In this search ω_p increases from 1e–5 in steps of 1e–5. For each ω_p, the system $\mathbf{Qa} = \mathbf{c}$ is formed, where $\mathbf{Q}$ and $\mathbf{c}$ consist of the first $L/2 + 1$ rows in $\mathbf{A}$ and $\mathbf{b}$. For a given ω_p, this system is linear, and its solution is obtained as $\mathbf{a} = \mathbf{Q}^{-1}\mathbf{c}$. Then, the solution is applied to calculate the left-hand side of the last equation in (5.19), as in [53]

$$D_n(\omega_p) = \begin{bmatrix} A_{M,1} & A_{M,2} & \cdots & A_{M,L/2+1} \end{bmatrix} \mathbf{a} \tag{5.23}$$

The optimum ω_p and, consequently, the optimum **a** are achieved for ω_p which results in $D_n(\omega_p) \approx 0$. Note that because of imposing flatness at $-\omega_p$ as well as at ω_p, an additional degree of flatness can only be achieved by increasing the polynomial order by 4, that is, for polynomials with $n = 1, 5, 9, 13$, etc. The optimum polynomial coefficients for $n = 1, 5, 9, 13, 17$, and 21 and the corresponding ω_p are given in Table 5.2.

The magnitude spectra and waveforms of optimum polynomially-weighted Gaussian pulses obtained for various even and odd n are shown in Figures 5.1 and 5.2. As expected, increasing n causes an increase in the bandwidth. Note that the pulses with $n = 2$ and $n = 5$, the pulses with $n = 4$ and $n = 9$, etc. exhibit the same degrees of flatness. Clearly, all pulses are well localized in time, even for high-order polynomials.

Table 5.2 Coefficients of optimum weighting polynomials a_m and corresponding frequencies ω_p, for odd n [53].

n	**a** = $[a_0, a_1, ..., a_{n/2}]$, for odd n	ω_p [rad/s]
1	**a** = [–1.31549]	$\sqrt{2}$
5	**a** = [–2.91916, 2.48477, $-5.72622\cdot10^{-1}$]	2.05287
9	**a** = [–4.53910, 7.73062, –4.41539, $9.02059\cdot10^{-1}$, $-6.24122\cdot10^{-2}$]	2.53720
13	**a** = [–6.16308, 15.7481, –14.3618, 5.63520, –1.05548, $9.17657\cdot10^{-2}$, $-3.02457\cdot10^{-3}$]	2.94326
17	**a** = [–7.78862, 26.5392, –33.2489, 19.2006, –5.81973, $9.73749\cdot10^{-1}$, $-9.00278\cdot10^{-2}$, $4.28795\cdot10^{-3}$, $-8.24614\cdot10^{-5}$]	3.29987
21	**a** = [–9.41494, 40.1044, –63.9146, 48.6727, –20.3458, 5.01133, $-7.53235\cdot10^{-1}$, $6.94380\cdot10^{-2}$, $-3.81480\cdot10^{-3}$, $1.14299\cdot10^{-4}$, $-1.43897\cdot10^{-6}$]	3.62159

An example of MATLAB code implementing the procedure for obtaining the peak frequencies, ω_p, polynomial coefficients, **a**, pulse's waveform, $f_n(t)$, and amplitude spectrum, $F_n(\omega)$, is given by Algorithm 5.1. The function is called *maxflatgauss*. Its input parameters are the order of polynomial, n, the vector of time points in s, t, and the vector of frequency points in rad/s, w. The function *maxflatgauss* calls the function *hermitepoly* which is given by Algorithm 3.2.

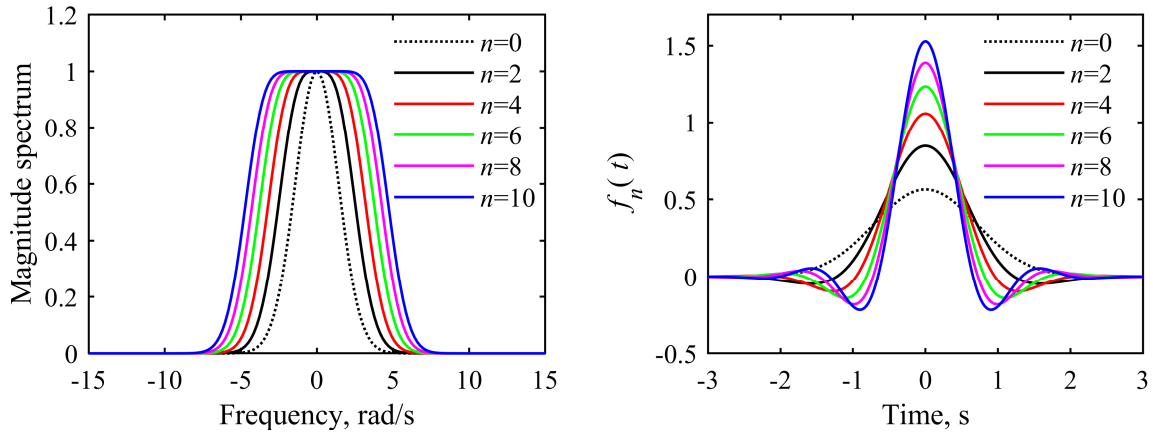

Figure 5.1 Magnitude spectra (left) and waveforms (right) of optimum polynomially-weighted Gaussian pulses obtained for even n [53].

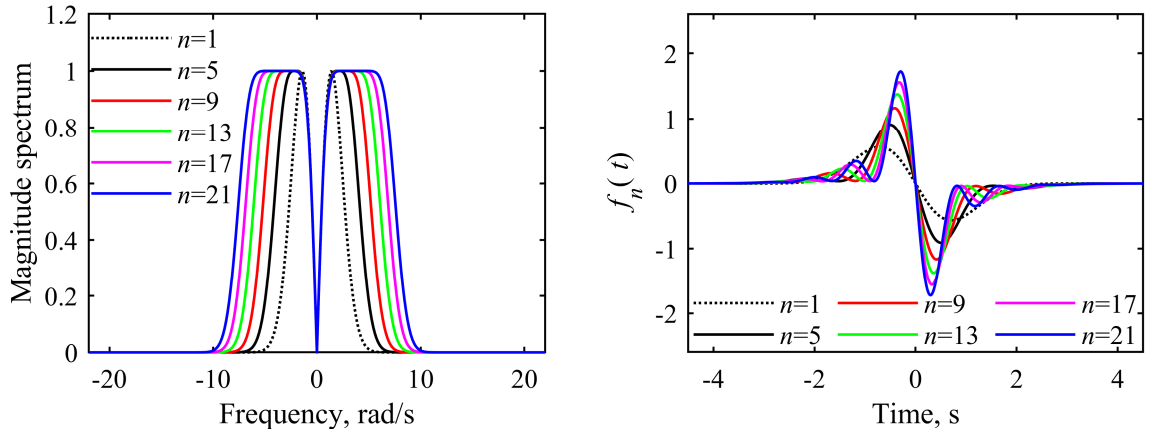

Figure 5.2 Magnitude spectra (left) and waveforms (right) of optimum polynomially-weighted Gaussian pulses obtained for odd n [53].

Algorithm 5.1 Design of maximally flat Gaussian pulse of order n.

```
function [wp,a,fn,Fn]=maxflatgauss(n,t,w)

if mod(n,2)==0, L=n/2;
else L=(n-1)/2;
end

% Optimum polynomial coefficients and peak frequencies
if n==0, wp=0; a=1/sqrt(pi);
elseif n==1, wp=sqrt(2); a=-sqrt(2*exp(1)/pi);
elseif mod(n,2)==0 % even n
 wp=0; a=zeros(n/2+1,1);
 for m=0:(n/2)
  if m==n/2, a(m+1)=(-1)^m/prod(1:m);
  else a(m+1)=(-1)^m*prod(2*m+3:2:n+1)/2^(n/2-m)/prod(1:n/2-m)/prod(1:m);
 end, end
 a=1/sqrt(pi)*a;
else % odd n
```

```
 if n==3,      wp=1.94333; elseif n==5,  wp=2.05287;
 elseif n==7,  wp=2.47976; elseif n==9,  wp=2.53720;
 elseif n==11, wp=2.91217; elseif n==13, wp=2.94326;
 elseif n==15, wp=3.28477; elseif n==17, wp=3.29987;
 elseif n==21, wp=3.62159;
 else error('The required n is not supported.');
 end
 % system of linear equations Aa=b
 A=zeros(L+1,L+1);
 for u=1:L+1, for v=1:L+1
   S=0;
   for k=0:(u-1)
    if k<=2*v-1
     S=S+prod(u-k:u-1)/prod(1:k)*(-1/2)^(u-k-1)*...
       prod(2*v-k:2*v-1)*hermitepoly(2*v-k-1,wp/2)*hermitepoly(u-k-1,wp/2);
    end, end
   A(u,v)=(-1)^(v-1)*2^(-2*(v-1))*S;
 end, end
 b=[-2/sqrt(pi)/exp(-(wp/2)^2); zeros(L,1)];
 % the system's solution
 a=A\b;
end

% Waveform fn(t)
if isempty(t), fn=[];
else g0=exp(-t.^2); pn=zeros(size(t));
 for m=0:L
  if mod(n,2)==0, pn=pn+a(m+1)*t.^(2*m);
  else pn=pn+a(m+1)*t.^(2*m+1);
 end, end
 fn=pn.*g0;
end

% Amplitude spectrum Fn(w)
if isempty(w), Fn=[];
else F=zeros(size(w));
 if mod(n,2)==0 % even n
  b=zeros(L+1,1);
  for m=0:L
   if m==L, b(m+1)=2^(-m)/prod(1:m);
   else b(m+1)=prod(2*m+3:2:n+1)/2^L/prod(1:L-m)/prod(1:m);
  end, end
  for m=0:L, F=F+2^(-m)*b(m+1)*hermitepoly(2*m,w/2); end
  F=1/sqrt(pi)*F;
 else % odd n
  for m=0:L
   F=F+(-1)^(m+1)*2^(-(2*m+1))*a(m+1)*hermitepoly(2*m+1,w/2);
 end, end
 Fn=sqrt(pi)*F.*exp(-(w/2).^2);
end
```

For example, the design of the maximally flat Gaussian pulse with $n = 10$ is given by the following call

```
n=10; t=linspace(-3,3,1001); w=linspace(-10,10,1001);
[wp,a,fn,Fn]=maxflatgauss(n,t,w);
figure, plot(t,fn); figure, plot(w,Fn);
```

5.4 Pulse shaping

To perform pulse shaping, the baseband pulse $f_n(t)$ is first transformed into a bandpass pulse $s_n(t)$. Then, $s_n(t)$ is scaled to fit its spectrum into a desired part of the spectral mask. This part is given by

$$P(\omega)=\begin{cases} A_L & \text{for} \quad \omega=\omega_L \\ C & \text{for} \quad \omega_L<\omega<\omega_U \\ A_U & \text{for} \quad \omega=\omega_U \end{cases} \tag{5.24}$$

where A_L, A_U, and C are magnitude limits whereas ω_L and ω_U are the lower and the upper band-edge frequency. To obtain the bandpass pulse, ω_p is transposed to some frequency ω_s, where $\omega_s > \omega_p$.

For pulse $f_n(t)$ synthesized by even order polynomial this transposition is obtained by forming $s_n(t)$ as a double-sideband signal

$$s_n(t)=f_n(t)\cos(\omega_s t) \tag{5.25}$$

Note that the pulse in (5.25) does not satisfy the requirement for zero DC [26]. This requirement is fulfilled by subtracting scaled version of the original pulse $f_n(t)$ rather than by subtracting a constant, thus preserving pulse's time localization. This technique is known from the wavelet theory, where it is used to implement the admissibility criterion [54]. Then, the expression in (5.25) becomes

$$s_n(t)=\frac{2f_n(t)\left[\cos(\omega_s t)-F_n(\omega_s)\right]}{1-2F_n^2(\omega_s)+F_n(2\omega_s)} \tag{5.26}$$

where $F_n(\omega_s)$ and $F_n(2\omega_s)$ are calculated by using (5.9). The amplitude spectrum of the pulse in (5.26) is given by

$$S_n(\omega)=\frac{F_n(\omega-\omega_s)+F_n(\omega+\omega_s)-2F_n(\omega_s)F_n(\omega)}{1-2F_n^2(\omega_s)+F_n(2\omega_s)} \tag{5.27}$$

Note that the denominator in (5.26) ensures $S_n(\omega_s) = 1$.

For pulse $f_n(t)$ synthesized by odd order polynomial, $s_n(t)$ is formed as an upper-sideband signal. Its canonical representation is given by [55]

$$s_n(t) = f_n(t)\cos(\omega_u t) - \hat{f}_n(t)\sin(\omega_u t) \tag{5.28}$$

where $\hat{f}_n(t)$ is the Hilbert transform of $f_n(t)$, $\omega_u = \omega_s - \omega_p$ and $\omega_u \neq 0$. The amplitude spectrum of the pulse in (5.28) is given by

$$S_n(\omega) = \frac{1}{2}\left\{\left[1+\text{sgn}(\omega-\omega_u)\right]F_n(\omega-\omega_u) + \left[1-\text{sgn}(\omega+\omega_u)\right]F_n(\omega+\omega_u)\right\} \tag{5.29}$$

The Hilbert transform of $f_n(t)$ is given by

$$\hat{f}_n(t) = \mathcal{H}\left\{\sum_{m=0}^{(n-1)/2} a_m t^{2m+1} e^{-t^2}\right\} = \sum_{m=0}^{(n-1)/2} a_m \mathcal{H}\left\{t^{2m+1} e^{-t^2}\right\} \tag{5.30}$$

The transform in (5.30) can be expressed in a closed form by following the procedure described in Section 4.3. It results in

$$\hat{f}_n(t) = f_n(t)\,\text{erfi}(t) + \frac{1}{\sqrt{\pi}} \sum_{m=0}^{(n-1)/2} a_m t^{2m} \sum_{q=0}^{m} \frac{2^{-q}}{t^{2q}} \prod_{i=0}^{q} (2i-1) \tag{5.31}$$

This expression is not defined for $t = 0$. Since $\hat{f}_n(t)$ for an odd n is an even function, the value of $\hat{f}_n(0)$ needs to be calculated. The Hilbert transform of $f_n(t)$ at $t = 0$ is

$$\hat{f}_n(0) = \frac{1}{\pi} P.V. \int_{-\infty}^{\infty} \frac{f_n(\tau)}{-\tau} d\tau = -\frac{1}{\pi} P.V. \int_{-\infty}^{\infty} \frac{f_n(\tau)}{\tau} d\tau \tag{5.32}$$

The integrand in (5.32) can be expressed as

$$\frac{f_n(t)}{t} = \sum_{m=0}^{(n-1)/2} a_m t^{2m} e^{-t^2} = f_{n-1}(t) \tag{5.33}$$

where $f_{n-1}(t)$ is an even function. Then, $\hat{f}_n(0)$ can be expressed as

$$\hat{f}_n(0) = -\frac{1}{\pi} P.V. \int_{-\infty}^{\infty} f_{n-1}(\tau) d\tau \tag{5.34}$$

Note that expression under the integral represents the Fourier transform of $f_{n-1}(t)$ calculated at $\omega = 0$. It follows

$$\hat{f}_n(0) = -\frac{1}{\pi} F_{n-1}(0) \tag{5.35}$$

where $F_{n-1}(\omega)$ takes the form as in (5.9). Finally, $\hat{f}_n(0)$ is equal to

$$\hat{f}_n(0) = -\frac{1}{\sqrt{\pi}} \sum_{m=0}^{(n-1)/2} (-1)^m 2^{-2m} a_m H_{2m}(0) \tag{5.36}$$

As elaborated in Section 5.3, the spectrum $F_n(\omega)$ is maximally flat at $\omega = \omega_p$. For an odd n, $S_n(\omega)$ is also maximally flat at $\omega = \omega_s$, assuming $\omega_u = \omega_s - \omega_p$. For an even n, $S_n(\omega)$ is approximately maximally flat, what is a consequence of overlapping the tails in the left- and the right-hand side of $S_n(\omega)$. However, such overlapping is negligible if $\omega_s > \omega_c$, where $\omega_c > 0$ is the band edge frequency of $F_n(\omega)$. For practical purposes, ω_c is estimated as the frequency at which $F_n(\omega) = 1e{-}2$. For $n = 0, 2, 4, 6, 8$, and 10, ω_c is obtained as 4.29194 rad/s, 5.15300 rad/s, 5.79861 rad/s, 6.33881 rad/s, 6.81312 rad/s, and 7.24113 rad/s.

The scaling of $s_n(t)$ is performed as

$$w_n(t) = \frac{C}{\tau} s_n\left(\frac{t}{\tau}\right) \tag{5.37}$$

where C and τ are amplitude and bandwidth scaling factors. The amplitude spectrum of $w_n(t)$ is given by

$$W_n(\omega) = C\, S_n(\omega\tau) \tag{5.38}$$

Note that, as a consequence of scaling, spectrum's peak is moved from ω_s to $\omega_w = \omega_s/\tau$. In addition, $W_n(0) = 0$ and $W_n(\omega_w) = C$.

The scaling ensures mapping the appropriate baseband frequencies ω_1 and ω_2 of $F_n(\omega)$ onto ω_L and ω_U. The values of ω_1 and ω_2 are obtained by solving the equations $F_n(\omega) = A_L/C$ and $F_n(\omega) = A_U/C$. It is clear from Figures 5.1 and 5.2 that two solutions for ω_1 as well as for ω_2 exist. These solutions have opposite signs for even n and positive sign for odd n. The choice is made $\omega_1 < 0$ and $\omega_2 > 0$ in the former, and $\omega_1 < \omega_2$ in the latter case. Finally, the values of τ and ω_w are obtained as

$$\tau = \frac{\omega_2 - \omega_1}{\omega_U - \omega_L} \tag{5.39}$$

$$\omega_w = \omega_U - \frac{\omega_2 - \omega_p}{\tau} \tag{5.40}$$

An example of MATLAB code implementing the procedure for obtaining the values of τ and ω_w, as well as the UWB pulse's waveform, $w_n(t)$, and amplitude spectrum, $W_n(\omega)$, is given by Algorithm 5.2. The function is called *uwbdesign_maxflatgauss*. Its input parameters are the order of polynomial, n, baseband frequencies, ω_1 and ω_2, the lower and the upper band-edge frequency of UWB region, f_L and f_U, the magnitude limit, C, vector of time points in s, t, and vector of frequency points in rad/s, w. The function *uwbdesign_maxflatgauss* calls the function *translated_maxflatgauss* which calculates $s_n(t)$ and $S_n(\omega)$, the function *ht_maxflatgauss* which calculates $\hat{f}_n(t)$, and the function *hermitepoly* which is given by Algorithm 3.2.

Algorithm 5.2 Design of UWB flat-spectrum Gaussian pulse of order n.

```
function [tau,fw,wn,Wn]=uwbdesign_maxflatgauss(n,w1,w2,fL,fU,C,t,w)

wp=maxflatgauss(n,[],[]);
tau=(w2-w1)/(2*pi*(fU-fL));
fw=fU+(wp-w2)/2/pi/tau;
ws=2*pi*fw*tau;
[sn,Sn]=translated_maxflatgauss(n,tau,ws,t,w);
wn=C*sn/tau; Wn=C*Sn/tau;

function [sn,Sn]=translated_maxflatgauss(n,tau,ws,t,w)

[wp,a,fn,Fn]=maxflatgauss(n,t/tau,w*tau);
Fn=tau*Fn;

if mod(n,2)==0 % even n
 % calculation of Fn(ws) and Fn(2ws)
 Fn_ws=0; Fn_2ws=0;
 for m=0:n/2
  Fn_ws=Fn_ws+(-1)^m*2^(-2*m)*a(m+1)*hermitepoly(2*m,ws/2);
  Fn_2ws=Fn_2ws+(-1)^m*2^(-2*m)*a(m+1)*hermitepoly(2*m,2*ws/2);
 end
 Fn_ws=sqrt(pi)*Fn_ws.*exp(-(ws/2).^2);
 Fn_2ws=sqrt(pi)*Fn_2ws.*exp(-(2*ws/2).^2);
 % waveform sn(t)
 sn=2*fn.*(cos(ws*t/tau)-Fn_ws)/(1-2*Fn_ws^2+Fn_2ws);
 % amplitude spectrum Sn(w)
 Fm=zeros(size(w)); Fp=zeros(size(w));
 for m=0:n/2
  Fm=Fm+(-1)^m*2^(-2*m)*a(m+1)*hermitepoly(2*m,(w*tau-ws)/2);
  Fp=Fp+(-1)^m*2^(-2*m)*a(m+1)*hermitepoly(2*m,(w*tau+ws)/2);
 end
 Fnm=sqrt(pi)*tau*Fm.*exp(-((w*tau-ws)/2).^2);
 Fnp=sqrt(pi)*tau*Fp.*exp(-((w*tau+ws)/2).^2);
 Sn=(Fnm+Fnp-2*Fn_ws*Fn)/(1-2*Fn_ws^2+Fn_2ws);
```

```
else % odd n
 % waveform sn(t)
 fnht=ht_maxflatgauss(n,a,t/tau);
 wu=ws-wp;
 sn=fn.*cos(wu*t/tau)-fnht.*sin(wu*t/tau);
 % amplitude spectrum Sn(w)
 Fm=zeros(size(w)); Fp=zeros(size(w));
 for m=0:(n-1)/2
  Fm=Fm+(-1)^(m+1)*2^(-(2*m+1))*a(m+1)*hermitepoly(2*m+1,(w*tau-wu)/2);
  Fp=Fp+(-1)^(m+1)*2^(-(2*m+1))*a(m+1)*hermitepoly(2*m+1,(w*tau+wu)/2);
 end
 Fnm=sqrt(pi)*tau*Fm.*exp(-((w*tau-wu)/2).^2);
 Fnp=sqrt(pi)*tau*Fp.*exp(-((w*tau+wu)/2).^2);
 Sn=1/2*(1+sign(w*tau-wu)).*Fnm+sign(wu)/2*(1-sign(w*tau+wu)).*Fnp;
end

function fnht=ht_maxflatgauss(n,a,t)
% Hilbert transform of Gaussian
ght=exp(-t.^2).*erfi(t);
% Hilbert transform of fn(t~=0)
fnht=zeros((size(t)));
for m=0:(n-1)/2
 fnht=fnht+a(m+1)*(t.^(2*m+1).*ght);
 for k=0:m
  Q=zeros(1,k);
  for q=0:k
   Q(1,q+1)=(2*q-1);
  end
  fnht=fnht+a(m+1)*t.^(2*m-2*k)*1/2^k/sqrt(pi)*prod(Q);
 end
end
% Hilbert transform of fn(t==0)
ind=find(t==0); fnht(ind)=0;
for m=0:(n-1)/2
 fnht(ind)=fnht(ind)+(-1)^m*2^(-2*m)*a(m+1)*hermitepoly(2*m,0);
end
fnht(ind)= -1/sqrt(pi)*fnht(ind);
```

5.5 FCC-compliant flat-spectrum Gaussian pulses

To illustrate the proposed design, several pulses that fill the FCC indoor and outdoor mask are presented. The pulses are shaped to fit the UWB region between $f_L = 3.1$ GHz and $f_U = 10.6$ GHz. In both masks, this region is bounded by the points that are 10 dB and 20 dB below the highest power spectral density (PSD), which equals –41.3 dBm/MHz. Therefore, the band-edge frequencies and upper magnitude limit in (5.24) are set to $\omega_L = 2\pi f_L$, $\omega_U = 2\pi f_U$, and $C = 8.610\text{e}{-3}$. For the outdoor mask, $A_L = A_U = 8.610\text{–}4$ is applied. For the indoor mask, $A_L = A_U = 2.723\text{e}{-3}$ is used for all n except for $n = 0$, 2, and 4. For these values of n, the pulses obtained do not meet the mask in the GPS band. Therefore, for $n = 0$, 2, and 4 the lower band edge is changed to $\omega_L = 2\pi f_{GPS}$, where $f_{GPS} = 1.61$ GHz, and $A_L = 1.718\text{e}{-4}$. For these values of ω_L and ω_U, the baseband frequencies ω_1 and ω_2 of $F_n(\omega)$ are given in Tables 5.3 and 5.4.

Table 5.5 provides numerical values of the obtained f_w and τ for various n. In addition, pulse's spectral efficiency and relative energy concentration are calculated as in (1.1) and (1.2) respectively. The energy concentration is calculated for $T = 0.5$ ns. As expected, an increase in n results in the increase of spectral efficiency. Clearly, a significant increase is achieved already for $n = 2$ and $n = 5$. In addition, since the indoor mask is less restrictive than the outdoor, the FCC-compliant indoor pulses exhibit higher efficiency. High energy concentration is obtained in all cases. The waveforms and the corresponding power spectral densities of the pulses compliant with the indoor and the outdoor FCC mask are shown in Figures 5.3 and 5.4 for even n, and in Figures 5.5 and 5.6 for odd n.

Table 5.3 Baseband frequencies ω_1 and ω_2 of $F_n(\omega)$ for even n.

n	indoor mask		outdoor mask	
	ω_1, rad/s	ω_2, rad/s	ω_1, rad/s	ω_2, rad/s
0	–3.95697	2.14597	–3.03486	
2	–4.83186	3.07546	–3.94448	
4	–5.48442	3.75506	–4.61404	
6	–4.31682		–5.16945	
8	–4.80646		–5.65459	
10	–5.24615		–6.09087	
12	–5.64862		–6.49064	
14	–6.02195		–6.86176	$\omega_2 = -\omega_1$
16	–6.37170		–7.20964	
18	–6.70182	$\omega_2 = -\omega_1$	–7.53817	
20	–7.01529		–7.85026	
30	–8.39871		–9.22874	
40	–9.57410		–10.4010	
50	–10.6141		–11.4388	
60	–11.5569		–12.3798	

Table 5.4 Baseband frequencies ω_1 and ω_2 of $F_n(\omega)$ for odd n.

n	indoor mask		outdoor mask	
	ω_1, rad/s	ω_2, rad/s	ω_1, rad/s	ω_2, rad/s
1	0.27648	3.12721	0.08593	3.90855
5	0.27281	4.59877	0.08444	5.36934
9	0.27150	5.68046	0.08393	6.44342
13	0.27084	6.57604	0.08368	7.33375
17	0.27044	7.35725	0.08353	8.11107
21	0.27017	8.05908	0.08343	8.80989

Table 5.5 Parameters and properties of FCC-compliant flat-spectrum Gaussian pulses. Properties are highlighted in bold [53].

	indoor mask				outdoor mask			
n	f_w, GHz	τ, ns	η, %	λ, %	f_w, GHz	τ, ns	η, %	λ, %
0	7.439	0.1080	**40.4**	**> 99.99**	6.850	0.1288	**41.2**	**> 99.99**
2	7.103	0.1400	**53.0**	**99.90**	6.850	0.1674	**53.5**	**99.74**
4	6.946	0.1636	**59.6**	**99.90**	6.850	0.1958	**60.0**	**99.50**
6	6.850	0.1832	**76.1**	**99.92**	6.850	0.2194	**64.2**	**99.37**
8	6.850	0.2040	**78.4**	**99.87**	6.850	0.2400	**67.2**	**99.28**
10	6.850	0.2227	**80.1**	**99.82**	6.850	0.2585	**69.6**	**99.21**
20	6.850	0.2977	**85.0**	**99.48**	6.850	0.3332	**76.4**	**98.98**
30	6.850	0.3565	**87.4**	**99.17**	6.850	0.3917	**79.9**	**98.77**
40	6.850	0.4063	**89.0**	**98.90**	6.850	0.4414	**82.2**	**98.59**
50	6.850	0.4505	**90.0**	**98.68**	6.850	0.4855	**83.8**	**98.42**
60	6.850	0.4905	**90.8**	**98.50**	6.850	0.5254	**85.0**	**98.28**
1	6.093	0.0605	**58.2**	**99.73**	5.706	0.0811	**44.5**	**99.41**
5	6.186	0.0918	**69.6**	**99.32**	5.893	0.1121	**57.8**	**98.74**
9	6.242	0.1148	**75.0**	**99.09**	5.993	0.1350	**64.4**	**98.36**
13	6.279	0.1338	**78.3**	**98.95**	6.058	0.1539	**68.6**	**98.16**
17	6.306	0.1504	**80.5**	**98.83**	6.105	0.1704	**71.6**	**98.03**
21	6.327	0.1653	**82.2**	**98.74**	6.141	0.1852	**73.8**	**97.94**

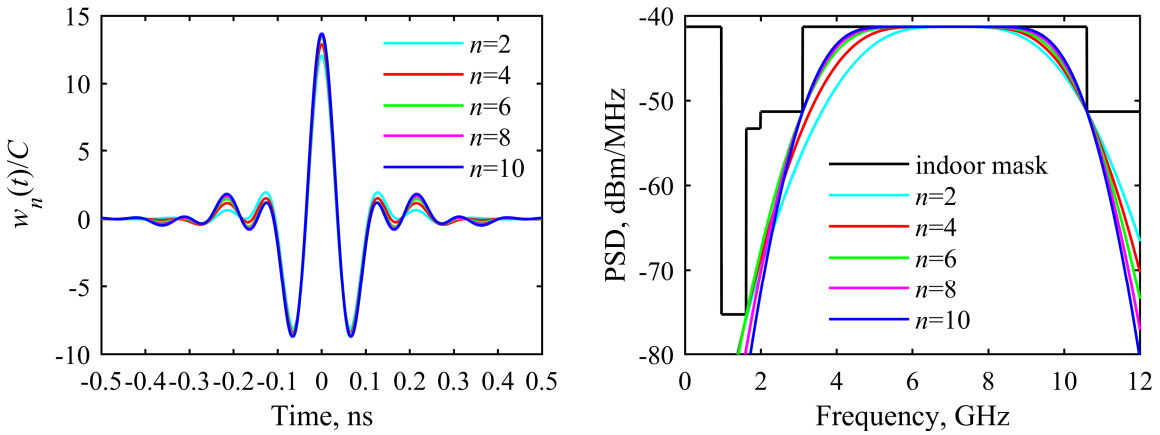

Figure 5.3 Waveforms (left) and power spectral densities (right) of flat-spectrum Gaussian pulses with even n, obtained for FCC indoor mask.

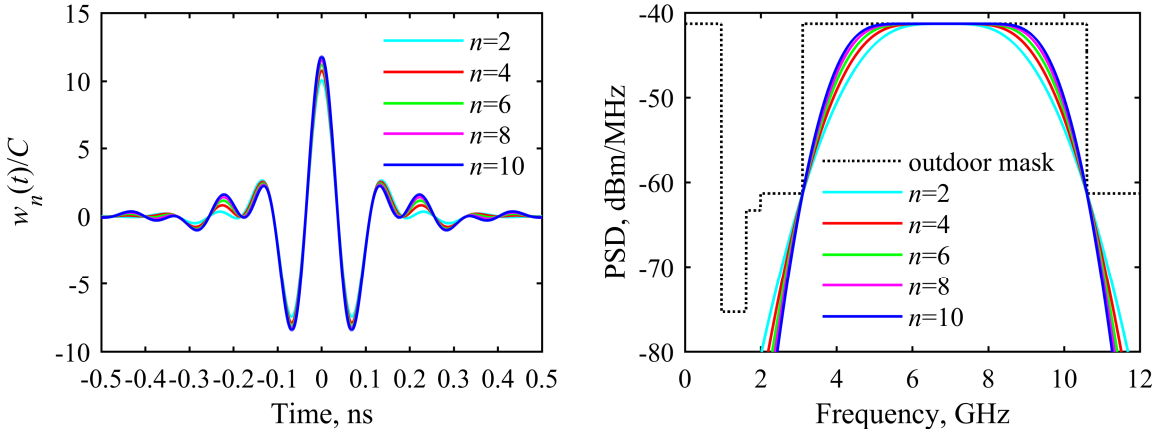

Figure 5.4 Waveforms (left) and power spectral densities (right) of flat-spectrum Gaussian pulses with even n, obtained for FCC outdoor mask.

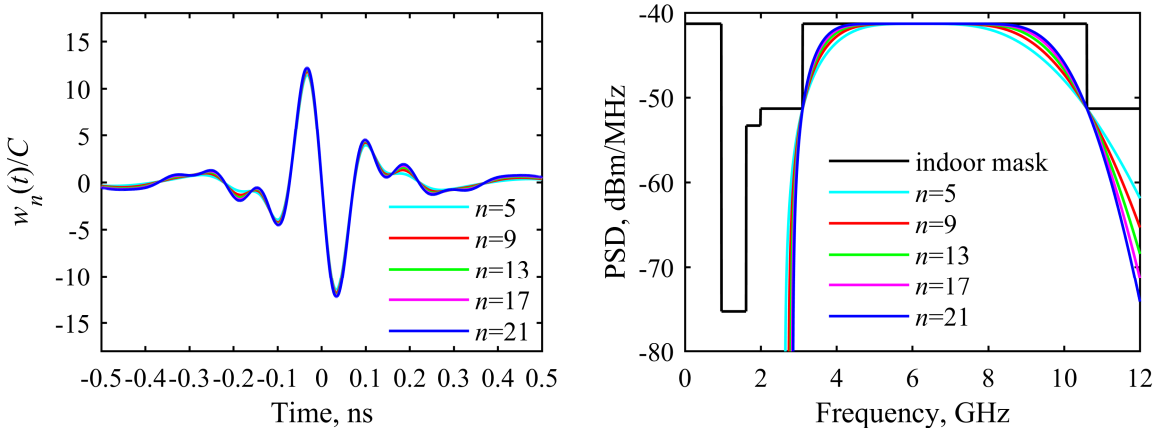

Figure 5.5 Waveforms (left) and power spectral densities (right) of flat-spectrum Gaussian pulses with odd n, obtained for FCC indoor mask.

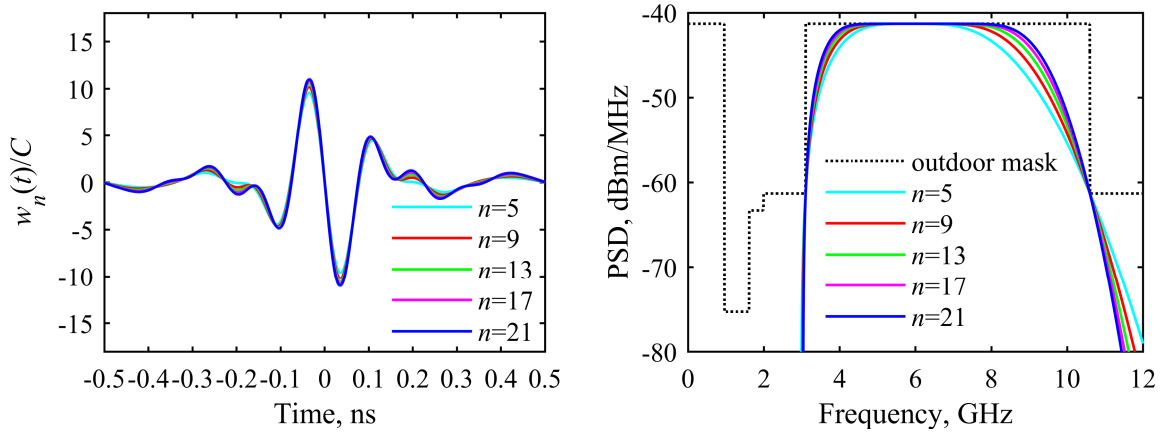

Figure 5.6 Waveforms (left) and power spectral densities (right) of flat-spectrum Gaussian pulses with odd n, obtained for FCC outdoor mask.

The spectral efficiency greater than 90 % is achieved for the indoor mask and even n, where $n \geq 50$. The waveforms and PSDs for $n = 60$ obtained for both masks are illustrated in Figure 5.7.

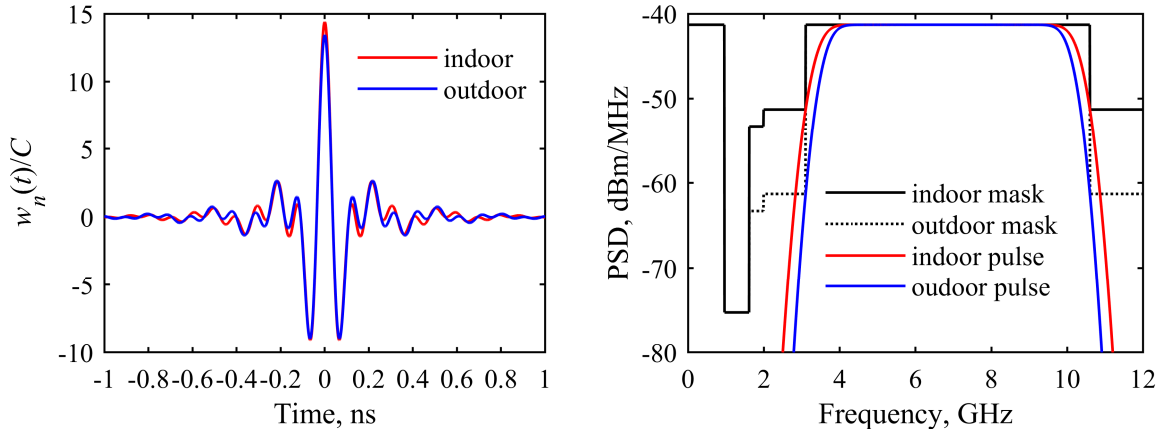

Figure 5.7 Waveforms (left) and power spectral densities (right) of FCC compliant flat-spectrum Gaussian pulses obtained for $n = 60$ [53].

Using Algorithm 5.2, the design of FCC-compliant indoor pulse with $n = 4$ is given by the call

```
n=4; w1=-5.48442; w2=3.75506; fL=1.61; fU=10.6; C=8.61e-3;
t=linspace(-0.5,0.5,1001); f=linspace(0,12,1001); w=2*pi*f;
[tau,fw,wn,Wn]=uwbdesign_maxflatgauss(n,w1,w2,fL,fU,C,t,w);
figure, plot(t,wn/C);
figure, plot(f,20*log10(abs(Wn)),'g',f,fccmask(f,'indoor'),'r');
axis([f(1) f(end) -80 -40]);
```

The design of the FCC-compliant indoor pulse with $n = 60$ is given by the call

```
n=60; w1=-11.55686; w2=-w1; fL=3.1; fU=10.6; C=8.61e-3;
t=linspace(-1,1,1001); f=linspace(0,12,1001); w=2*pi*f;
[tau,fw,wn,Wn]=uwbdesign_maxflatgauss(n,w1,w2,fL,fU,C,t,w);
figure, plot(t,wn/C);
figure, plot(f,20*log10(abs(Wn)),'g',f,fccmask(f,'indoor'),'r');
axis([f(1) f(end) -80 -40]);
```

The design of the FCC-compliant outdoor pulse with $n = 5$ is given by the call

```
n=5; w1=0.08444; w2=5.36934; fL=3.1; fU=10.6; C=8.61e-3;
t=linspace(-0.5,0.5,1001); f=linspace(0,12,1001); w=2*pi*f;
[tau,fw,wn,Wn]=uwbdesign_maxflatgauss(n,w1,w2,fL,fU,C,t,w);
figure, plot(t,wn/C);
figure, plot(f,20*log10(abs(Wn)),'g',f,fccmask(f,'outdoor'),'r');
axis([f(1) f(end) -80 -40]);
```

5.6 Comparison with other FCC-compliant pulses

To illustrate features of the proposed method, several examples of the designed pulses that fill the FCC masks are described. First, the original Gaussian derivatives which fill the indoor and the outdoor mask with maximum efficiencies, obtained for $n = 4$ and $n = 7$, are compared with optimum flat-spectrum Gaussian pulses having $n = 2$ and $n = 5$. Their PSDs and waveforms are shown in Figure 5.8. It is clear that the proposed pulses fill the UWB region more tightly.

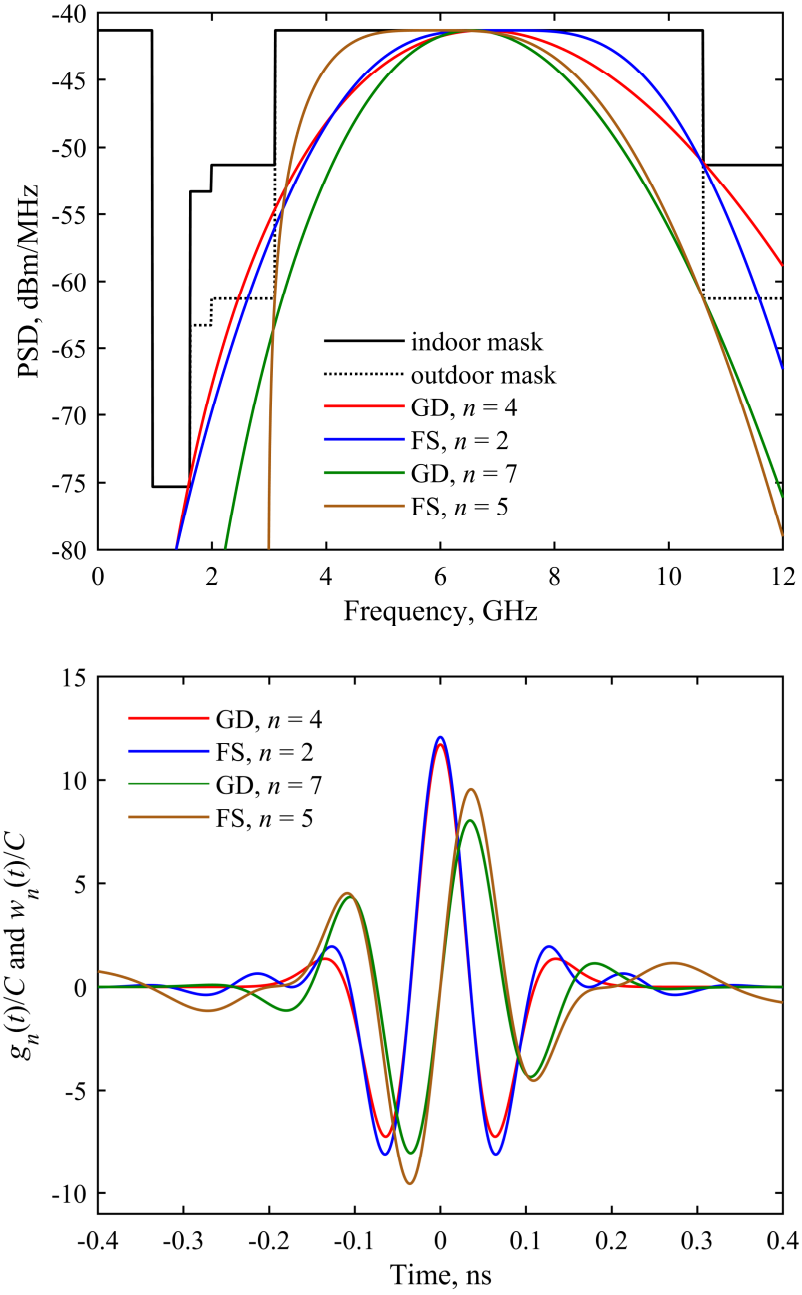

Figure 5.8 Power spectral densities (up) and waveforms (down) of *n*th Gaussian derivatives (GD) [9] and *n*th order flat-spectrum Gaussian pulses (FS) [53].

In the second example, the sixth-order flat-spectrum Gaussian pulse is compared with a linear combination of three translated Gaussian pulses [34], both filling the FCC indoor mask. The PSDs and waveforms of the pulses are shown in Figure 5.9. Both pulses are very well localized in time. However, somewhat better filling of the UWB region is encountered in the proposed pulse.

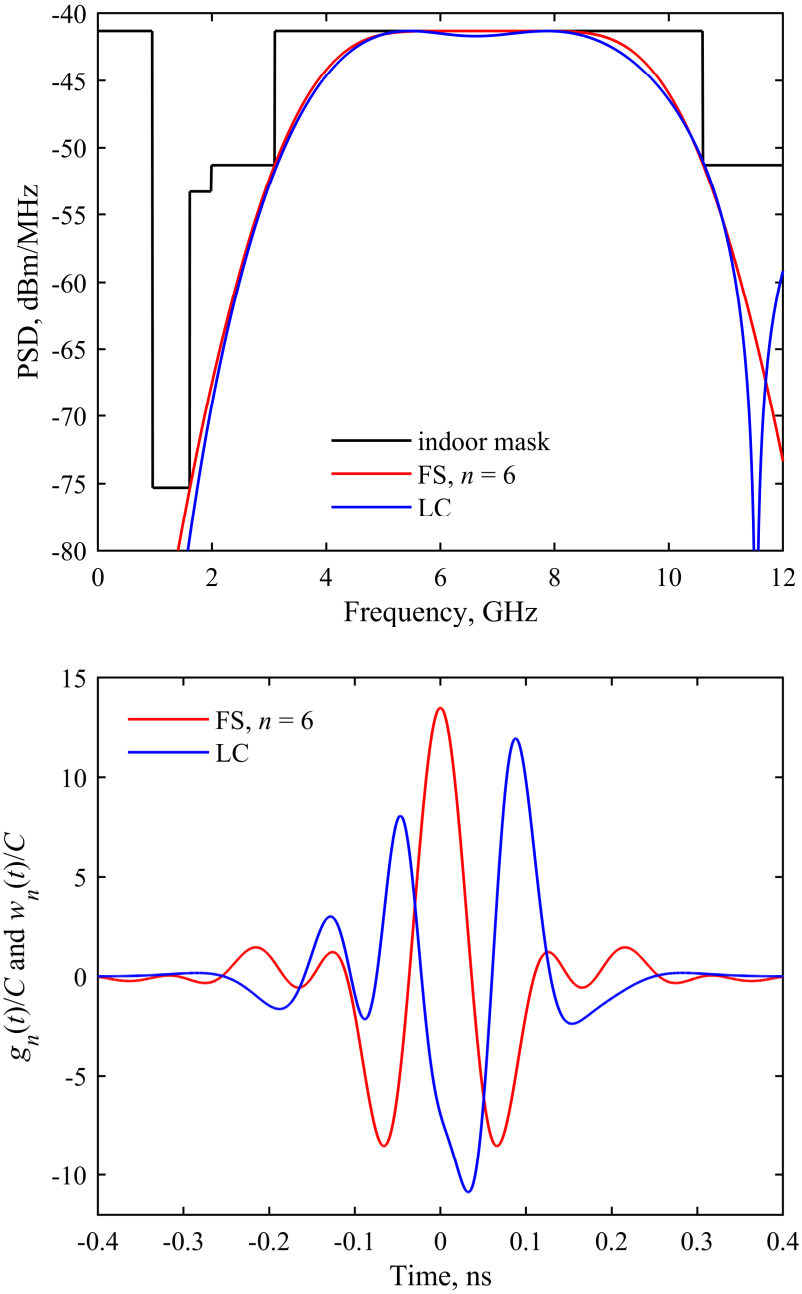

Figure 5.9 Power spectral densities (up) and waveforms (down) of sixth-order flat-spectrum Gaussian pulse (FS) and linear combination of one sixth-order and two seventh-order Gaussian derivatives (LC) [53].

In the last example, the proposed flat-spectrum Gaussian pulses are compared with the sharpened Gaussian derivatives [48]. The flat-spectrum pulses with $n = 20$ and $n = 21$ are considered, filling the indoor and the outdoor mask, respectively. They are compared with the sharpened second and first Gaussian derivatives with $p = 8$. The PSDs and waveforms of these pulses are shown in Figure 5.10. All pulses exhibit high spectral efficiency and energy

concentration. However, for the indoor mask, better results are obtained for the flat-spectrum pulse, whereas for the outdoor mask, the sharpened Gaussian derivative is favorable.

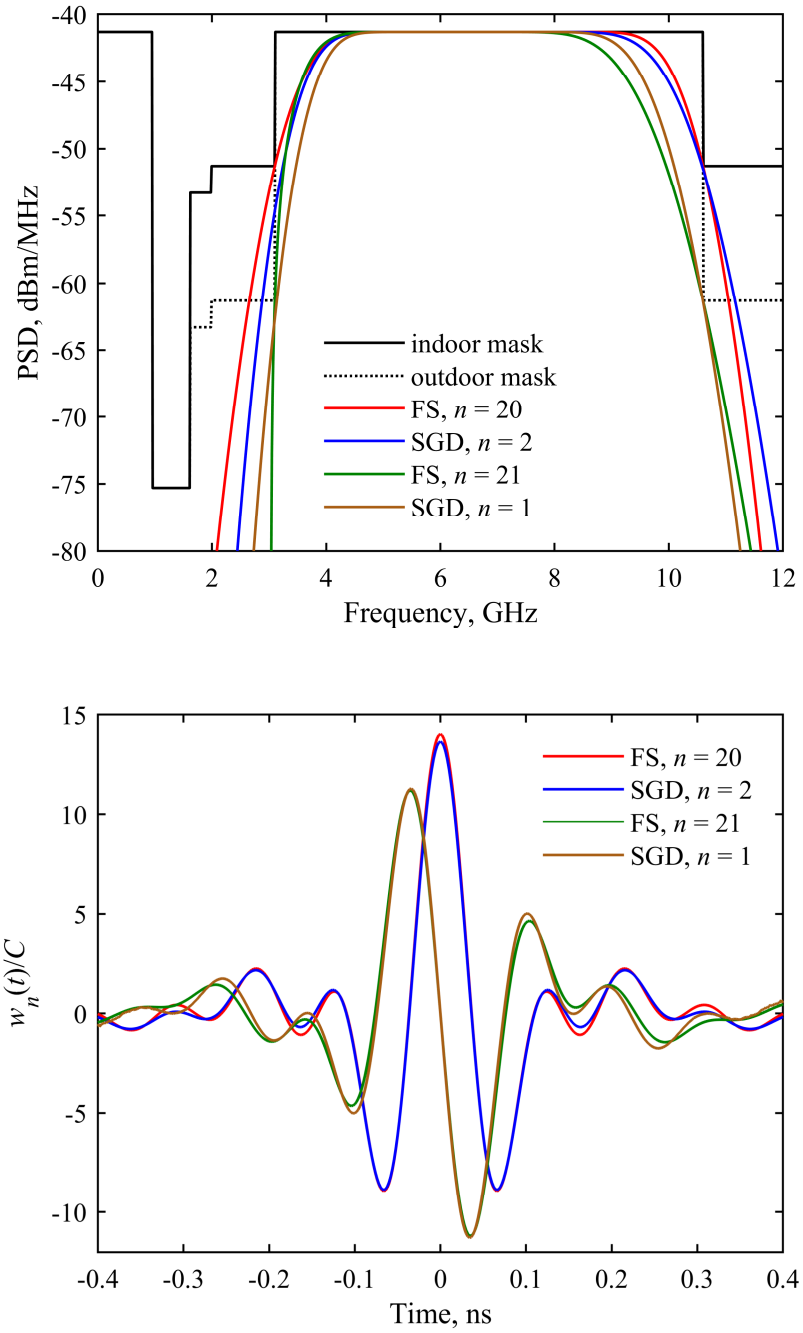

Figure 5.10 Power spectral densities (up) and waveforms (down) of *n*th-order flat-spectrum Gaussian pulses (FS) and sharpened *n*th Gaussian derivatives (SGD) obtained for $p = 8$.

Table 5.6 shows the spectral efficiency and energy concentration of the pulses from [9], [20], [31], [32], [34], optimally sharpened Gaussian derivative with $n = 1$ and $p = 8$, as well as optimal flat-spectrum Gaussian pulses with $n = 20$, $n = 40$ and $n = 20$, all obtained for the FCC indoor mask. The flat-spectrum Gaussian pulses reach the efficiency of 90.8 % with the concentration of 98.5 %.

Table 5.6 Comparison of various sinc-based and Gaussian-based pulses with flat-spectrum Gaussian pulses. All pulses are compliant with FCC indoor mask.

	Pulse	η, %	λ, %
Sinc	Translated and truncated sinc pulse [20]	98.9	95.82
	Linear combination of three translated sinc pulses [31]	82.6	98.53
Gaussian	Fourth Gaussian derivative [9]	54.3	>99.99
	Linear combination of Gaussian derivatives [34]	72.0	99.97
	Linear combination of three translated Gaussians [31]	77.5	99.78
	Linear combination of eight translated Gaussians [32]	82.8	99.56
	Sharpened Gaussian derivative with $n = 1$ and $p = 8$	83.2	99.11
	Flat-spectrum Gaussian, $n = 20$	85.0	99.48
	Flat-spectrum Gaussian, $n = 40$	89.0	98.90
	Flat-spectrum Gaussian, $n = 60$	90.8	98.50

6. TRANSFER FUNCTIONS OF FCC-COMPLIANT PULSE SHAPERS

As shown in Figure 1.2, UWB pulses are formed by shaping filters called pulse shapers. In this chapter, the synthesis of pulse shapers whose impulse responses efficiently approximate ideal FCC-compliant UWB pulses is described. As a result of this synthesis, several sets of transfer functions are provided, which cover the approximations of the original and sharpened Gaussian derivatives as well as the approximations of modified Hermite, prolate-spheroidal, and flat-spectrum-Gaussian pulses.

6.1 Time-domain synthesis based on least squares approximation

The time-domain synthesis of pulse shaper approximates an ideal pulse $p(t)$ with the impulse response of a causal continuous-time filter. To ensure causality, $p(t)$ should be delayed and zeroed for $t < 0$, thus forming a desired impulse response

$$h_d(t) = \begin{cases} p(t - t_d) & \text{for} \quad t \geq 0 \\ 0 & \text{for} \quad t < 0 \end{cases} \tag{6.1}$$

where t_d is the delay. The objective is to design a filter whose impulse response approximates the response in (6.1) in the least-squares sense. Therefore, the approximation error is given by

$$\varepsilon(\mathbf{x}) = \int_0^{T_U} \left[h(t, \mathbf{x}) - h_d(t) \right]^2 dt \tag{6.2}$$

where $h(t, \mathbf{x})$ is filter's impulse response, $\mathbf{x}$ is the vector of filter's parameters, and T_U is high enough to ensure $h(t, \mathbf{x}) \approx 0$ and $h_d(t) \approx 0$ for $t > T_U$.

The filter parameters that minimize error in (6.2) can be found by solving the problem

$$\hat{\mathbf{x}} = \arg\min_{\mathbf{x}} \left[\varepsilon(\mathbf{x}) \right] \tag{6.3}$$

To solve the problem in (6.3), the method proposed in [56] is used. In the method referred to, the function $\varepsilon(\mathbf{x})$ is approximated as

$$\varepsilon(\mathbf{x}) \approx T_s \sum_{q=0}^{Q} \left[h\left(t_q, \mathbf{x}\right) - h_d\left(t_q\right) \right]^2 \tag{6.4}$$

where $h(t, \mathbf{x})$ and $h_d(t)$ are evaluated on uniformly spaced grid $t_q = qT_s$, $q = 0, ..., Q$, with $T_s = T_U/Q$. The method deals with the zero-pole-gain model of the filter, thus enabling simple control of filter stability. The optimum parameters are found by iterative procedure in which a second-order cone program is solved in each iteration.

To apply the method in [56], the value of t_d should be known in advance. For a given T_U, t_d is chosen to ensure that $h_d(t)$ contains at least 99.9 % of the total energy of $p(t)$, as in

$$\int_0^{\infty} h_d^2\left(t\right) dt \geq 0.999 \int_{-\infty}^{\infty} p^2\left(t\right) dt \tag{6.5}$$

Clearly, the condition in (6.5) determines a lower bound for t_d. Its exact value can be found experimentally. The experiments show that this value is placed near this bound.

6.2 Zero-pole-gain model of pulse shaper

The transfer function of an Nth order filter with M zeros is given by

$$H(s) = H_0 \frac{\prod_{i=1}^{M_1} \left(s - z_i\right)}{\prod_{k=1}^{N_1} \left(s - p_k\right)} \tag{6.6}$$

where H_0 is the gain constant, and p_k and z_i denote transfer function poles and zeros. If the poles are simple and $M < N$, the impulse response $h(t)$ can be obtained as

$$h(t) = \sum_{r=1}^{N} K_r e^{p_r t} \quad \text{for } t \geq 0 \tag{6.7}$$

where K_r; $r = 1, ..., N$; are pole residues given by

$$K_r = H_0 \frac{\prod_{i=1}^{M}(p_r - z_i)}{\prod_{k=1,k\neq r}^{N}(p_r - p_k)} \tag{6.8}$$

Since the filter is uniquely described by p_k, z_i, and H_0, these parameters represent the components of **x**. To form **x** as a real vector, complex pairs of the poles and the zeros are described by their real and imaginary parts. If the transfer function contains M_1 real zeros, M_2 complex zeros, M_3 imaginary zeros, N_1 real poles, and N_2 complex poles, where $M_1+M_2+M_3=M$ and $N_1+N_2=N$, then **x** can be defined as [56]

$$\begin{aligned}\mathbf{x} = \big[& H_0, \\ & z_1,...,z_{M_1}, \alpha_1, \beta_1,...,\alpha_{M_2/2}, \beta_{M_2/2}, \gamma_1,...,\gamma_{M_3/2}, \\ & p_1,...,p_{N_1}, \sigma_1, \omega_1,...,\sigma_{N_2/2}, \omega_{N_2/2} \big]^T\end{aligned} \tag{6.9}$$

where α_i, β_i, γ_k, σ_l, and ω_l are real and imaginary parts of complex zeros and poles, as given in

$$z_{M_1+i} = \alpha_i + j\beta_i; \quad z^*_{M_1+i} = \alpha_i - j\beta_i; \quad i = 1,...,M_2/2 \tag{6.10}$$

$$z_{M_1+M_2+k} = j\gamma_k; \quad z^*_{M_1+M_2+k} = -j\gamma_k; \quad k = 1,...,M_3/2 \tag{6.11}$$

$$p_{N_1+l} = \sigma_l + j\omega_l; \quad p^*_{N_1+l} = \sigma_l - j\omega_l; \quad l = 1,...,N_2/2 \tag{6.12}$$

The procedure in [56] requires the appropriate value of **x** as an optimization starting point. The choice of the starting point is not critical, provided it describes a stable filter [56]. However, the convergence rate can be significantly reduced if the starting point is far from the optimum. Furthermore, since the transfer function in (6.6) vanishes for $H_0 = 0$, it is recommended to start the optimization with H_0 of the appropriate sign or run the optimizations for both signs [56].

6.3 Spectral efficiency and energy concentration of impulse response

The spectral efficiency of $h(t)$ in the UWB region $f_L \le f \le f_U$ is obtained as

$$\eta = \frac{\int_{f_L}^{f_U} |H(f)|^2 \, df}{\int_{f_L}^{f_U} M(f) \, df} \tag{6.13}$$

where $|H(f)|$ is filter's magnitude response and $M(f)$ is PSD mask. Since $M(f) = C^2$ for $f_L < f < f_U$, the denominator in (6.13) equals $C^2(f_U - f_L)$. The integral in the numerator can be expressed as

$$\int_{f_L}^{f_U} |H(f)|^2 \, df = \frac{E(\omega_c)\big|_{\omega_c = 2\pi f_U} - E(\omega_c)\big|_{\omega_c = 2\pi f_L}}{2} \tag{6.14}$$

where $E(\omega_c)$ denotes the total energy of the filter's response to a sinc pulse occupying the band $-\omega_c \le \omega \le \omega_c$. This energy is given by [57]

$$E(\omega_c) = -\frac{1}{j\pi} \sum_{r=1}^{N} K_r \left(\sum_{q=1}^{N} \frac{K_q}{p_r + p_q} \right) \ln \frac{-p_r + j\omega_c}{-p_r - j\omega_c} \tag{6.15}$$

The energy concentration of $h(t)$ in the interval $0 \le t \le T$ is obtained as

$$\lambda = \frac{1}{e_h} \int_0^T h^2(t) \, dt \tag{6.16}$$

where e_h is the total energy of $h(t)$, given by [58]

$$e_h = \int_0^\infty h^2(t) \, \mathrm{d}t = -\sum_{r=1}^{N} \sum_{q=1}^{N} \frac{K_r K_q}{p_r + p_q} \tag{6.17}$$

By using (6.7), the integral in (6.16) is calculated as

$$\begin{aligned}\int_0^T h^2(t)dt &= \int_0^T \sum_{r=1}^{N} K_r e^{p_r t} \sum_{q=1}^{N} K_q e^{p_q t} \\ &= \sum_{r=1}^{N}\sum_{q=1}^{N} K_r K_q \int_0^T e^{\left(p_r+p_q\right)t} dt \\ &= \sum_{r=1}^{N}\sum_{q=1}^{N} \frac{K_r K_q}{p_r+p_q}\left(e^{\left(p_r+p_q\right)T}-1\right)\end{aligned} \tag{6.18}$$

The expression in (6.17) is recognized as a part of (6.18). Consequently, the energy of $h(t)$ occupying the interval $0 \le t \le T$ can be simplified as

$$\int_0^T h^2(t)dt = e_h + \sum_{r=1}^{N}\sum_{q=1}^{N} \frac{K_r K_q}{p_r+p_q} e^{(p_r+p_q)T} \tag{6.19}$$

6.4 Optimum pulse shapers

In this section, the optimum transfer functions approximating FCC-compliant Gaussian derivatives, modified Hermite pulses, prolate spheroidal wave functions, sharpened Gaussian derivatives, and flat-spectrum Gaussian pulses are provided. All transfer functions are obtained by minimizing the error in (6.4), assuming $Q = 2000$. For each transfer function, the spectral efficiency and energy concentration of its impulse response, calculated for $f_L = 3.1$ GHz, $f_U = 10.6$ GHz, and $T = 2t_d$, are provided. Finally, the time axis is normalized to 1 ns. Consequently, the zeros and poles are normalized to 1 Grad/s.

6.4.1 Pulse shapers forming Gaussian derivatives

The pulse shapers forming nth-order Gaussian derivative were obtained by approximating $p(t) = w_n(t)$, where $w_n(t)$ is given in (3.8), and by utilizing $T_U = 10\tau$. The optimum zeros, poles, and gain constants for $n = 4$, 5, 6, and 7 are given in Tables 6.1 and 6.2. For each n, the sixth- and eighth-order transfer function is obtained. In the tables, the spectral efficiencies and energy concentrations of the corresponding impulse responses are also given. The impulse response of eighth-order pulse shaper forming fourth-order Gaussian derivative is shown in Figure 6.1. Figure 6.2 and 6.3 show the power spectral densities of the impulse responses of the proposed sixth- and eighth-order pulse shapers for various derivative orders,

together with the FCC indoor mask. It is clear that the shapers are compliant with the mask in the UWB region. The only exception is the shaper with $N = 8$, $M = 4$ and $n=6$, where a small violation is encountered at the upper band edge. However, outside the UWB region, some violations occur in many cases. Nevertheless, all these violations are considered tolerable since the UWB antennas have bandpass responses which additionally filter the pulses [14], [15].

Figure 6.4 shows the impulse responses and the corresponding PSDs of the pulse shaper with $N = 6$ and $M = 4$ forming fourth-order Gaussian derivative and the elliptic pulse shaper having $N = 6$ and $M = 5$, which is proposed in [12]. Within the UWB region, the former shaper ensures $\eta = 50.8\%$, whereas the latter results in $\eta = 56.6\%$. Clearly, the elliptic shaper generates the pulse with higher spectral efficiency. However, this pulse exhibit poor time localization, which is a consequence of its sharp transition bands.

Table 6.1 Zeros, poles, and gain constants of various pulse shapers forming even order Gaussian derivatives, together with pulses' spectral efficiency and energy concentration [59].

$n = 4$ with $\tau = 0.06647$ ns and $t_d = 0.18688$ ns, $M = 4$ and $N = 6$		
z_i	$24.3772 \pm 63.6343j$, $4.41124 \pm 1.52466j$	$\eta = 50.8$ % $\lambda = 99.67$ %
p_k	$-7.05717 \pm 59.4434j$, $-8.17639 \pm 42.9447j$, $-6.84788 \pm 27.4355j$	
H_0	2.05990	
$n = 4$ with $\tau = 0.06647$ ns and $t_d = 0.18688$ ns, $M = 6$ and $N = 8$		
z_i	$13.3323 \pm 79.0313j$, $\pm 8.36727j$, 38.9955, 38.9955	$\eta = 55.6$ % $\lambda = 99.94$ %
p_k	$-9.05537 \pm 66.1232j$, $-10.7319 \pm 48.7615j$, $-10.4152 \pm 32.5719j$, $-9.67026 \pm 13.0463j$	
H_0	-6.46810	
$n = 6$ with $\tau = 0.07495$ ns and $t_d = 0.22071$ ns, $M = 3$ and $N = 6$		
z_i	$29.9416 \pm 47.8954j$, 2.39398	$\eta = 46.5$ % $\lambda = 99.50$ %
p_k	$-5.38548 \pm 60.6325j$, $-6.42499 \pm 47.1044j$, $-5.52264 \pm 33.9556j$	
H_0	-233.974	
$n = 6$ with $\tau = 0.07495$ ns and $t_d = 0.22071$ ns, $M = 4$ and $N = 8$		
z_i	$40.0656 \pm 57.1491j$, $\pm 14.3802j$	$\eta = 51.6$ % $\lambda = 99.88$ %
p_k	$-6.01416 \pm 65.1139j$, $-7.55214 \pm 51.7788j$, $-7.49202 \pm 39.0740j$, $-6.14528 \pm 26.0428j$	
H_0	-9207.52	

Table 6.2 Zeros, poles, and gain constants of various pulse shapers forming odd order Gaussian derivatives, together with pulses' spectral efficiency and energy concentration [59].

$n = 5$ with $\tau = 0.07212$ ns and $t_d = 0.20922$ ns, $M = 4$ and $N = 6$		
z_i	$23.2788 \pm 63.4835j$, 21.6042, 0	$\eta = 47.5$ % $\lambda = 99.61$ %
p_k	$-6.25793 \pm 59.9713j$, $-7.26166 \pm 45.1554j$, $-6.09085 \pm 31.1535j$	
H_0	5.20835	
$n = 5$ with $\tau = 0.07212$ ns and $t_d = 0.20922$ ns, $M = 5$ and $N = 8$		
z_i	$19.1303 \pm 71.3904j$, 12.9017, 0, 0	$\eta = 51.7$ % $\lambda = 99.93$ %
p_k	$-7.39071 \pm 65.7296j$, $-8.85083 \pm 50.9586j$, $-8.58172 \pm 37.4470j$, $-6.73907 \pm 24.1066j$	
H_0	296.149	
$n = 7$ with $\tau = 0.08061$ ns and $t_d = 0.23093$ ns, $M = 3$ and $N = 6$		
z_i	$20.7203 \pm 64.6888j$, 0	$\eta = 43.9$ % $\lambda = 99.33$ %
p_k	$-5.15940 \pm 63.5246j$, $-5.94215 \pm 50.4177j$, $-4.84870 \pm 38.1205j$	
H_0	−222.469	
$n = 7$ with $\tau = 0.08061$ ns and $t_d = 0.23093$ ns, $M = 4$ and $N = 8$		
z_i	$28.8548 \pm 74.8823j$, 1.62664, 1.62452	$\eta = 46.3$ % $\lambda = 99.93$ %
p_k	$-6.17274 \pm 67.1398j$, $-7.57758 \pm 54.5552j$, $-7.45103 \pm 42.8736j$, $-6.00026 \pm 31.3212j$	
H_0	−7052.51	

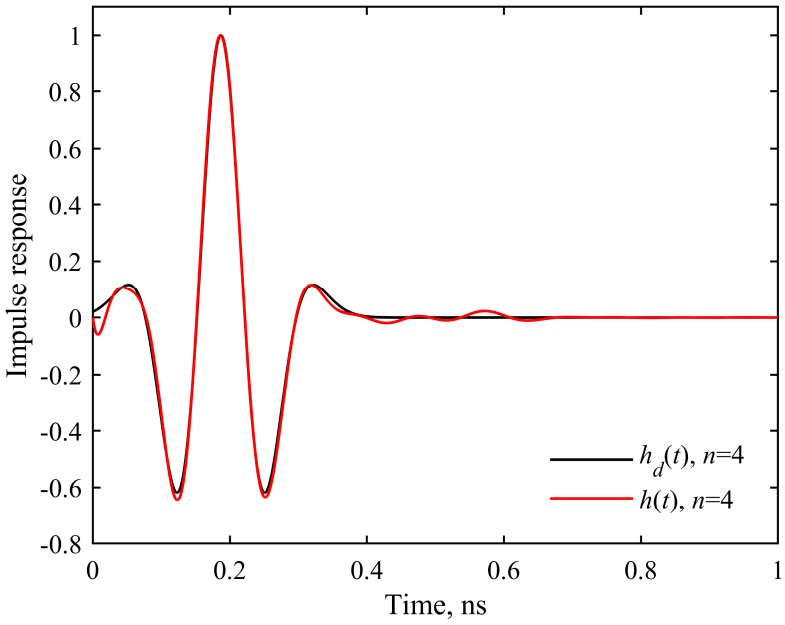

Figure 6.1 Desired impulse response of pulse shaper forming fourth-order Gaussian derivative and its approximation obtained by pulse shaper with $N = 8$ and $M = 6$.

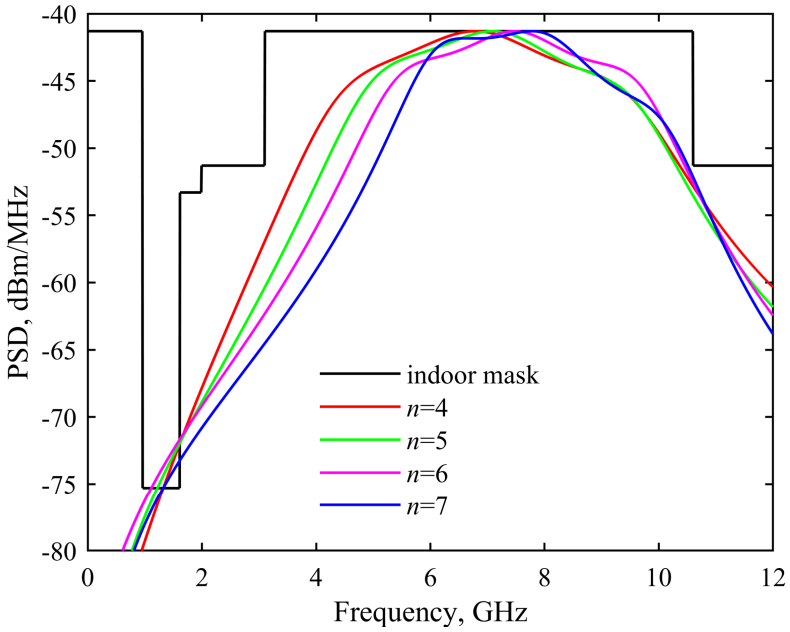

Figure 6.2 Power spectral densities of impulse responses approximating nth Gaussian derivatives obtained by shapers with $N = 6$, together with FCC indoor mask [59].

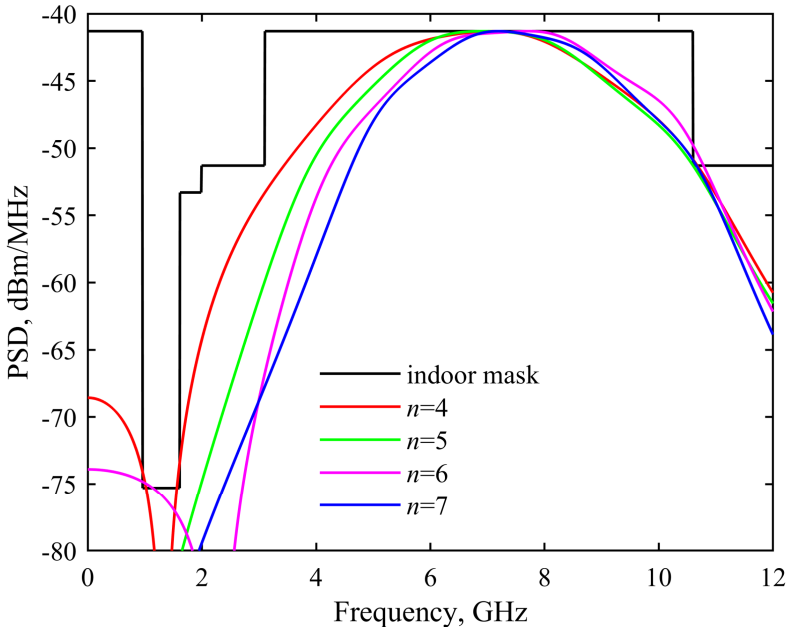

Figure 6.3 Power spectral densities of impulse responses approximating *n*th Gaussian derivatives obtained by shapers with $N = 8$, together with FCC indoor mask [59].

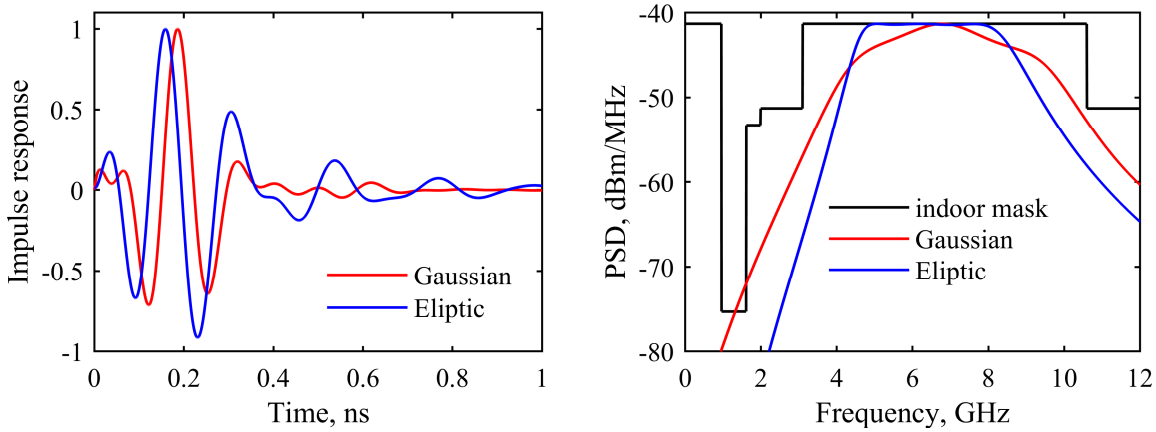

Figure 6.4 Impulse responses (left) and their power spectral densities (right) obtained for pulse shaper with $N = 6$ and $M = 4$ forming fourth Gaussian derivative and elliptic pulse shaper with $N = 6$ and $M = 5$ [12], [59].

6.4.2 Pulse shapers forming modified Hermite pulses

Pulse shapers whose impulse responses approximate modified-Hermite pulses with $n = 2$, 3, and 4, are considered. The were obtained with $p(t) = Cm_n(t)$, where $m_n(t)$ is given in (2.8), and by utilizing $T = 20\tau$. In addition, according to [17], the magnitude responses of the modified-Hermite pulses contain zeros. Therefore, in the approximations of these pulses, the transfer functions with imaginary zeros are used. The optimum zeros, poles, and gain constants of the obtained pulse shapers are given in Table 6.3, together with the obtained spectral efficiency and energy concentration. It should be noted that high order modified-Hermite pulses require higher transfer function's order.

Figure 6.5 shows the impulse response and the PSD obtained for the pulse shaper forming the fourth-order modified-Hermite pulse. It is clear that this shaper is not FCC compliant. It is expected since the ideal modified-Hermite pulses is also not FCC-compliant [9]. Therefore, the pulses obtained by the proposed pulse shapers require additional bandpass filtering.

Table 6.3 Zeros, poles, and gain constants of various pulse shapers forming nth-order modified-Hermite pulses, together with pulses' spectral efficiency and energy concentration [59].

$n = 2$ with $\tau = 0.05515$ ns and $t_d = 0.20074$ ns, $M = 4$ and $N = 6$		
z_i	$23.9001 \pm 44.3637j,\ \pm 12.4314j$	$\eta = 38.7$ % $\lambda = 99.58$ %
p_k	$-6.42630 \pm 39.6797j, -7.06111 \pm 24.3636j, -6.06555 \pm 7.56470j$	
H_0	1.78995	
$n = 3$ with $\tau = 0.06223$ ns and $t_d = 0.24734$ ns, $M = 6$ and $N = 8$		
z_i	$20.6618 \pm 39.4412j, \pm 19.5214j, \pm 0.99368j$	$\eta = 37.2$ % $\lambda = 99.06$ %
p_k	$-4.81876 \pm 39.7134j, -5.07600 \pm 27.0069j, -4.70509 \pm 13.2715j,$ $-1.78883 \pm 1.01560j$	
H_0	1.95497	
$n = 4$ with $\tau = 0.06647$ ns and $t_d = 0.28410$ ns, $M = 8$ and $N = 10$		
z_i	$\pm 75.9298j, 19.9731 \pm 46.1548j, \pm 24.8823j, \pm 7.80364j$	$\eta = 32.7$ % $\lambda = 99.93$ %
p_k	$-5.36191 \pm 49.7136j, -6.60265 \pm 38.5947j, -6.10334 \pm 27.7797j,$ $-6.25259 \pm 16.3914j, -5.90958 \pm 5.33935j$	
H_0	0.75294	

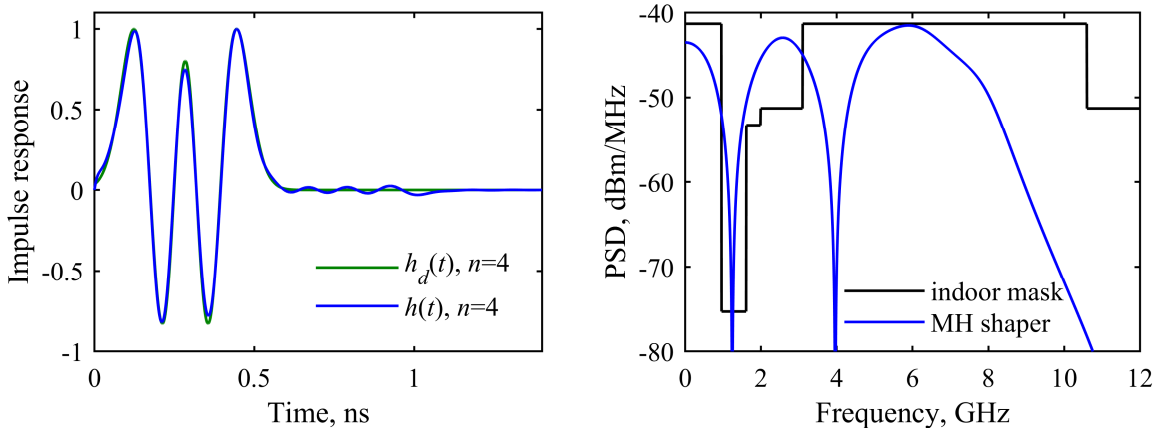

Figure 6.5 Desired impulse response of pulse shaper forming modified-Hermite indoor pulse with $n = 4$ and its approximation obtained by pulse shaper with $N = 6$ and $M = 8$ (left), and power spectral density of approximated pulse together with FCC indoor mask (right) [59].

6.4.3 Pulse shapers forming prolate spheroidal pulses

Pulse shapers forming prolate spheroidal pulses are designed for an orthogonal pair used in multiple access. However, due to generation imperfections, the generated pulses cannot be completely orthogonal. Therefore, a measure for the orthogonality of the generated pulses is required.

Let $H_1(s)$ and $H_2(s)$ denote the transfer functions of the pulse shapers whose impulse responses approximate ψ_1 and ψ_2. Assuming $H_1(s)$ and $H_2(s)$ contain N_1 and N_2 poles, as well as M_1 and M_2 zeros, they are given by

$$H_1(s) = H_{01} \frac{\prod_{i=1}^{M_1} (s - z_i)}{\prod_{k=1}^{N_1} (s - p_k)} \tag{6.20}$$

$$H_2(s) = H_{02} \frac{\prod_{i=1}^{M_2} (s - c_i)}{\prod_{k=1}^{N_2} (s - d_k)} \tag{6.21}$$

where H_{01} and H_{02} are gain constants, z_i and c_i are transfer function zeros, and p_k and d_k are transfer function poles. If the poles are simple, $M_1 < N_1$, and $M_2 < N_2$, the impulse responses are obtained as

$$h_1(t) = \sum_{r=1}^{N_1} K_r e^{(p_r t)} \quad \text{for } t \geq 0 \tag{6.22}$$

$$h_2(t) = \sum_{n=1}^{N_2} A_n e^{(d_n t)} \quad \text{for } t \geq 0 \tag{6.23}$$

where K_r and A_n are pole residues given by

$$K_r = H_{01} \frac{\prod_{i=1}^{M_1} (p_r - z_i)}{\prod_{k=1, k \neq r}^{N_1} (p_r - p_k)} \tag{6.24}$$

$$A_n = H_{02} \frac{\prod_{i=1}^{M_2} (d_n - c_i)}{\prod_{k=1, k \neq n}^{N_2} (d_n - d_k)} \tag{6.25}$$

Assuming perfect synchronization, the measure for orthogonality of the impulse responses $h_1(t)$ and $h_2(t)$ is defined via their normalized cross-correlation calculated for the zero lag, as in [60]

$$\mu = \left. \frac{(h_1 \circ h_2)(\tau)}{\sqrt{e_1 e_2}} \right|_{\tau=0} \tag{6.26}$$

where

$$(h_1 \circ h_2)(\tau) = \int_0^{\infty} h_1(t) h_2(t+\tau) \mathrm{d}t \tag{6.27}$$

and e_1 and e_2 denote the total energies of impulse responses $h_1(t)$ and $h_2(t)$. These energies are given by [58]

$$e_1 = \int_0^{\infty} h_1^2(t)\,\mathrm{d}t = -\sum_{r=1}^{N_1}\sum_{q=1}^{N_1}\frac{K_r K_q}{p_r + p_q} \tag{6.28}$$

$$e_2 = \int_0^{\infty} h_2^2(t)\,\mathrm{d}t = -\sum_{n=1}^{N_2}\sum_{k=1}^{N_2}\frac{A_n A_k}{d_n + d_k} \tag{6.29}$$

It can be shown that for simple poles located in the left half-plane of the complex plane, the cross-correlation in (6.27) takes the form [60]

$$\left(h_1 \circ h_2\right)(\tau) = -\sum_{r=1}^{N_1}\sum_{n=1}^{N_2}\frac{K_r A_n}{p_r + d_n} e^{(d_n \tau)} \tag{6.30}$$

By substituting (6.30) into (6.26), analytic expression for the measure of orthogonality is obtained as [60]

$$\mu = -\frac{1}{\sqrt{e_1 e_2}}\sum_{r=1}^{N_1}\sum_{n=1}^{N_2}\frac{K_r A_n}{p_r + d_n} \tag{6.31}$$

It is clear that highly orthogonal pulses have $\mu \approx 0$.

The time-domain synthesis of prolate-spheroidal pulse shapers approximates delayed pulses ψ_1 and ψ_2 by using causal impulse responses in (6.22) and (6.23). Since the ideal pulses are zero outside the interval $-T_P/2 \le t \le T_P/2$, the desired impulse responses take the forms [18]

$$h_{d1}(t) = \begin{cases} \psi_1\left(t - \dfrac{T_P}{2}\right) & \text{for} \quad 0 \le t \le T_P \\ 0 & \text{for} \quad \text{otherwise} \end{cases} \tag{6.32}$$

$$h_{d2}(t) = \begin{cases} \psi_2\left(t - \dfrac{T_P}{2}\right) & \text{for} \quad 0 \le t \le T_P \\ 0 & \text{for} \quad \text{otherwise} \end{cases} \tag{6.33}$$

The approximated error functions are obtained by using (6.4) and $T_U = 2T_P$. They are given by [60]

$$\varepsilon_1(\mathbf{x}) = T_S \sum_{q=0}^{Q} \left[h_1(t_q, \mathbf{x}) - h_{d1}(t_q) \right]^2 \tag{6.34}$$

$$\varepsilon_2(\mathbf{x}) = T_S \sum_{q=0}^{Q} \left[h_2(t_q, \mathbf{x}) - h_{d2}(t_q) \right]^2 \tag{6.35}$$

The parameters of pulse shapers that minimize errors in (6.34) and (6.35) are found by solving the problem in (6.3).

The pulse shapers are obtained by approximating the ideal pulses with the duration of T_P = 1 ns. The pulses are represented with 65 points, that is, with Q = 64. For each pulse, the sixth-, eighth-, and tenth-order transfer functions are optimized. The optimum zeros, poles, and gain constants obtained for ψ_1 and ψ_2 are given in Table 6.4 and Table 6.5, together with the obtained spectral efficiency and energy concentration. In addition, for the pairs of transfer functions with equal complexity, the orthogonality of the impulse responses is provided. It is clear that for the eighth- and tenth-order pulse shapers the orthogonality is less than 1e–3, whereas the efficiency is close to 25%. The latter is expected since the prolate spheroidal pulses belong to the class of orthogonal UWB pulses with low spectral efficiency.

Table 6.4 Zeros, poles, and gain constants of various pulse shapers forming prolate-spheroidal pulse ψ_1, together with pulse's spectral efficiency, energy concentration, and orthogonality with their counterparts from Table 6.5 [60].

$M = 4, N = 6$		
z_i	$8.39436 \pm 47.0141j, \pm 10.9794j$	$\eta_1 = 22.2$ % $\lambda_1 = 99.12$ % $\mu = 6.91\text{e}{-3}$
p_k	$-2.32565 \pm 49.1046j, -2.70852 \pm 42.7923j, -2.13370 \pm 36.7477j$	
H_{01}	0.43243	
$M = 6, N = 8$		
z_i	$7.73952 \pm 55.8954j, 12.7742 \pm 35.2706j, \pm 16.8938j$	$\eta_1 = 26.2$ % $\lambda_1 = 99.90$ % $\mu = 2.17\text{e}{-4}$
p_k	$-3.01165 \pm 51.4290j, -3.71406 \pm 45.0846j, -3.67363 \pm 38.9992j,$ $-2.89246 \pm 32.8404j$	
H_{01}	–0.35375	
$M = 6, N = 10$		
z_i	$7.52737 \pm 61.3555j, 31.7015 \pm 36.7887j, 6.26145 \pm 23.2928j$	$\eta_1 = 25.3$ % $\lambda_1 = 99.99$ % $\mu = 1.01\text{e}{-5}$
p_k	$-3.40210 \pm 54.6866j, -4.28802 \pm 48.6866j, -4.54515 \pm 42.9541j,$ $-4.31194 \pm 37.2215j, -3.45030 \pm 31.2181j$	
H_{01}	–173.588	

Table 6.5 Zeros, poles, and gain constants of various pulse shapers forming prolate-spheroidal pulse ψ_2, together with pulse's spectral efficiency, energy concentration, and orthogonality with their counterparts from Table 6.4 [60].

$M = 4, N = 6$		
c_i	11.5187 ± 44.1935j, 42.1453, 42.1453	$\eta_2 = 23.1$ % $\lambda_2 = 99.29$ % $\mu = 6.91\text{e}{-3}$
d_k	–2.36742 ± 49.7739j, –2.83391 ± 43.4868j, –2.38244 ± 37.1900j	
H_{02}	–0.19318	
$M = 6, N = 8$		
c_i	12.3902 ± 48.7513j, 2.92240, 2.92240, 0, 0	$\eta_2 = 25.5$ % $\lambda_2 = 99.80$ % $\mu = 2.17\text{e}{-4}$
d_k	–2.61145 ± 51.2162j, –3.23008 ± 45.2111j, –3.14462 ± 39.4264j, –2.28670 ± 33.7071j	
H_{02}	–0.15718	
$M = 6, N = 10$		
c_i	9.80439 ± 58.7597j, 11.6355 ± 26.8504j, 0.75866 ± 13.9595j	$\eta_2 = 24.9$ % $\lambda_2 = 99.98$ % $\mu = 1.01\text{e}{-5}$
d_k	–3.27600 ± 54.3405j, –4.14431 ± 48.4190j, –4.39378 ± 42.7537j, –4.15336 ± 37.0925j, –3.28685 ± 31.1931j	
H_{02}	–278.009	

Figure 6.6 shows the impulse responses of the pulse shapers with $N_1 = N_2 = 8$ and $M_1 = M_2 = 6$ together with the desired impulse responses. It is clear that both pulse shapers generate the desired pulses with a small error. Figure 6.7 shows the pulses' power spectral densities together with the FCC masks, for convenience.

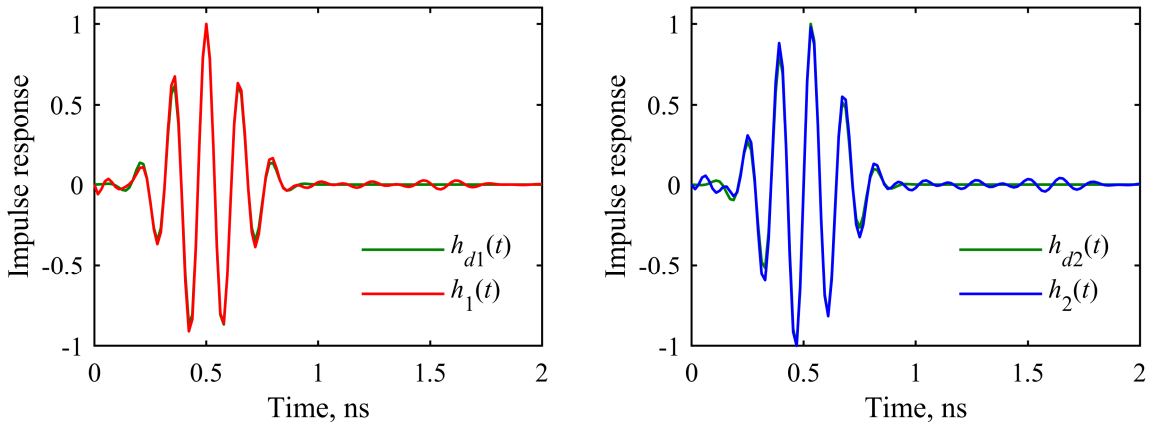

Figure 6.6 Impulse responses of pulse shapers with $N_1 = N_2 = 8$ and $M_1 = M_2 = 6$ forming delayed prolate-spheroidal pulses ψ_1 (left) and ψ_2 (right), together with corresponding desired impulse responses [60].

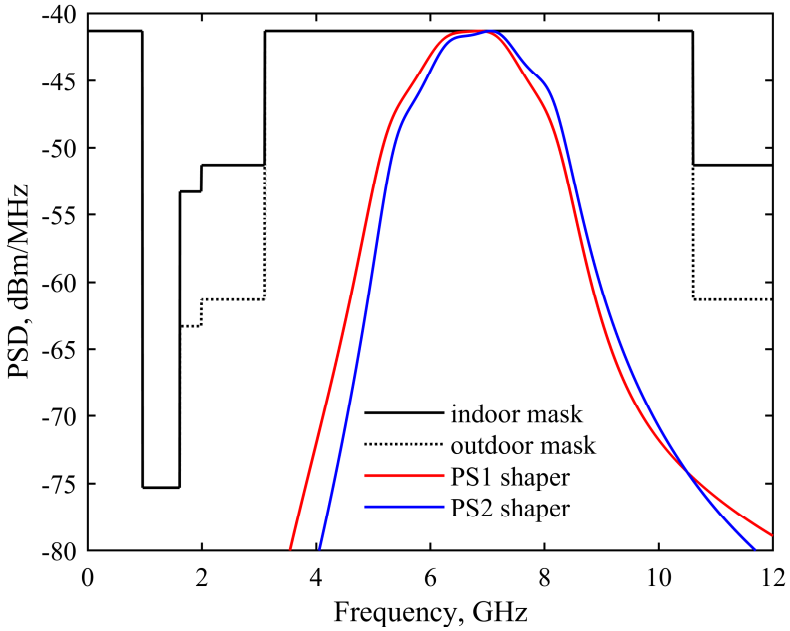

Figure 6.7 Power spectral densities of impulse responses approximating delayed prolate-spheroidal pulses ψ_1 and ψ_2 with $N_1 = N_2 = 8$ and $M_1 = M_2 = 6$, together with FCC masks [60].

6.4.4 Pulse shapers forming sharpened Gaussian derivatives

In this section, the pulse shapers whose impulse responses approximate sharpened Gaussian derivatives with $n = 2$ and $p = 8$ from Table 4.1 are considered. The pulse shapers are optimized assuming $T_U = 15\,\tau$. The zeros, poles, and gain constants of the optimum shapers are given in Table 6.6, together with pulse's spectral efficiency and energy concentration. An efficient approximation of the FCC-compliant indoor and outdoor pulse is achieved with 12th- and 14th-order transfer functions, resulting in the spectral efficiency of 78.4% for the indoor and 71.3% for the outdoor pulse. The corresponding impulse responses and their power spectral densities are shown in Figures 6.8 and 6.9.

Table 6.6 Zeros, poles, and gain constants of pulse shapers forming sharpened Gaussian derivatives with $n = 2$ and $p = 8$, together with pulse's spectral efficiency and energy concentration.

indoor mask, $t_d = 0.4042$ ns, $M = 9$, $N = 12$		
z_i	$9.55380 \pm 74.5862j$, $10.7889 \pm 49.7172j$, $10.5129 \pm 35.0886j$, $\pm 13.7414j$, 0	$\eta = 78.4$ % $\lambda = 99.92$ %
p_k	$-3.84132 \pm 64.0258j$, $-5.66522 \pm 56.0146j$, $-6.57212 \pm 46.4578j$, $-6.70120 \pm 35.9577j$, $-5.35748 \pm 26.2801j$, $-4.31093 \pm 19.8174j$	
H_0	-71.9335	
outdoor mask, $t_d = 0.5040$ ns, $M = 9$, $N = 14$		
z_i	$5.47365 \pm 71.0651j$, $8.87791 \pm 48.8466j$, $8.47769 \pm 35.7927j$, $\pm 15.9573j$, 0	$\eta = 71.3$ % $\lambda = 99.96$ %
p_k	$-3.55734 \pm 63.2944j$, $-4.66959 \pm 57.4548j$, $-5.97048 \pm 50.5432j$, $-6.33009 \pm 42.8853j$, $-6.08789 \pm 35.2177j$, $-4.85209 \pm 28.0375j$, $-3.34908 \pm 23.0890j$	
H_0	84863	

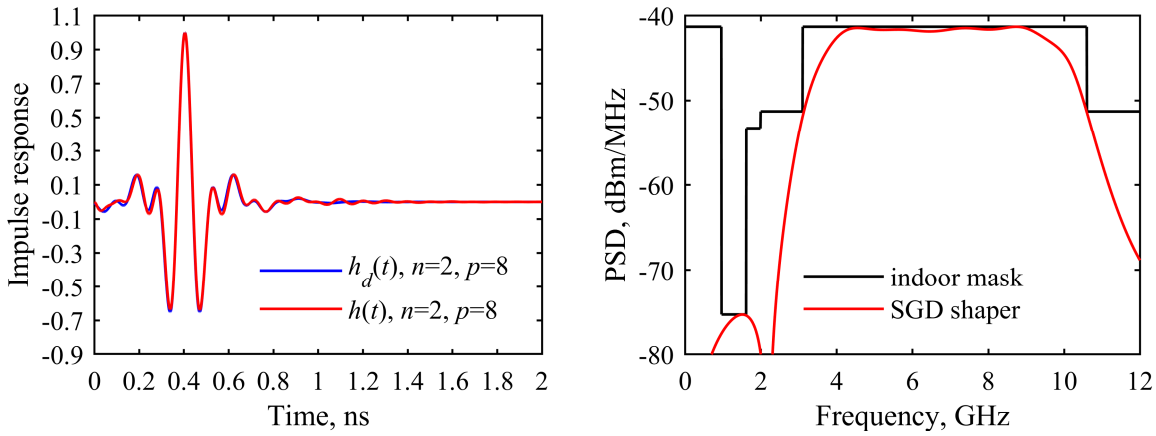

Figure 6.8 Desired impulse response of pulse shaper forming sharpened Gaussian derivative with $n = 2$ and $p = 8$ and its approximation obtained by pulse shaper with $N = 12$ and $M = 9$ (left), and power spectral density of approximated pulse together with FCC indoor mask (right).

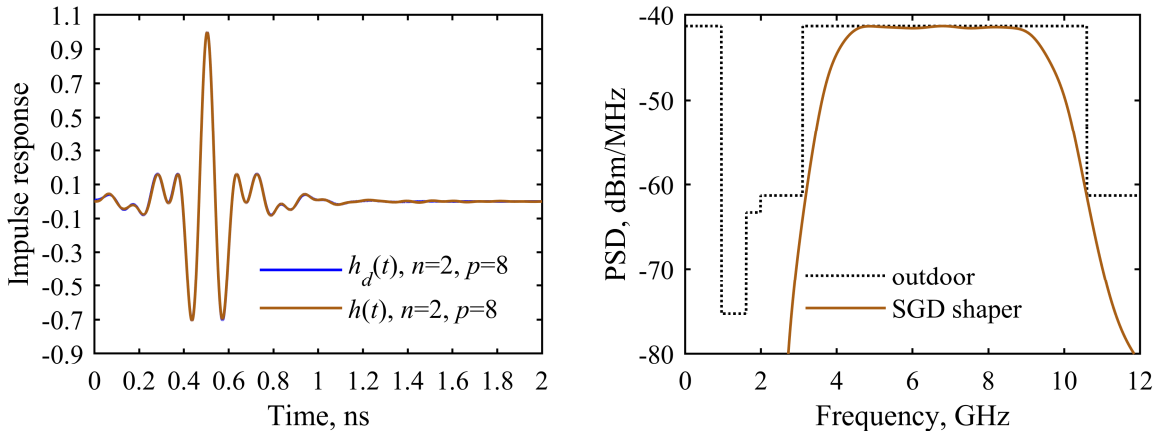

Figure 6.9 Desired impulse response of pulse shaper forming sharpened Gaussian derivative with $n = 2$ and $p = 8$ and its approximation obtained by pulse shaper with $N = 14$ and $M = 9$ (left), and power spectral density of approximated pulse together with FCC outdoor mask (right).

6.4.5 Pulse shapers forming flat-spectrum Gaussian pulses

As shown in Chapter 5, the flat-spectrum Gaussian pulses obtained for even and odd polynomial orders behave differently. Therefore, in further text, these two classes are considered separately. In both cases, the pulses are synthesized assuming $T = 15\,\tau$.

6.4.5.1 Flat-spectrum Gaussian pulses with even polynomial orders

After experimenting with various numbers of zeros and poles, efficient approximations of ideal FCC-compliant indoor pulses are obtained by using the tenth-order transfer function for $n = 2$ and by the 12th-order transfer functions for $n = 4$ and $n = 6$. Efficient approximations of ideal FCC-compliant outdoor pulses are achieved with the 12th-order transfer functions for $n = 2$ and $n = 4$, and with the 14th-order transfer function for $n = 6$.

The optimum zeros, poles, and gain constants of the pulse shapers forming flat-spectrum Gaussian pulses with even n, compliant with FCC indoor and outdoor mask, are given in Tables 6.7 and 6.8. In both tables, the spectral efficiencies and energy concentrations of the corresponding impulse responses are also given. It should be noted that these spectral efficiencies are close to those provided by the ideal pulses given in Table 5.5. The obtained impulse responses and their power spectral densities are shown in Figures 6.10 and 6.11 for both FCC masks.

Table 6.7 Zeros, poles, and gain constants of various pulse shapers forming flat-spectrum Gaussian pulses with even n compliant with FCC indoor mask, together with pulse's spectral efficiency and energy concentration.

$n = 2$, $t_d = 0.3074$ ns, $M = 7$, $N = 10$		
z_i	8.26640±74.8274j, 14.0789±44.3345j, 0,0,0	$\eta = 62.8\%$ $\lambda = 99.94\%$
p_k	–5.48610±66.7521j, –6.79072±56.4203j, –7.72134±45.6240j, –6.41113±34.5937j, –4.33054±24.7381j	
H_0	–67.2060	
$n = 4$, $t_d = 0.3605$ ns, $M = 7$, $N = 12$		
z_i	17.7185±70.0258j, 12.5786±41.6633j, 0,0,0	$\eta = 68.1\%$ $\lambda = 99.96\%$
p_k	–4.53626±66.5192j, –5.83079±58.0152j, –6.95387±48.9761j, –6.86823±38.9683j, –5.53416±29.7980j, –3.68565±21.5125j	
H_0	–90478.5	
$n = 6$, $t_d = 0.3851$ ns, $M = 9$, $N = 12$		
z_i	5.15633 ± 75.6110j, 13.9518±50.4316j, 13.3563±36.1040j, 0,0,0	$\eta = 74.5\%$ $\lambda = 99.97\%$
p_k	–4.62858±66.2378j, –5.97356±57.9576j, –7.25476±48.6274j, –7.17348±38.4707j, –5.75447±28.9733j¸–3.98401±20.8141j	
H_0	–58.7661	

Table 6.8 Zeros, poles, and gain constants of various pulse shapers forming flat-spectrum Gaussian pulses with even n compliant with FCC outdoor mask, together with pulse's spectral efficiency and energy concentration.

$n = 2$, $t_d = 0.3470$ ns, $M = 7$, $N = 12$		
z_i	3.99395±73.5956j, 16.2706±41.9552j, ±11.8263j, 0	η=52.8% λ>99.99%
p_k	–5.64583±65.5680j, –6.80756±57.0742j, –7.70583±49.0605j, –7.98014±39.3269j, –6.64944±31.0674j, –4.95372±22.6029j	
H_0	–84462.9	
$n = 4$, $t_d = 0.4211$ ns, $M = 9$, $N = 12$		
z_i	9.53595±68.5894j, 11.0584±43.7695j, 20.8890±14.3229j, 0,0,0	η=58.9% λ=99.98%
p_k	–4.04647±61.6085j, –5.29162±54.0044j, –6.38632±45.5863j, –6.18430±36.6779j, –5.13735±29.0586j, –3.95956±21.5530j	
H_0	–25.5522	
$n = 6$, $t_d = 0.4985$ ns, $M = 9$, $N = 14$		
z_i	6.72496±70.9040j, 11.2801±47.2774j, 12.6693±35.6687j, ±10.9387j, 0	η=63.5% λ=99.99%
p_k	–3.65455±64.2156j, –4.67158±57.8925j, –5.65027±51.3844j, –5.99696±43.8411j, –5.63423±36.2446j, –4.50279±29.5113j, –3.20864±23.2617j	
H_0	48336.4	

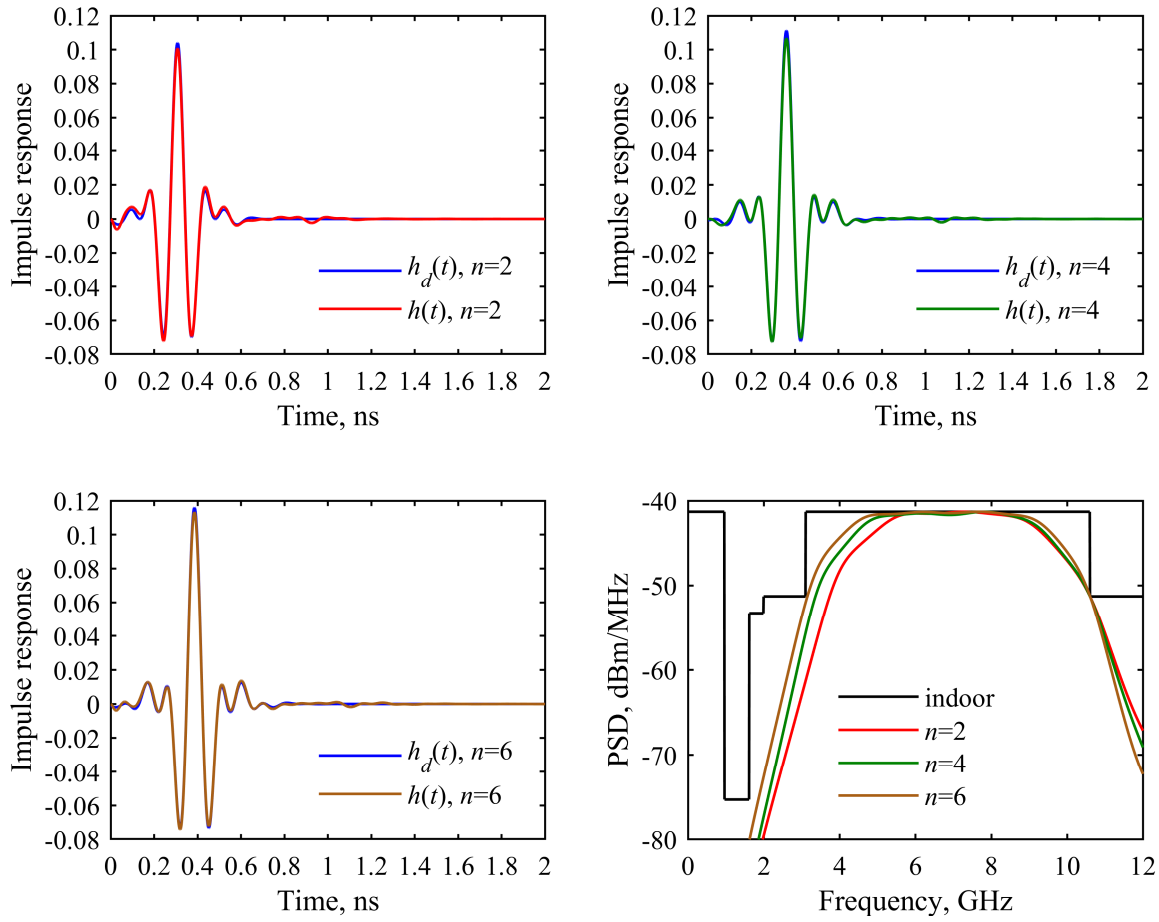

Figure 6.10 Desired impulse responses of pulse shapers forming flat-spectrum Gaussian pulses and their approximations obtained for $n = 2$, $N = 10$ and $M = 7$ (top left), $n = 4$, $N = 12$ and $M = 7$ (top right), $n = 6$, $N = 12$ and $M = 9$ (bottom left), together with power spectral densities of approximated pulses (bottom right). All pulse shapers are compliant with FCC indoor mask.

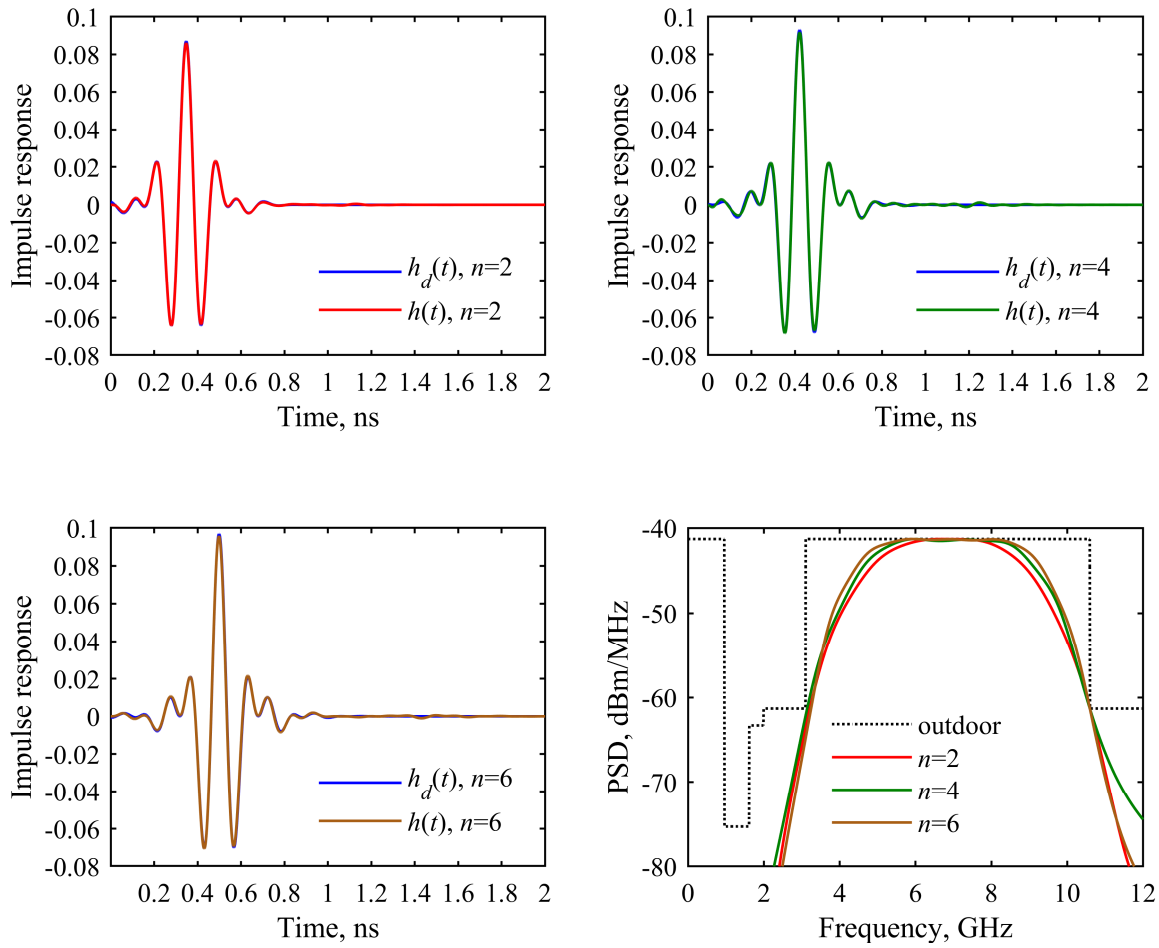

Figure 6.11 Desired impulse responses of pulse shapers forming flat-spectrum Gaussian pulses and their approximations obtained for $n = 2$, $N = 12$ and $M = 7$ (top left), $n = 4$, $N = 12$ and $M = 9$ (top right), $n = 6$, $N = 14$ and $M = 9$ (bottom left), together with power spectral densities of approximated pulses (bottom right). All pulse shapers are compliant with FCC outdoor mask.

6.4.5.2 Flat-spectrum Gaussian pulses with odd polynomial orders

In this section, the FCC-compliant flat-spectrum Gaussian pulses with $n = 5$, 9 and 13 are considered. Note that these pulses exhibit the same order of flatness as the pulses with $n = 2$, 4 and 6, which were approximated in the previous section. The optimum zeros, poles, and gain constants of the pulse shapers approximating the aforementioned pulses are given in Tables 6.9 and 6.10 for the FCC indoor and the outdoor mask. For both masks, the 12th-, 14th- and 16th-order transfer functions are found appropriate for the approximation of the pulses with $n = 5$, 9, and 13. The obtained impulse responses and their power spectral densities are shown in Figures 6.12 and 6.13 for the FCC indoor and the outdoor mask, respectively.

Table 6.9 Zeros, poles, and gain constants of various pulse shapers forming flat-spectrum Gaussian pulses with odd n compliant with FCC indoor mask, together with pulse's spectral efficiency and energy concentration.

$n = 5$, $t_d = 0.4527$ ns, $M = 9$, $N = 12$		
z_i	8.17092±62.5009j, 10.0589±46.7728j, 10.1108±33.0004j, ±10.2861j, 0	η=66.2% λ=99.80%
p_k	–3.17615±64.2742j, –4.46317±55.2349j, –5.10085±46.1783j, –5.19496±36.8827j, –4.40050±28.3405j, –2.81333±21.2510j	
H_0	–72.9407	
$n = 9$, $t_d = 0.4978$ ns, $M = 9$, $N = 14$		
z_i	8.56421±60.8318j, 9.14098±45.4491j, 8.93030±32.3676j, ±15.3966j, 0	η=71.5% λ=99.90%
p_k	–2.93232±65.0832j, –4.14973±57.4008j, –4.89371±49.5391j, –5.25414±41.1886j, –5.05398±32.8938j, –4.08661±25.5142j, –2.34706±19.6225j	
H_0	–132553	
$n = 13$, $t_d = 0.5225$ ns, $M = 9$, $N = 16$		
z_i	10.3127±63.1151j, 9.49650±46.2420j, 8.72559±32.9462j, ±15.6517j, 0	η=77.3% λ=99.95%
p_k	–3.01610±67.2740j, –4.23878±60.4548j, –4.99055±53.5829j, –5.62922±46.1728j, –5.85701±38.4728j, –5.37522±30.9456j, –4.18992±24.3647j, –2.30493±19.4268j	
H_0	–2.05604e8	

Table 6.10 Zeros, poles, and gain constants of various pulse shapers forming flat-spectrum Gaussian pulses with odd n compliant with FCC outdoor mask, together with pulse's spectral efficiency and energy concentration.

$n = 5$, $t_d = 0.4296$ ns, $M = 7$, $N = 12$		
z_i	10.3806±57.3166j, 10.0511±38.2123j, ±14.4478j, 0	η=58.3% λ=99.93%
p_k	–3.55511±61.5076j, –4.86778±53.1647j, –5.56597±44.9766j, –5.75258±36.4237j, –4.73218±28.6072j, –2.90313±22.3376j	
H_0	–85531.9	
$n = 9$, $t_d = 0.4690$ ns, $M = 9$, $N = 14$		
z_i	5.70771±68.2733j, 12.1512±50.5142j, 9.43089±35.9289j, ±17.0634j, 0	η=63.3% λ=99.93%
p_k	– 4.56650±65.5678j, – 5.76226±57.8235j, – 6.47344±50.5644j, –7.12754±42.8231j, –6.68092±34.6871j, –5.12548±27.2355j, –2.89054±21.9192j	
H_0	–109075	
$n = 13$, $t_d = 0.5358$ ns, $M = 11$, $N = 16$		
z_i	6.94159±64.7165j, 9.39100±47.8593j, 8.38226±35.1047j, ±19.0888j, 7.52255, 7.52255, 0	η=67.1% λ=99.83%
p_k	–3.51527±63.7467j, –4.62871±56.9629j, –5.14586±50.3286j, –5.94074±43.0729j, –5.62079±35.7032j, –4.89712±28.7284j, –3.16675±23.1703j, –0.66108±19.6254j	
H_0	71725.6	

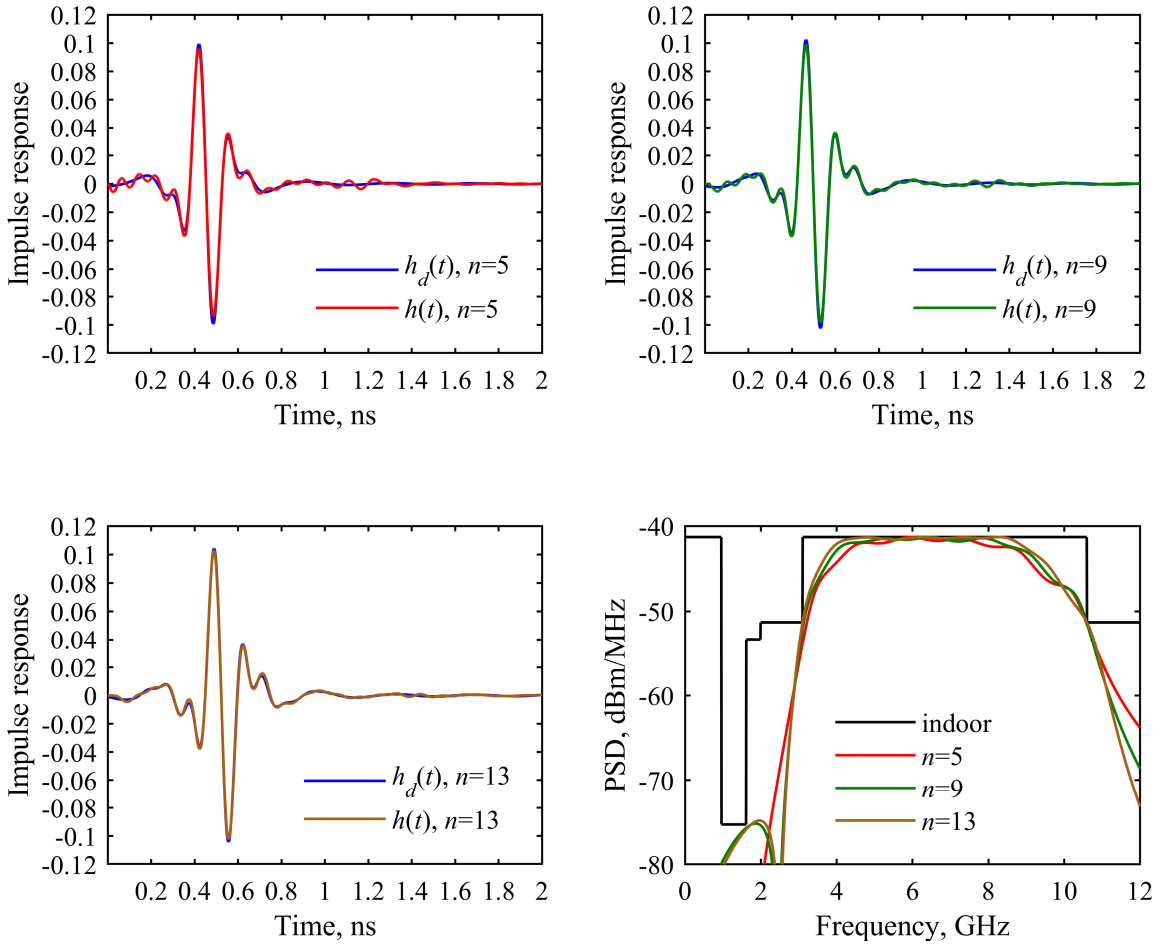

Figure 6.12 Desired impulse responses of pulse shapers forming flat-spectrum Gaussian pulses and their approximations obtained for $n = 5$, $N = 12$ and $M = 9$ (top left), $n = 9$, $N = 14$ and $M = 9$ (top right), $n = 13$, $N = 16$ and $M = 9$ (bottom left), together with power spectral densities of approximated pulses (bottom right). All pulse shapers are compliant with FCC indoor mask.

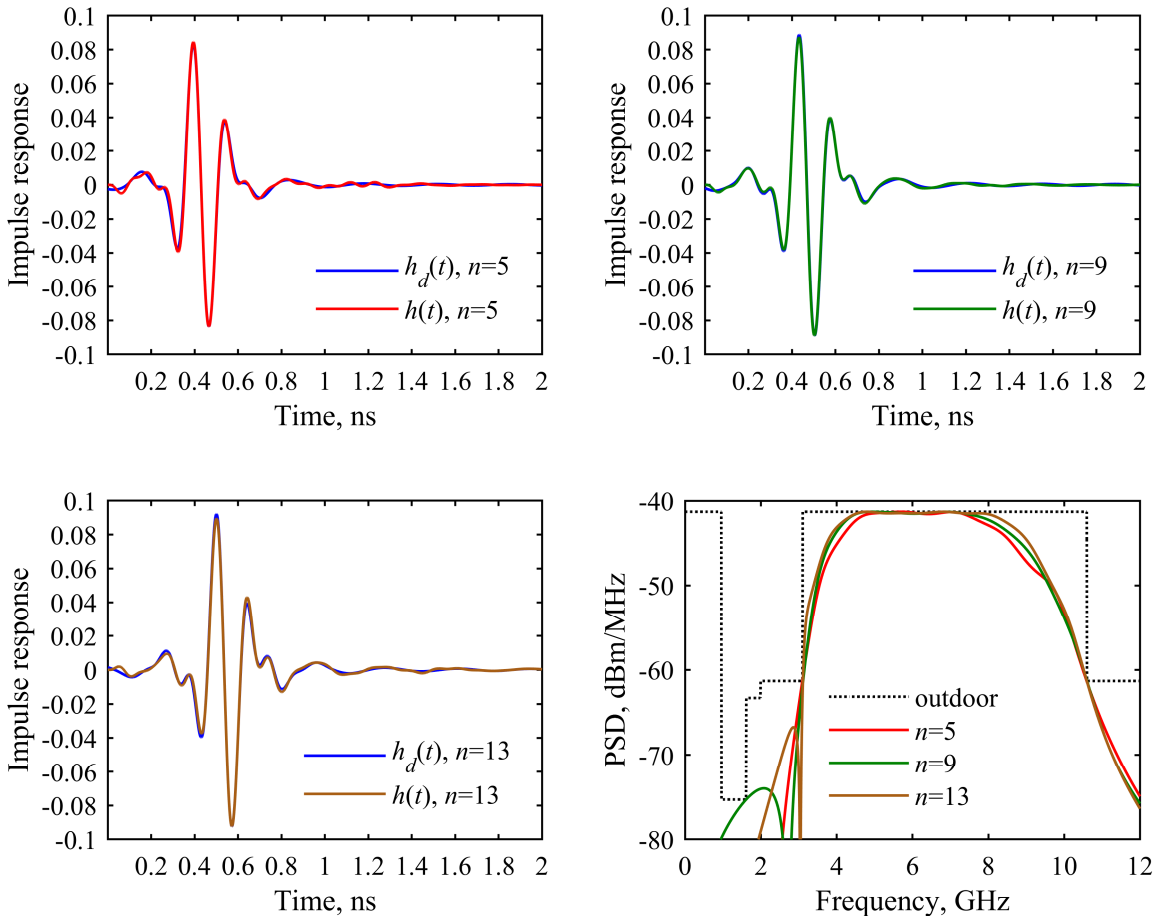

Figure 6.13 Desired impulse responses of pulse shapers forming flat-spectrum Gaussian pulses and their approximations obtained for $n = 5$, $N = 12$ and $M = 7$ (top left), $n = 9$, $N = 14$ and $M = 9$ (top right), $n = 13$, $N = 16$ and $M = 11$ (bottom left), together with power spectral densities of approximated pulses (bottom right). All pulse shapers are compliant with FCC outdoor mask.

7. CONCLUSION

Two methods for the design of spectrally and energy efficient UWB pulses were developed. Both methods are based on shaping the pulses' magnitude spectra. In such shaping, the research has explored new analytical techniques which ensure the filling of the desired spectral mask in a spectrally efficient way, while maintaining a high energy concentration. Furthermore, to obtain the corresponding pulse shaping filters, the rational transfer functions which efficiently approximate ideal pulses were proposed. More specifically, three contributions have been made.

First, a simple method for the design of UWB pulses based on sharpening technique was developed. In this method, the spectral properties of Gaussian derivatives were significantly improved by polynomial sharpening of their magnitude spectra. To obtain the pulses with good frequency and time localization, the spectrum flatness was introduced as a sharpening criterion. The method supports arbitrary UWB masks. Considering the FCC masks, the obtained waveforms outperform the spectral efficiency of other Gaussian-based pulses, while retaining high energy concentration.

In the scope of second contribution, polynomial weighting of the Gaussian pulse was exploited to develop a method for the waveform design. In this method, maximum flatness was introduced as a spectrum shaping criterion, thus resulting in the pulses with very high time and frequency localization. The presented shaping relies on frequency shift and bandwidth scaling. Such an approach allows very efficient filling of a given spectral mask. Considering the FCC masks, the obtained spectral shapes significantly outperform state-of-the-art pulses, while maintaining a high energy concentration.

Finally, the transfer functions whose impulse responses efficiently approximate the ideal UWB pulses and comply the FCC spectral masks were investigated. In their synthesis, the zero-pole-gain model was used because it describes the impulse response simply. The transfer functions were obtained by minimizing the mean squared error in the time domain, where special attention was paid to maintaining a high spectral efficiency.

8. REFERENCES

[1] Ghavami, M., Michael, L. B., Kohno, R., "Ultra wideband signals and systems in communication engineering", Second edition, John Wiley & Sons Ltd, 2007.

[2] Oppermann, I. J., Hämäläinen, M., Iinatti. J. H., "UWB Theory and Applications", John Wiley & Sons Ltd, 2005.

[3] "Signaling of the New York City Subway", available on https://en.wikipedia.org/wiki/Signaling_of_the_New_York_City_Subway (2023., November 2nd).

[4] "Ultra Wideband security in iOS", available on https://support.apple.com/guide/security/ultra-wideband-security-sec1e6108efd/web (2021., February 18th).

[5] "What's the deal with Ultra Wideband?", available on https://www.bmw.com/en/innovation/bmw-digital-key-plus-ultra-wideband.html (2021., March 11th).

[6] FCC 02-48, "FCC first report and order: Revision of part 15 of the Commission's rules regarding ultra-wideband transmission systems", February 2002.

[7] ECC/DEC/(06)04, "Electronic Communications Committee (2006) ECC Decision of 24 March 2006 on the harmonic conditions for devices using ultra-wideband (UWB) technology in bands below 10.6 GHz", amended July 2007., amended December 2011.

[8] Association of Radio Industries and Businesses (2015) UWB (Ultra-Wideband) radio systems. STD-T91, Version 2.0, English translation, March 2015.

[9] Hu, B., Beaulieu, N. C., "Pulse shapes for ultrawideband communication systems", *IEEE Transactions on Wireless Communications*, Vol. 4, No. 4, July 2005., pp. 1789–1797.

[10] Zhu, Y., Zuegel, J. D., Marciante, J. R., Wu, H., "Distributed waveform generator: a new circuit technique for UWB pulse generation, shaping and modulation", *IEEE Journal of Solid-State Circuits*, Vol. 44, No. 3, March 2009., pp. 808–823.

[11] Haddad, S. A. P., Verwaal, N., Houben, R., Serdijn, W. A., "Optimized dynamic translinear implementation of the Gaussian wavelet transform", *Proceedings of the IEEE International Symposium on Circuits and Systems*, Vancouver, Canada, May 2004., pp. 145–148.

[12] Shamsa, Y., Serdijn, W. A., "A 21pJ/pulse FCC compliant UWB pulse generator", *Proceedings of the IEEE International Symposium on Circuits and Systems*, Paris, France, May/June 2010., pp. 497–500.

[13] Neves, L. C., de Araujo, G. M., da Costa, J. C., Haddad, S. A. P., "Design of a PSWF impulse response filter for UWB systems", *Proceedings of the IEEE International Symposium on Circuits and Systems*, Seoul, Korea, May 2012., pp. 1935–1938.

[14] Mirshafiei, M., Abtahi, M., Rusch, L. A., "Ultra-wideband pulse shaping: bypassing the inherent limitations of the Gaussian monocycle", *IET Communications*, Vol. 6, No. 9, June 2012., pp. 1068–1074.

[15] Bagga, S., Vorobyov, A. V., Haddad, S. A. P., Yarovoy, A. G., Serdijn, W. A., Long, J. R., "Codesign of an impulse generator and miniaturized antennas for IR-UWB", *IEEE Transactions on Microwave Theory and Techiques*, Vol. 54, No. 4, April 2006., pp. 1656–1666.

[16] Sheng, H., Orlik, P., Haimovich, A. M., Cimini Jr., L. J., Zhang, J., "On the spectral and power requirements for ultra-wideband transmission", *Proceedings of the IEEE International Conference on Communications*, Anchorage, Alaska, USA, May 2003., pp. 738–742.

[17] Ghavami, M., Michael, L. B., Haruyama, S., and Kohno, R., "A novel UWB pulse shape modulation system", *Wireless Personal Communications*, Vol. 23, October 2002., pp. 105–120.

[18] Parr, B., Cho, B., Wallace, K., Ding, Z., "A novel ultrawideband pulse design algorithm", *IEEE Communications Letters*, Vol. 7, No. 5, May 2003., pp. 219–221.

[19] Ghavami, M., Amini, A., and Marvasti, F., "Unified structure of basic UWB waveforms", *IEEE Transactions on Circuits and Systems II: Express Briefs*, Vol. 55, No. 12, December 2008., pp. 1304–1308.

[20] Beaulieu, N. C., Hu, B., "On determining a best pulse shape for multiple access ultra-wideband communication systems", *IEEE Transactions on Wireless Communications*, Vol. 7, No. 9, September 2008., pp. 3589–3596.

[21] Sharma, S., Bhatia, V., "UWB pulse design using constraint convex sets method", *International Journal of Communication Systems*, Vol. 30, No. 14, September 2017., e3290.

[22] Zaki, A., Ommar, M., Yousry, I., "A novel doublet hermite pulse for performance enhancement and interference mitigation in UWB STC systems", *2017 Progress in Electromagnetics Research Symposium - Fall (PIERS - FALL)*, Singapore, November 2017., pp. 2715-2721.

[23] Kim, S., Kim, Y., Li, X., Kang, J., "Orthogonal pulse design in consideration of FCC and IEEE 802.15.4a constraints", *IEEE Communications Letters*, Vol. 17, No. 5, May 2013., pp. 896–899.

[24] Sharma, A., Sharma, S. K., "Spectral efficient pulse shape design for UWB communication with reduced ringing effect and performance evaluation for IEEE 802.15.4a channel", *Wireless Networks*, Vol. 25, April 2019., pp. 2723–2740.

[25] Yin, L., Hongbo, Z., “UWB pulse design using the approximate prolate spheroidal wave functions,” *Proceedings of the International Symposium on Microwave, Antenna, Propagation and EMC Technologies for Wireless Communications*, Beijing, Vol. 1, August 2005., pp. 450–453.

[26] Amini, A., Esfahani, P. M., Ghavami, M., Marvasti, F., "UWB orthogonal pulse design using Sturm-Liouville boundary value problem", *Signal Processing*, Vol. 159, June 2019., pp. 147–158.

[27] Beaulieu, N. C., Hu, B., "A pulse design paradigm for ultra-wideband communication systems", *IEEE Transactions on Wireless Communications*, Vol. 5, No. 6, June 2006., pp. 1274–1278.

[28] Vauche, R., Bourdel, S., Dehaese, N., Fourquin, O., Gaubert, J., "Fully tunable UWB pulse generator with zero DC power consumption", *Proceedings of the IEEE International Conference on Ultra-Wideband*, Vancouver, Canada, September 2009, pp. 418–422.

[29] Popa, A., Alexandru, N. D., "Waveform and CMOS generator for a pulse designated for UWB European band 6–8.5 GHz", *Proceedings of the International Symposium on Signals, Circuits and Systems*, Iasi, Romania, July 2015, pp. 1–4.

[30] Pohoata, S., Popa, A., Alexandru, N. D., "Approximation of the third derivative of the Gaussian pulse", *Proceedings of the International Symposium on Signals, Circuits and Systems*, Iasi, Romania, July 2011, pp. 1–4.

[31] Taki, H., Abou-Rjeily, C., "On enhancing the transmission efficiency of modulated UWB signals under different emission standards", *Annals of Telecommunications*, Vol. 77, June 2022., pp. 847–865.

[32] Bai, Z., Liu, J., Chen, H.-H., "Design of ultra-wideband pulses based on spectrum shifted Gaussian waveforms", *IET Communications.*, Vol. 7, No. 6, April 2013., pp. 512–520.

[33] Lu, G., Spasojevic, P., Greenstein, L., "Antenna and pulse designs for meeting UWB spectrum density requirements", *IEEE Conference on Ultra Wideband Systems and Technologies*, Reston, VA, USA, November 2003., pp. 162–166

[34] Taki, H., Abou-Rjeily, C., "Spectrally efficient IR-UWB pulse designs based on linear combinations of Gaussian derivatives", *Telecommunication Systems*, Vol. 81, August 2022., pp. 269–288.

[35] Silva, J. A., Campos, M. L., "Spectrally efficient UWB pulse shaping with application in orthogonal PSM", *IEEE Transactions on Communications,* Vol. 55, No. 2, February 2007., pp. 313–322.

[36] Yin, Z., Wu, M., Wu, S., Wu, Z., Chen, Y., "IA-OPD: An optimized orthogonal pulse design scheme for waveform division multiple access UWB systems", *IEEE Systems Journal*, Vol. 13, No. 3, September 2019., pp. 2386–2395.

[37] Akansu, A. N., Serdijn, W. A., Selesnick, I. W., "Emerging applications of wavelets: A review, " *Physical Communication*, Vol. 3, No. 1, March 2010., pp. 1–18.

[38] Rodrigues, J., Menon M. K, D., Lonappan, L., Gudino, L. J., "Spectral Efficient Pulse Shaping for Impulse Radio Ultra Wideband Communications", *Helix*, Vol. 10, No. 02, April 2020., pp. 226-231.

[39] Miao, G. J., Clements, M. A., "Digital shaped Gaussian monocyles in ultra wideband communications", *United States Patent Application Publication*, US 2004/0086001 A1, May 2004.

[40] Luo, X., Yang, L., Giannakis, G. B., "Designing optimal pulse-shapers for ultra-wideband radios, " *Journal of Communications and Networks*, Vol. 5, No. 4, December 2003., pp. 344–353.

[41] Wu, X., Tian, Z., Davidson, T. N., Giannakis, G. B., "Optimal waveform design for UWB radios", *IEEE Transactions on Signal Processing*, Vol. 54, No. 6, June 2006., pp. 2009–2021.

[42] Gradshteyn, I. S., Ryzhik, I. M., "Table of Integrals, Series, and Products", Elsevier, 2007.

[43] Martens, J.-B., "The Hermite transform - theory", *IEEE Transactions on Acoustics, Speech, and Signal Processing*, Vol. 38, No. 9, September 1990., pp. 1595–1606.

[44] Di Benedetto, M. G., Vojcic, B., "Ultra-wideband wireless communications: A Tutorial", *Journal of Communications and Networks*, Vol. 5, No. 4, December 2003., pp. 290–302.

[45] Slepian, D., Pollak, H. O., "Prolate spheroidal wave functions, Fourier analysis, and uncertainty-I", *The Bell System Techical Journal*, Vol. 40, No. 1, January 1961., pp. 43–46.

[46] Hayes, M. H., "Statistical Digital Signal Processing and Modeling", Wiley, New York, 1996.

[47] *MATLAB,* version 9.7.0 (R2019b), The MathWorks Inc, Natick, Massachusetts, USA 2019.

[48] Molnar, G., Milos, A., Vucic, M., "Sharpened Gaussian Derivatives and Their Application in UWB Pulse Design", *2023 International Symposium on Image and Signal Processing and Analysis (ISPA)*, Rome, Italy, September 2023., pp. 1-6.

[49] Kaiser, J., Hamming, R., "Sharpening the response of a symmetric nonrecursive filter by multiple use of the same filter", *IEEE Transactions on Acoustics, Speech, and Signal Processing*, Vol. ASSP-25, No. 5, October 1977., pp. 415–422.

[50] Hahn, S. L., “Hilbert transforms in signal processing”, Artech House, Inc., Boston, 1996.

[51] Molnar, G., Milos, A., Vucic, M., "Closed-form approximation of Hilbert transforms of Gaussian derivatives based on weighted polynomial fitting". *Proceedings of the IEEE International Convention MIPRO*, Opatija, Croatia, May 2018., pp. 117–121.

[52] Temme, N. M. "Error Functions, Dawson's and Fresnel Integrals", in NIST Handbook of Mathematical Functions, Olver, Frank W. J.; Lozier, Daniel M.; Boisvert, Ronald F.; Clark, Charles W. (eds.), Cambridge University Press, 2010.

[53] Milos, A., Molnar, G., Vucic, M., "Spectrally Efficient UWB Pulse Shaping Based on Polynomially Weighted Gaussian Pulses with Maximally Flat Amplitude Spectra," *IEEE Communications Letters*, Vol. 27, No. 7, July 2023., pp. 1869-1873.

[54] Daubechies, I., "Ten Lectures on Wavelets", SIAM, Philadelphia, PA, USA, 1992.

[55] Haykin, S., "Digital Communication Systems", Wiley, Hoboken, NJ, USA, 2014.

[56] Vucic, M., Molnar, G., "Time-domain synthesis of continuous-time systems based on second-order cone programming", *IEEE Transactions on Circuits and Systems I: Regular Papers*, Vol. 55, No. 10, November 2008., pp. 3110–3118.

[57] Vucic, M., Molnar, G., "Measure for phase linearity based on symmetry of time-domain response", *IET Electronics Letters*, Vol. 39, No. 19, September 2003., pp. 1425–1426.

[58] Vucic, M., Babic, H., "A class of systems with symmetric impulse response", *Proceedings of the IEEE International Symposium on Circuits and Systems*, Monterey, CA, USA, Vol. 3, May/June 1998., pp. 485–488.

[59] Milos, A., Molnar, G., Vucic, M., "Spectral-efficient UWB pulse shapers generating Gaussian and modified Hermitian monocycles", *Proceedings of the IEEE International Convention MIPRO*, Opatija, Croatia, May 2017., pp. 121–126.

[60] Molnar, G., Miloš, A., Vučić, M., "Prolate-spheroidal UWB pulse shapers with highly orthogonal impulse responses", *Proceedings of the 10th International Symposium on Image and Signal Processing and Analysis (ISPA)*, Ljubljana, Slovenia, September 2017., pp. 171–176.

Biography

Ante Miloš was born in 1989 in Mostar, Republic of Bosnia and Herzegovina. He received the master's degree in electrical engineering and information technology from the University of Zagreb Faculty of Electrical Engineering and Computing, Zagreb, Croatia, in 2013. In 2016 he enrolled in the Doctoral study at the same faculty in the field of pulse-shaping techniques and filter design for ultra-wideband impulse radio. After the Master study, he has been employed in the Research and Development Centre of Ericsson Nikola Tesla d.d. in Zagreb, where he works as a Software/Hardware Developer in the Radio Development Unit. In the unit, he is also a member of the Scientific Radio group, where he participates in various research activities of the project Improvements for LTE Radio Access Equipment (ILTERA) - an educational and research collaboration project between Ericsson Nikola Tesla d.d. and the Department of Electronic Systems and Information Processing of the Faculty of Electrical Engineering and Computing, University of Zagreb. Additionally, he participates in the project Efficient Signal Processing Systems for Software Defined Radio funded by Croatian Science Foundation. He is a member of IEEE societies on Signal Processing, Antennas and Propagation, and Circuits and Systems.

Publications:

[1] **Miloš**, **A**., Molnar, G., Vučić, M., "Spectral-efficient UWB pulse shapers generating Gaussian and modified Hermitian monocycles", *Proceedings of 40th International Convention on Information and Communication Technology, Electronics and Microelectronics (MIPRO 2017)*, Opatija, Croatia, May 2017, pp. 121–126.

[2] Molnar, G., **Miloš, A.**, Vučić, M., "Prolate-spheroidal UWB pulse shapers with highly orthogonal impulse responses", *Proceedings of the 10th International Symposium on Image and Signal Processing and Analysis (ISPA 2017)*, Ljubljana, Slovenia, September 2017, pp. 171–176.

[3] Molnar, G., **Miloš**, **A**., Vučić, M., "Closed-form approximation of Hilbert transforms of Gaussian derivatives based on weighted polynomial fittin", *Proceedings of 41st International Convention on Information and Communication Technology, Electronics and Microelectronics (MIPRO 2018)*, Opatija, Croatia, May 2018, pp. 117–121.

[4] Molnar, G., **Miloš**, **A**., Vučić, M., "Time-domain synthesis of pulse shapers for ultra-wideband impulse radio", *Abstract Book of Third International Workshop on Data Science (IWDS)*, Zagreb, Croatia, October 2018, pp. 1415.

[5] **Milos, A.**, Molnar, G., Vucic, M., "Spectrally efficient UWB pulse shaping based on polynomially weighted Gaussian pulses with maximally flat amplitude spectra," *IEEE Communications Letters*, Vol. 27, No. 7, July 2023, pp. 18691873.

[6] Molnar, G., **Milos, A**., Vucic, M., "Sharpened Gaussian derivatives and their application in UWB pulse design", *2023 International Symposium on Image and Signal Processing and Analysis (ISPA 2023)*, Rome, Italy, September 2023, pp. 16.

Životopis

Ante Miloš rođen je 1989. godine u Mostaru, Republika Bosna i Hercegovina. Diplomirao je 2013. godine elektrotehniku i informacijsku tehnologiju na Sveučilištu u Zagrebu, Fakultet elektrotehnike i računarstva. Godine 2016., upisao je doktorski studij na istom fakultetu u području dizajna pulsova i filtara za ultra-širokopojasne impulsne radio sustave. Nakon magistarskog studija zaposlio se kao razvojni programer u kompaniji Ericsson Nikola Tesla d. d., Centar za istraživanje i razvoj, Jedinica za razvoj radija u Zagrebu. U jedinici je član znanstvene radio skupine, gdje sudjeluje u istraživačkim aktivnostima projekta Improvements for LTE Radio Access Equipment (ILTERA) - obrazovano-istraživački kolaboracijski projekt između kompanije Ericsson Nikola Tesla d. d. i Zavoda za elektroničke sustave i obradu informacija na Fakulteta elektrotehnike i računarstva, Sveučilište u Zagrebu. Također sudjeluje u projektu Učinkoviti sustavi za obradu signala namijenjeni programski definiranom radiju, financiran od strane Hrvatske Zaklade za Znanost, *HRZZ IP-2019-04-4189.* Član je IEEE društava za Obradu Signala, Antene i Rasprostiranje Elektromagnetskih Valova i Električne Krugove i Sustave.